HEAT TRANSFER IN A TWO-PASS CHANNEL WITH VORTEX GENERATORS

by

Pavin Ganmol

B.Eng, Chulalongkorn University, Thailand, 1996

M.S., University of Pittsburgh, USA, 1999

Submitted to the Graduate Faculty of

Swanson School of Engineering in partial fulfillment

of the requirements for the degree of

Doctor of Philosophy

University of Pittsburgh

2010

UNIVERSITY OF PITTSBURGH

SWANSON SCHOOL OF ENGINEERING

This dissertation was presented

by

Pavin Ganmol

It was defended on

July 28, 2010

and approved by

Dr. Phouc X. Tran, Research Engineer, NETL, U.S. Department of Energy

Dr. Laura Schaefer, Associate Professor, Department of Mechanical Engineering & Materials Science

Dr. Sung Kwon Cho, Assistant Professor, Department of Mechanical Engineering & Materials Science

Dissertation Director: Dr. Minking K. Chyu, Professor, Department of Mechanical Engineering & Materials Science

HEAT TRANSFER IN A TWO-PASS CHANNEL WITH VORTEX GENERATORS

Pavin Ganmol, PhD

University of Pittsburgh, 2010

Cooling channels in modern turbine airfoils often include surface features for enhanced heat convection and near 180-degree turns. A sharp turn further induces turbulence level and increases heat transfer rate. However, it also causes significant pressure loss. While significant level of studies have been focused on either surface enhancement, such as vortex generators/turbulators, or turn effects, virtually no study in the open literature has been directed to the combined effects of sharp turn and surface-feature induced heat transfer enhancement. In this study, series of experiments were performed to investigate the heat transfer and pressure characteristics in a high aspect ratio, (4.5:1 width-to-height), two-pass channel, with delta-wing-shaped, cube-shaped and diamond-shaped element arrays placed in both channel passes before and after a 180-degree sharp turn. Transient liquid crystal technique is applied to acquire detailed local heat transfer data both on the channel surface and the turbulator elements, for Reynolds number between 13000 and 32000. To further explore potential design alternatives for enhancement cooling, the density effects of the delta wing turbulators are investigated and the effects of block height of the cube-shaped and diamond-shaped, ranging from ¼, ½, ¾ and full span of the channel height are also evaluated. Present results suggest that a staggered delta wing array can enhance heat transfer rate up to 3.1 fold in the first pass and up to 1.6 fold in the second pass, relative to the fully-developed smooth channel counterpart. When coupled with the 90-degree bend inlet, heat transfer rate can be enhanced up to another 1.9 and 1.3 fold for the

first and second pass respectively. The cube-array can enhance heat transfer rate up to 3.5 folds in the first pass and approximately 1.9 fold in the second pass. For the corresponding diamond-shaped block array, the enhancement is up to 3.4 and 1.9 respectively. It is interesting to note that even though the post-turn turbulence transport in the second pass is generally higher than the first turn, the effects of surface-element induced heat transfer enhancement are, in fact, less prominent, in the post-turn region in the second pass. Pressure loss for a diamond block arrays is generally higher than that of the corresponding cube-block array. Pressure losses for sparse and dense delta arrays are approximately the same as the pressure losses of the half height cube and diamond arrays respectively.

TABLE OF CONTENTS

ACKNOWLEDGEMENTS ..... **XII**

LIST OF TABLES ..... **VIII**

LIST OF FIGURES ..... **IX**

1.0 INTRODUCTION **1**

1.1 BACKGROUND **1**

1.2 PREVIOUS STUDY **6**

1.3 PRESENT WORK STATEMENT **12**

2.0 HEAT TRANSFER MEASUREMENT **13**

2.1 TRANSIENT LIQUID CRYSTAL METHOD **13**

3.0 EXPERIMENT SETUP AND APPARATUS **19**

3.1 OVERALL TEST SETUP **19**

3.2 TEST SURFACE PREPARATION **21**

3.3 EXPERIMENT PROCEDURE **22**

4.0 HEAT TRANSFER ENHANCEMENT EXPERIMENT **23**

4.1 2-PASS SMOOTH CHANNEL **23**

4.1.1 Result and discussion **24**

4.2 3-PASS SMOOTH CHANNEL **27**

4.2.1 Result and discussion **28**

4.3 2-PASS CHANNEL WITH SPARSE DELTA WING ARRAYS 30

4.3.1 Result and discussion 32

4.4 2-PASS CHANNEL WITH DENSE DELTA WING ARRAYS 37

4.4.1 Result and discussion 38

4.5 90-DEGREE BEND INLET 44

4.5.1 Result and discussion 44

4.6 2-PASS CHANNEL WITH PIN-FIN ARRAYS 49

4.6.1 Result and discussion 50

4.7 2-PASS CHANNEL WITH CUBE-SHAPED BLOCK ARRAYS 52

4.7.1 Result and discussion 53

4.8 2-PASS CHANNEL WITH DIAMOND-SHAPED BLOCK ARRAYS 59

4.8.1 Result and discussion 60

5.0 RESULTS COMPARISON 66

6.0 CONCLUSIONS 69

7.0 FUTURE WORK 72

BIBLIOGRAPHY 73

LIST OF TABLES

Table 1: Average heat transfer coefficient in the 2-pass smooth channel 25

Table 2: Average heat transfer coefficient in the 3-pass smooth channel 28

Table 3: Average heat transfer coefficient of 2-pass channel with sparse delta-wing arrays..... 33

Table 4: Average heat transfer coefficient of 2-pass with dense delta-wing arrays 39

Table 5: Average heat transfer coefficient of 2-pass channel with straight and 90-degree bend inlet at Re=20,000..... 46

Table 6: Average heat transfer coefficient of 2-pass channel with pin-fin arrays 51

Table 7: Average heat transfer coefficient of 2-pass channel with cube-shaped block arrays 54

Table 8: Average heat transfer coefficient of 2-pass channel with diamond-shaped block arrays61

LIST OF FIGURES

Figure 1 (a) Convection cooling, (b) Impingement cooling, (c) Film cooling, (d) Transpiration cooling [5] 4

Figure 2 Turbine blade Internal Cooling [6] 5

Figure 3 Typical coolant channels in turbine airfoil and internal rib arrangement [25] 7

Figure 4 Wedge- and delta-shaped ribs [33] 8

Figure 5 Relative heat transfer coefficient on pin elements, Re = 16,800 [37] 10

Figure 6 Relative pin-resolved heat (mass) transfer within an array [43] 11

Figure 7 Thermochromic liquid crystal (TLC) temperature range (bandwidth) 14

Figure 8 Liquid crystal color intensity vs. temperature 15

Figure 9 One-dimensional heat transfer over solid surface 16

Figure 10 Experiment setup diagram 20

Figure 11 Experiment setup 21

Figure 12 2-pass smooth channel test section 24

Figure 13 Local heat transfer coefficient of 2-pass channel with Reynolds number of 13000, 20000, 28000 and 32000 respectively 26

Figure 14 Column average Nu/Nu_0 of 2-pass channel with Reynolds number of 13000, 20000, 28000 and 32000 respectively 27

Figure 15 3-pass channel 27

Figure 16 Local heat transfer coefficient of 3-pass channels at 3 different Reynolds number; .. 29

Figure 17 Column average Nu/Nu_0 of 3-pass channel at Re_{Dh}=13000, 20000 and 28,000 30

Figure 18 2-pass channel with sparse delta wing arrays configuration 31

Figure 19 Test section with sparse delta wing arrays 31

Figure 20 Local heat transfer coefficient and column average Nu/Nu_0 of 2-pass channel with sparse array delta wings configuration at Re_{Dh}=13000..... 33

Figure 21 Local heat transfer coefficient and column average Nu/Nu_0 of 2-pass channel with sparse array delta wings configuration at Re_{Dh}=20000..... 34

Figure 22 Local heat transfer coefficient and column average Nu/Nu_0 of 2-pass channel with sparse array delta wings configuration at Re_{Dh}=28000..... 35

Figure 23 Local heat transfer coefficient and column average Nu/Nu_0 of 2-pass channel with sparse array delta wings configuration at Re_{Dh}=32000..... 36

Figure 24 2-pass channel with dense delta wing arrays configuration 37

Figure 25 Test section with dense delta wing arrays 38

Figure 26 Local heat transfer coefficient and column average Nu/Nu_0 of 2-pass channel with dense array delta wings configuration at Re_{Dh}=13000 40

Figure 27 Local heat transfer coefficient and column average Nu/Nu_0 of 2-pass channel with dense array delta wings configuration at Re_{Dh}=20000 41

Figure 28 Local heat transfer coefficient and column average Nu/Nu_0 of 2-pass channel with dense array delta wings configuration at Re_{Dh}=28000 42

Figure 29 Local heat transfer coefficient and column average Nu/Nu_0 of 2-pass channel with dense array delta wings configuration at Re_{Dh}=32000 43

Figure 30 90-degree bend inlet 44

Figure 31 Local heat transfer coefficient and column average Nu/Nu_0 of 2-pass channel with 90-degree bend inlet at Re_{Dh}=20000 46

Figure 32 Local heat transfer coefficient and column average Nu/Nu_0 of 90-degree bend inlet 2-pass channel with sparse array delta wings configuration at Re_{Dh}=20000 47

Figure 33 Local heat transfer coefficient and column average Nu/Nu_0 of 90-degree bend inlet 2-pass channel with dense array delta wings configuration at Re_{Dh}=20000 48

Figure 34 2-pass channel with pin-fin arrays..... 49

Figure 35 Local heat transfer coefficient of 2-pass channel with pin-fin arrays at Re_{Dh}=13000, 20000 and 28000 51

Figure 36 2-pass channel with cube-shaped block arrays 52

Figure 37 Local heat transfer coefficient of 2-pass channel with ¼ channel height cube-shaped block arrays at Re_{Dh}=13000, 20000, 28000 and column average Nu/Nu_0 55

Figure 38 Local heat transfer coefficient of 2-pass channel with ½ channel height cube-shaped block arrays at Re_{Dh}=13000, 20000, 28000 and column average Nu/Nu_0 56

Figure 39 Local heat transfer coefficient of 2-pass channel with ¾ channel height cube-shaped block arrays at Re_{Dh}=13000, 20000, 28000 and column average Nu/Nu_0 57

Figure 40 Local heat transfer coefficient of 2-pass channel with full channel height cube-shaped block arrays at Re_{Dh}=13000, 20000, 28000 and column average Nu/Nu_0 58

Figure 41 2-pass channel with diamond-shaped block arrays 59

Figure 42 Local heat transfer coefficient of 2-pass channel with ¼ channel height diamond-shaped block arrays at Re_{Dh}=13000, 20000, 28000 and column average Nu/Nu_0 62

Figure 43 Local heat transfer coefficient of 2-pass channel with ½ channel height diamond-shaped block arrays at Re_{Dh}=13000, 20000, 28000 and column average Nu/Nu_0 63

Figure 44 Local heat transfer coefficient of 2-pass channel with ¾ channel height diamond-shaped block arrays at Re_{Dh}=13000, 20000, 28000 and column average Nu/Nu_0 64

Figure 45 Local heat transfer coefficient of 2-pass channel with full channel height diamond-shaped block arrays at Re_{Dh}=13000, 20000, 28000 and column average Nu/Nu_0 conclusion 65

Figure 46 Comparison of Nu_{ave}/Nu_0 vs. Re_{Dh} with different channel configurations 67

Figure 47 Comparison of f_{ave}/f_0 vs. Re_{Dh} with different channel configurations 68

Figure 48 Overall cooling performance factor vs. Re_{Dh} with different channel configurations ... 68

ACKNOWLEDGEMENTS

During the course of my study, many people provided great assistance. First, I would like to acknowledge my advisor, Dr. Minking K. Chyu, for his support, advice and patient guidance throughout the years.

I also would like to thank my committee members, Dr. Laura Schaefer, Dr. Sung K. Cho, and Dr. Phuoc X. Tran for their time and valuable advice. I would like to extend my thanks to the faculty and staff members in the Department of Mechanical Engineering and Material Science.

Special thanks go to my colleagues in the heat transfer group, Sin Chien Siw, Shuping Chen, Emmanuel Olayede and Danny Mazzotta, for their support, help, and inspiration.

1.0 INTRODUCTION

1.1 BACKGROUND

The history of gas turbine has been dated back for more than two centuries. Since then, it has been continuously developed into a reliable and versatile engine with good efficiency and high power-to-weight ratio. Simple open-cycle gas turbines can achieve about 40% efficiency while the high efficiency gas turbines coupling with a combined cycle could reach 60% thermal efficiency. Gas turbine systems in modern world, both land and air based, need improvement in efficiency and power output due to the competition in business, the rising fuel cost and national security. Government agencies, such as the Department of Energy in the United States and major turbine power companies worldwide, are striving for developing higher efficiency gas turbine systems [1, 2]. The maximum Carnot heat engine thermal efficiency that any heat engine could ideally have can be shown by the equation;

$$\eta = 1 - \frac{T_L}{T_H} \tag{1}$$

where T_H is the absolute temperature of the high-temperature pool and T_L is the absolute temperature of the low-temperature pool. For turbine engines, this correlation shows that the high inlet temperature directly affects the efficiency. To achieve the highest efficiency, the turbines have to operate at the highest inlet temperature possible.

The desire to improve the thermal efficiency and power output of modern jet engines has increased turbine inlet temperature up to 2000 K [3]. This operating temperature is well above the permissible temperature of currently available thermal-resistive materials, even for the most advance alloys with advanced coating. The thermal load induced by high *turbine inlet temperature (TIT)* will lead to immense challenge in maintaining material integrity of turbine components. In order to manage stress and improve heat transfer inside the channel of the turbine blade, various techniques have been employed. Manufacturing techniques such as *Directional Solidification (DS)*, which makes grain orientation paralleled to the major axis of the components, increase the strength by a large margin. Protective ceramic coating, such as *thermal barrier coating (TBC)*, also helps the components withstand higher temperature. Operating condition also affects TIT and engine efficiency. For example, adding more air than the stoichiometric air to fuel ratio makes engine burn lean, resulting in lower combustion temperature; thus resulting in lower efficiency due to the lower turbine inlet temperature.

While the advance in developing more effective materials is rather limited, a viable solution to increase the turbine inlet temperature while maintaining the turbine components temperature under their limits is the use of cooling technology. Therefore, advance cooling techniques have to be established to prevent the thermal degradation of turbine components. The first stage rotor and stator are the components that require the highest cooling rate due to high turbine inlet temperature up to 1400 degree centigrade in standard gas turbines. A very good cooling system is needed to create a higher efficiency gas turbine engine. If sufficient cooling is provided, the inlet temperature and combustion temperature can be raised. An increase of 100 °F (56 °C) in combustion temperature could increase 8% to 13% power output and 2% to 4% in simple-cycle efficiency [4].

Turbine could be cooled by various fluids. The coolant is normally air since it is readily available by bleeding from the compressor. Some land based turbines use water or other liquids for the cooling system. The liquid cooling is more effective than the air cooling since liquid has much higher thermal conductivity and is also able to cool the components by evaporation, but it also has disadvantage that it needs large liquid reservoir and requires heat exchanger; thus it is not suitable for the aircraft application.

Gas turbine cooling designs can be separated into two different categories: internal cooling and external cooling. With internal cooling approach, coolant is forced and directed through the cooling channels inside turbine components. External cooling, on the other hand, the coolant is injected or bred from a coolant manifold inside components directly into a hot gas path to protect the exposed component surfaces. There are four major methods to cool the turbine blade. Convection cooling and impingement cooling are used for internal cooling; film cooling and transpiration cooling are used for external cooling.

The convection cooling is the simplest way to cool the turbine blade but in the modern application it exists only when combined with other methods. The general concept of the convection cooling is to force coolant through the channel inside the turbine blade from the base of the blade and discharging out at the tip as shown in Figure 1a. Forced convective heat transfer is the dominant mechanism to transport thermal energy from the component body into the coolant. The impingement cooling, shown in Figure 1b, is the method that directs the air flow inside the blade to impinge directly to the point that requires intensive cooling, usually opposite to the leading edge stagnation point. The impingement cooling is very effective for the local area that needs high rate of heat transfer. Currently, double-walled cooling is considered to be a type of impingement cooling.

As for the film cooling, shown in Figure 1c, the cooling air is forced through small holes into the boundary layer of the hot gas to create cool film along the surface of the blade. The cool film is effectively protecting the surface from the extreme temperature. The transpiration cooling, shown in Figure 1d, is referred to as the full-blade film cooling or porous blade cooling. It is basically the same concept as film cooling but there are many more small holes placed all along the surface.

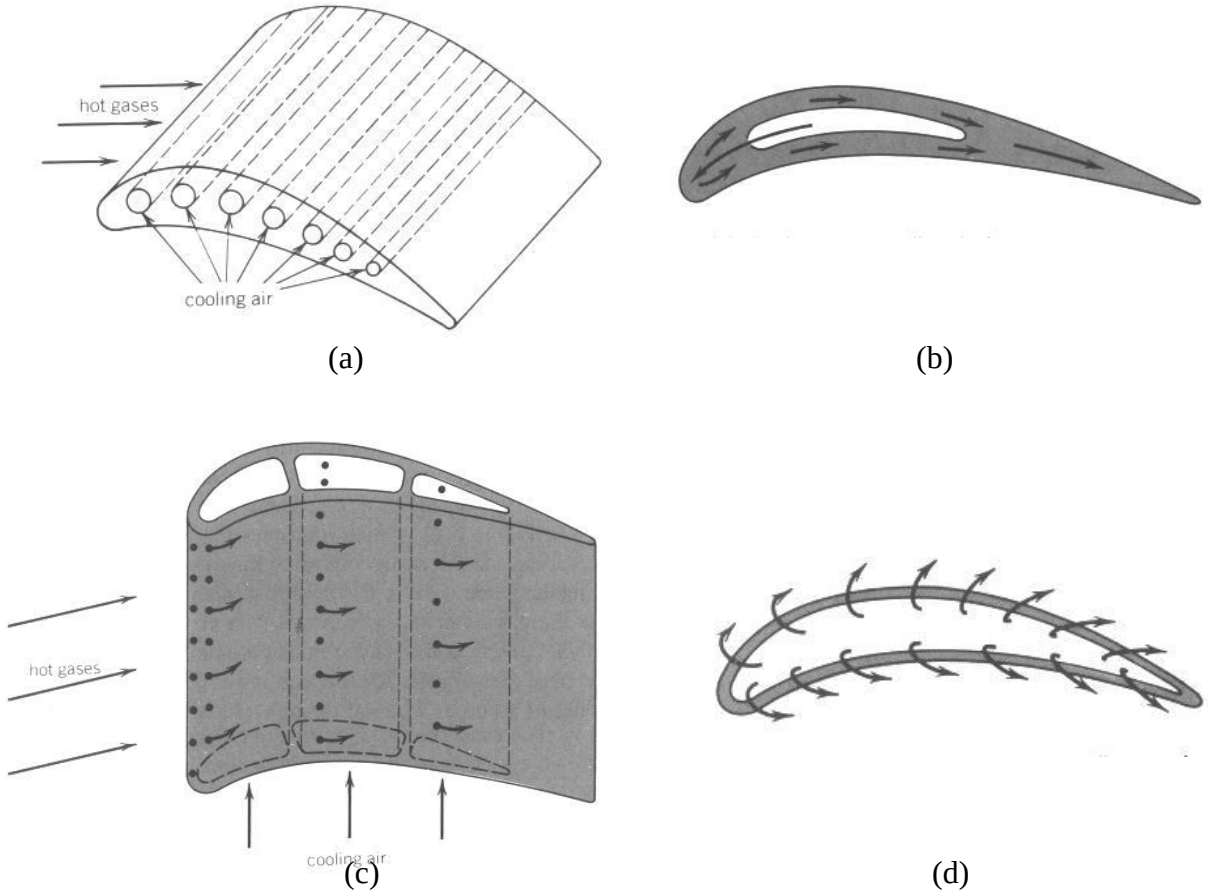

Figure 1 (a) Convection cooling, (b) Impingement cooling, (c) Film cooling, (d) Transpiration cooling [5]

Each cooling method has its advantages and disadvantages. Depending on the application, designers have to choose the best suitable method or combine some of them together to optimize the efficiency of the engine. For example, to cool the first stage turbine blade, a few cooling methods are combined together as shown in Figure 2. Coolant is forced into serpentine channels inside of the turbine blade creating convection cooling while part of it is directed to impinge at the leading edge of the blade and then discharged out to provide film cooling.

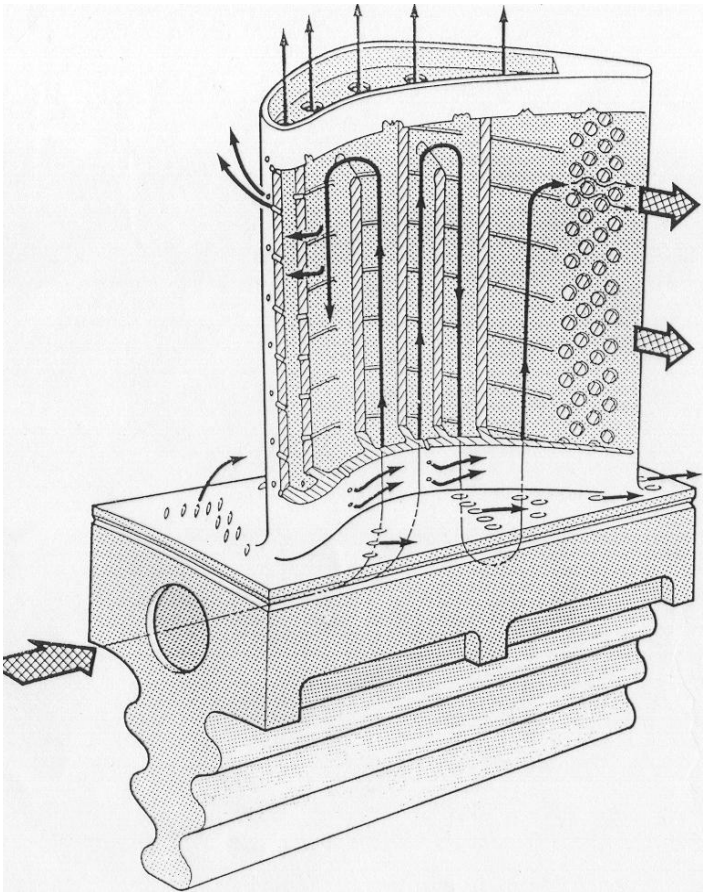

Figure 2 Turbine blade Internal Cooling [6]

Turbine researchers always look for heat transfer designs to increase the heat transfer rate in internal cooling. To improve the heat transfer performance of the convection cooling in the channel inside turbine blade is the main objective of this research since the internal channel is

one of the vital parts in turbine blade cooling and is in much need of improvement. Not only the channel provides the internal forced convective cooling, it is also served as a circuit for the external cooling. Due to the complex flow and heat transfer characteristic in internal cooling channel, there has been extensive research on this topic for the past several decades. To increase heat transfer enhancement and to explore new design alternatives, more research need to be conducted.

1.2 PREVIOUS STUDY

The channel within the turbine blade in general is comprised of sharp turn and has surface features incorporated on channel surface. When fluid flows through a bend, the secondary flow occurs because of the imbalance of the centrifugal force and redial pressure gradient causing the fluid in the midplane of the channel to move outward and circle back along the top and bottom walls. Then the flow merges at the midplane near inner wall of the bend. This flow is called Dean-type secondary motion [7].

Wang and Chyu [8] numerically investigated the effects of secondary flow on the heat transfer along the channel with a 180-degree turn. In their study, three different turn configurations, the straight-corner turn, rounded-corner turn and circular turn were observed. Their study shows that the heat transfer in the turning region of the straight-corner and rounded-corner channels is approximately 30 percent higher than that of the circular turn. However, the overall heat transfer of the entire channels is comparable among the three configurations.

Over past two decades, heat transfer, flow characteristics and pressure drop in 2-pass channel with 180-degree sharp turn have been investigated by both experimental and numerical

methods [9-15]. Other researchers also studied on the different configurations of the channels such as three-pass channels [16, 17] or channels with series of 90-degree turns [18]. The effects of channels aspect ratio on heat transfer had been studied by several researchers [19-21]. In general, channels of high aspect ratio have lower azimuthal heat transfer variations and higher overall heat transfer than low aspect ratio channels, but they have higher friction factor and pressure loss. However, high aspect ratio channels, if positioned properly such as in skin cooling technique, can offer effective cooling and consume less coolant than low aspect ratio channel.

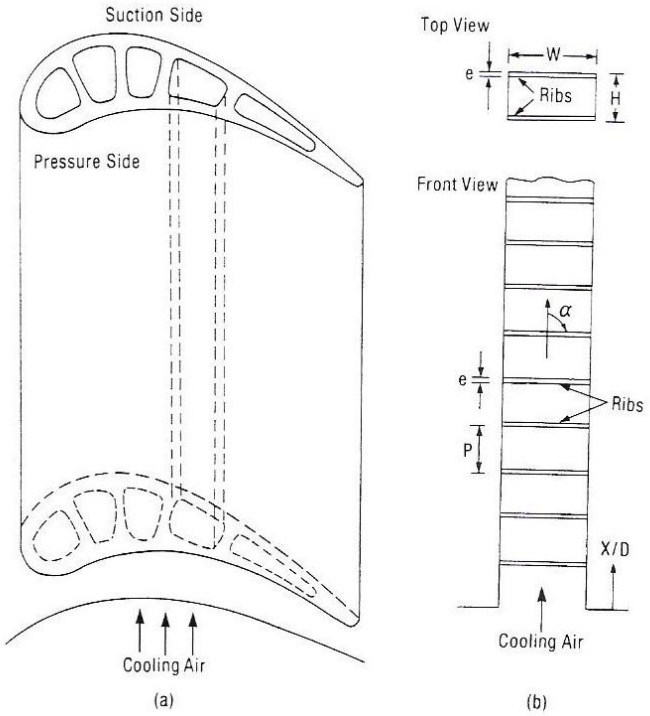

Figure 3 Typical coolant channels in turbine airfoil and internal rib arrangement [25]

In turbine cooling channels, surface features such as ribs, grooves, dimples and pin-fins are always added to promote turbulence flow to enhance heat transfer. Han et al. [19], are one of the first to investigate heat transfer and friction factor of the surfaces with rib turbulators. Since then, several studies [23-32] on various configurations of rib turbulators have been conducted. Figure 3 is an example of turbine airfoil channels with ribs turbulators. Surface ribs can increase

heat transfer rate by several folds comparing to smooth surface channel, but they also create higher pressure loss. To reduce pressure loss, ribs can be placed at an angle to the main flow. They create pressure loss less than ribs that are perpendicular to the flow, while receiving the same heat transfer enhancement level. Han et al. [33], in 1993, had studied heat transfer enhancement of the wedge-shaped and delta-shaped turbulence promoters as shown in Figure 4. Their study shows that the delta-shaped turbulators renders higher heat transfer and lower pressure loss than the wedge-shaped turbulators.

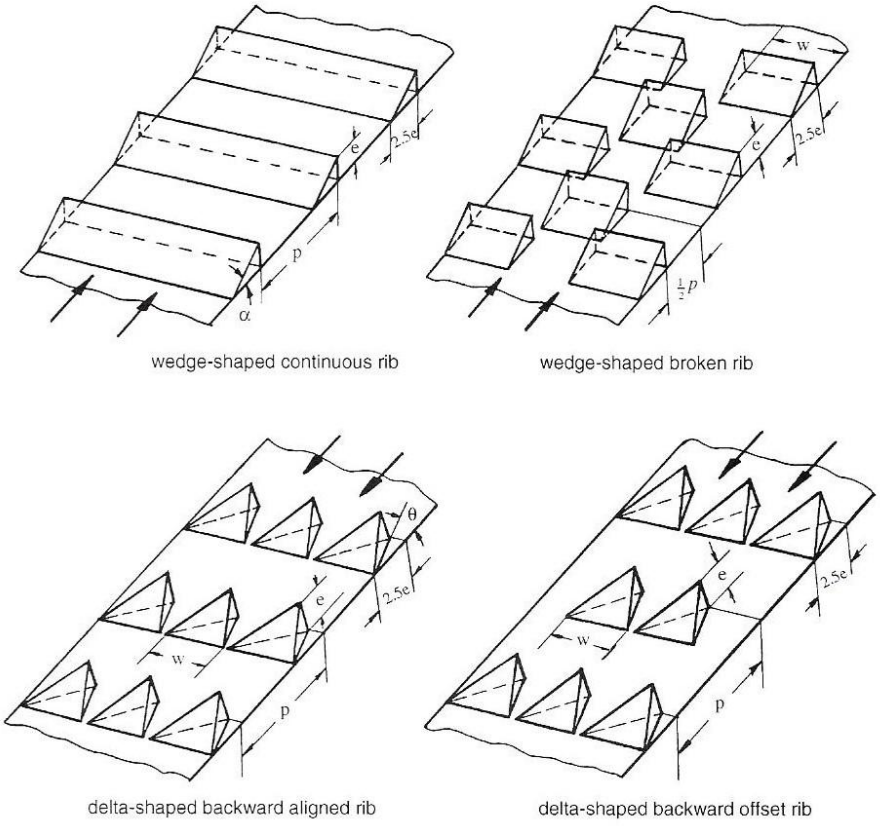

Figure 4 Wedge- and delta-shaped ribs [33]

Pin-fins are round cylindrical elements protruding from endwall surface and oriented in a cylinder-in-cross flow setting. The pins in the flow field induce wakes downstream and generate vortices near the base of the pins, promoting turbulent in the region. Besides the enhanced

turbulence, the pins increase wetted surface area leading to higher heat transfer. Pin-fins in heat transfer applications are normally in array form to cover the areas that need heat transfer enhancement. Heat transfer in long pin-fin arrays (H/D > 10) is dominated by pin-fins' surfaces where as in the short pin-fin arrays (H/D < ½), heat transfer is dominated by endwall effects. Armstrong and Winstanley [34] review heat transfer in staggered pin-fin arrays and found that heat transfer coefficient in intermediate length pin-fin array, usually used in turbine airfoil, cannot be interpolated from short and long pin-fin arrays cases since they have they own characteristics. They also observe that average heat transfer coefficient in short pins is lower than that of the long pins since the short pins have less wetted surface area.

Ames and Dvorak [35] study turbulent transport in staggered pin-fin arrays to better understand the flow characteristic of the pin-fin arrays. They find that the shedding strength, the strong driving force of pins' backside heat transfer, increases significantly with increasing Reynolds number. Furthermore, they observe that there is clear evidence of flow separation in the first two rows and the subsequent rows show very high near-wall turbulence from unsteady separation.

Chyu et al [36, 37] studied two most common pin fin arrays configuration, the inline and staggered arrays as shown in Figure 5. They find that mass (heat) transfer in the immediate region, ahead and alongside, at the base of the each pin is high and not sensitive to array geometry and it is similar to that of the single pin study. In contrary, the heat transfer downstream of the pin is strongly affected by the array pattern. For staggered array, the local maximum and minimum heat transfer exist along the symmetry behind each pin; while the heat transfer between pins in the streamwise direction is low and it increase almost linearly from the area behind the pin to the area ahead of the pin in the next row for the inline array. Pins in both

arrays have 10 to 20 percent higher heat transfer than the endwalls. Their results also suggest that the staggered arrays induce higher heat transfer than the inline arrays. Metzger et al. [38, 39] and Chyu [40] report that while the staggered pin fin arrays post higher heat transfer coefficient, they suffer higher pressure lost.

Pin-fins in actual turbine blades, typically, are not perfect cylinders, due to manufacturing limitation. Chyu [40] and Goldstein et al. [41] study the effect of the pin shape on heat transfer. Chyu [40] studies pin-fins with fillet and reports that they have higher pressure lost and lower heat transfer than the pin-fins without fillet. The effects are much stronger for the staggered array than for the inline array. On the other hand, Goldstein et al. [41] study and compare uniform diameter pin-fins with stepped-diameter pin-fins which have smaller diameter in the center section. They find that the step-diameter pin-fin arrays not only have higher heat transfer coefficient, but also have less pressure drop than the uniform-diameter pin fin array. Furthermore, the effects of pin inclination have been studied by Chyu et al. [42] and they reported that inclination reduces pin array heat transfer and pressure loss significantly.

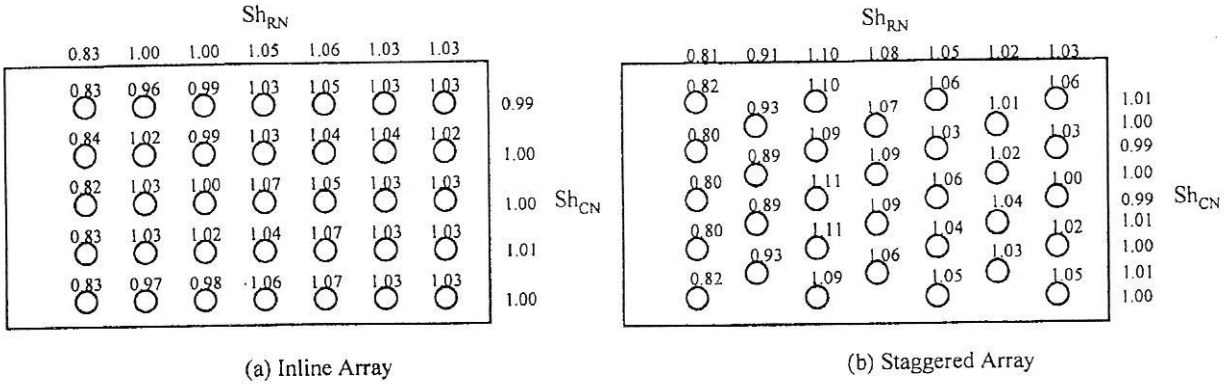

Figure 5 Relative heat transfer coefficient on pin elements, Re = 16,800 [37]

To further explore potential design alternatives for enhancement cooling, researchers have investigated different pin-fin shapes outside cylindrical domain. For example, Chyu et al.

[43, 44] study the effect of the cube- and diamond- shaped pins in different array arrangements, shown in Figure 6. They found that the diamond-shaped pin array has the highest heat transfer coefficient and the cylindrical pin array has the lowest heat transfer rate among the three shapes considered. On the contrary, when consider the performance factor which includes pressure lost into account, the diamond-shaped pin array has the lowest performance factor since it suffer from highest pressure lost among all three configurations. The cylindrical pin array achieve highest performance factor.

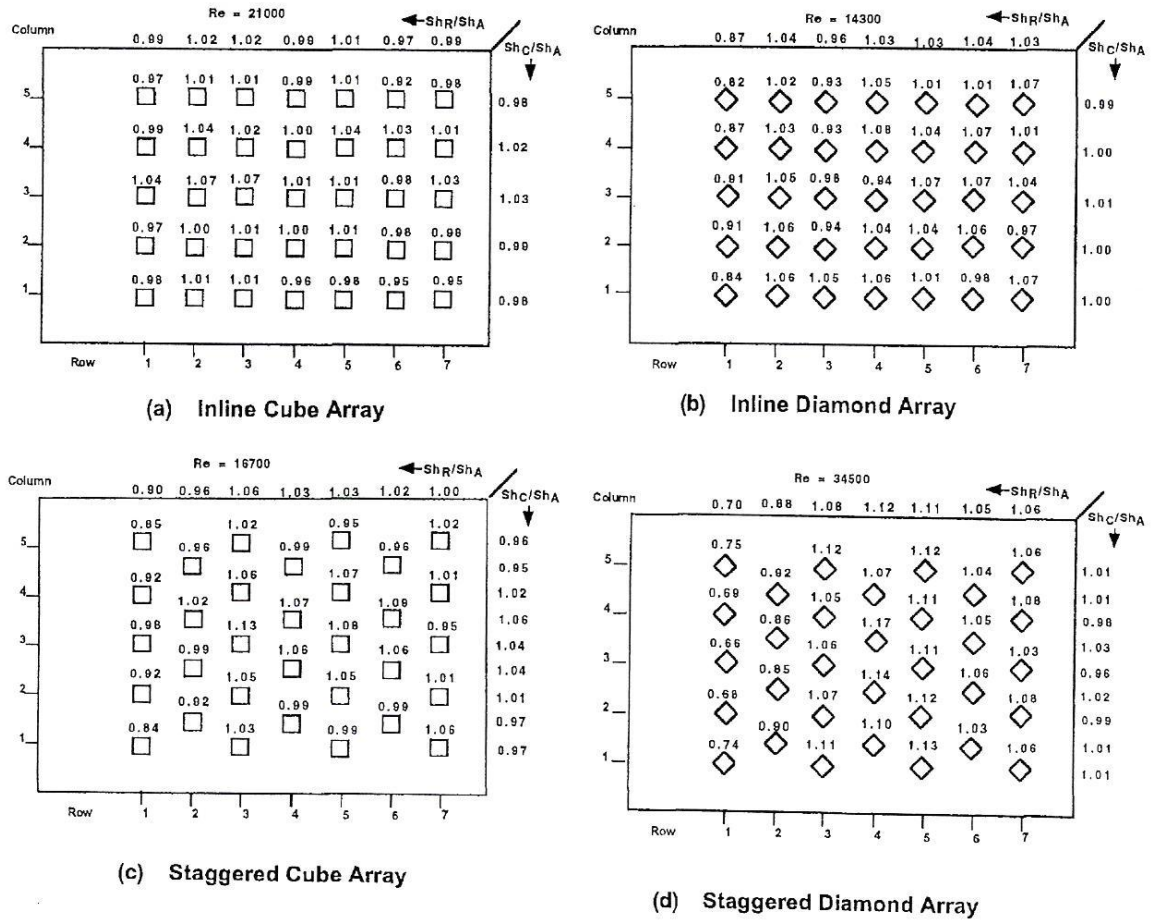

Figure 6 Relative pin-resolved heat (mass) transfer within an array [43]

1.3 PRESENT WORK STATEMENT

While significant level of studies have been focused on either surface enhancement, such as vortex generators/turbulators, or turn effects, virtually no study in the open literature has been directed to the combined effects of sharp turn in the high aspect ratio channel and surface-feature induced heat transfer enhancement. The objective of this study is to investigate the combined effects of the turn and the vortex generators induced turbulence and heat transfer enhancement.

The research in this present dissertation is emphasized on the experimental study of the 2-pass channel, which is a channel with one 180-degree sharp turn. Different shape pins are added to the surface of the channel to promote higher turbulence flow. All the vortex generator elements are made of aluminum which have high thermal conductivity to ensure very small Biot number so that each element can be consider as a lump unit with uniform temperature. The vortex generators included in this study are delta-wing-shaped, cylinder-shaped, cube-shaped and diamond-shaped elements. The heat transfer results of both endwalls (top and bottom), necessary for double-walled/skin cooling approach, are analyzed and then compared among all the different configurations and previous studies.

2.0 HEAT TRANSFER MEASUREMENT

In order to evaluate cooling performance, heat transfer rate has to be measured. In this chapter, the method for heat transfer measurement, as well as the heat transfer theory is described in detail.

2.1 TRANSIENT LIQUID CRYSTAL METHOD

Transient liquid crystal technique is a useful and effective technique which becomes one of the standard techniques for determining heat transfer coefficient, h, in the heat transfer community. By using *thermochromic liquid crystal (TLC)* thermography, one can obtain required parameters for calculating heat transfer coefficient. Several researchers [31, 44-51] have used this technique to find the local heat transfer distribution. In this research, it also has been utilized to find the local heat transfer in the channel. When subject to heat in specific temperature range (bandwidth), the liquid crystal colors change from red to green and then blue as shown in Figure 7. Outside the specific temperature range, the liquid crystal is colorless. The starting temperature and temperature range can be custom made to order by the user.

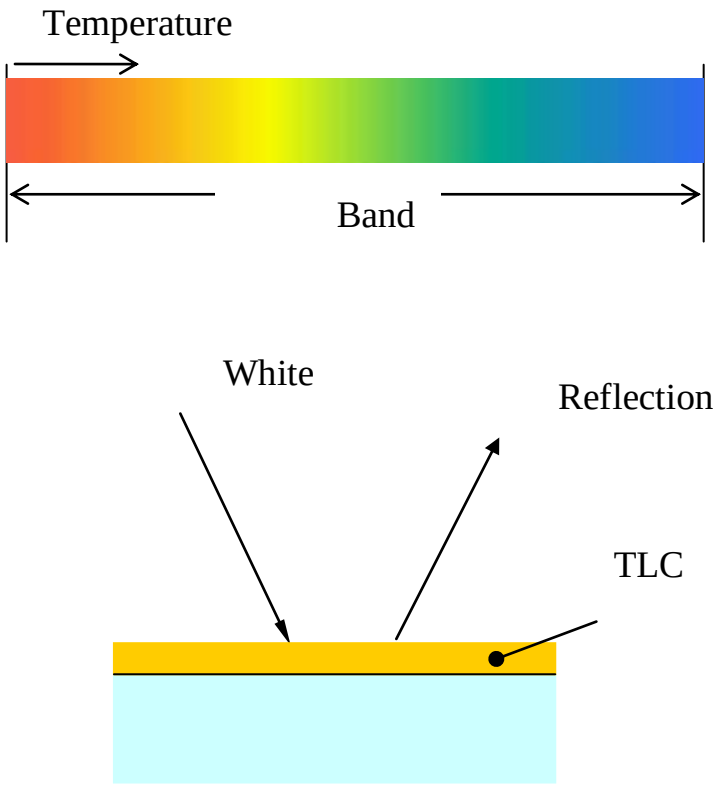

Figure 7 Thermochromic liquid crystal (TLC) temperature range (bandwidth)

Figure 8 shows the color property of the liquid crystal being used in this research. The liquid crystal has peak color intensity when it displays green shade and the green intensity also gives the best contrast and signal/noise ratio among all the reflecting colors. In this case the highest intensity occurs at 38.2 degree Celsius. During the experiment, the digital video capturing device records the color changing process of the liquid crystal. With liquid crystal imaging analyzer program, the user knows exactly when the maximum intensity occurs. The program analyzes each pixel's intensity in every frame of the video recorded during the experiment. The result shows the time of which the certain pixel has highest intensity.

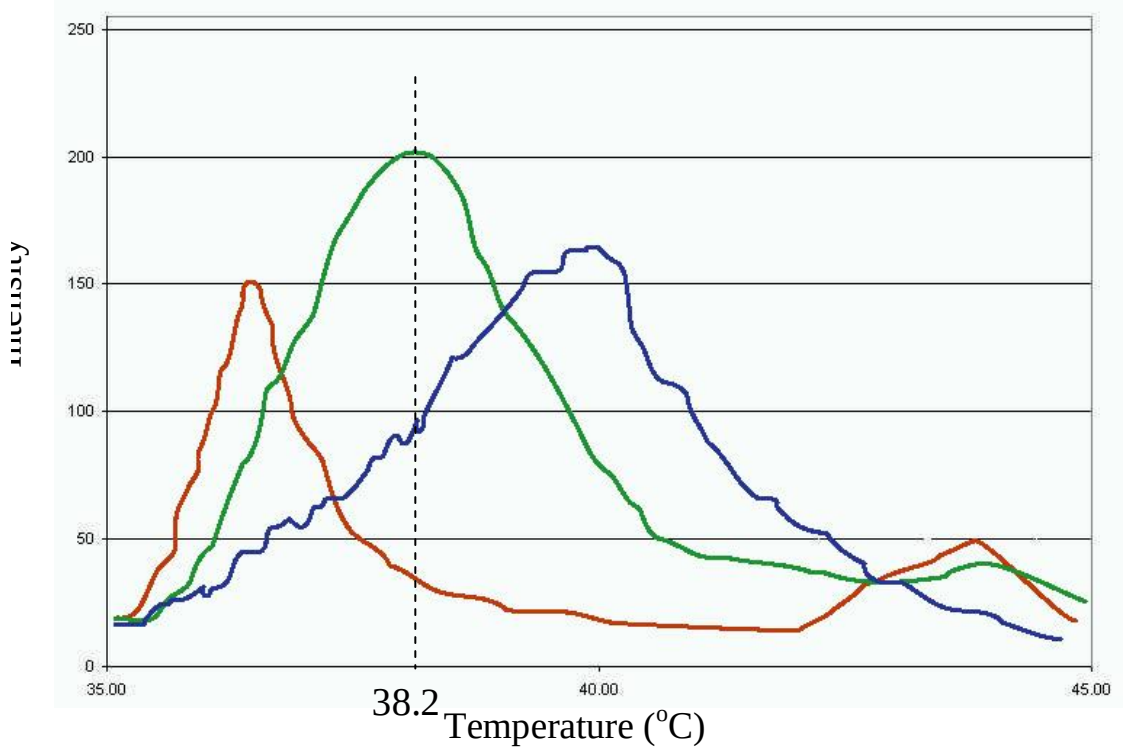

Figure 8 Liquid crystal color intensity vs. temperature

One of the key features for using transient liquid crystal technique in the transient mode is assuming that the heat transfer through the housing wall or substrate is one dimensional, shown in Figure 9. The local heat transfer coefficient can be determined under this assumption. The assumption is reasonable only when the test duration is sufficiently short and the depth of heat penetration is shallower than the wall thickness. If this is the case, the one-dimensional transient heat conduction equation can be represent as

$$k\frac{\partial^2 T}{\partial z^2} = \rho C_p \frac{\partial T}{\partial t} \tag{2}$$

The boundary and initial conditions are

$$-k\left.\frac{\partial T}{\partial z}\right|_{z=0} = h(T_w - T_r) \tag{3}$$

$$T\big|_{z=\infty} = T_i \tag{4}$$

$$T\big|_{t=0} = T_i \tag{5}$$

where T_i is initial temperature of the channel wall, T_w is the local surface temperature of the channel wall and T_r is the flow reference temperature.

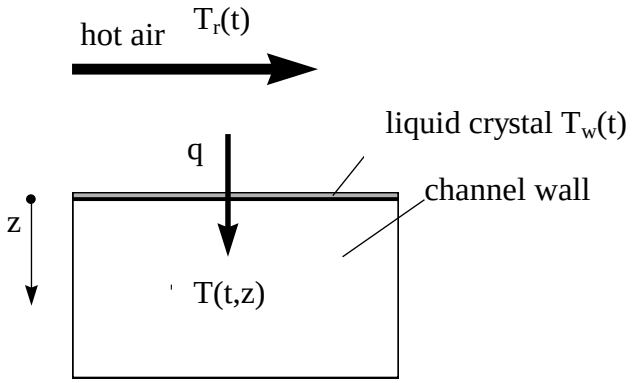

Figure 9 One-dimensional heat transfer over solid surface

From the equations (2)-(5), wall temperature T_w can be express as

$$\frac{T_w - T_i}{T_r - T_i} = 1 - \exp\left[\frac{h^2 \alpha t}{k^2}\right] erfc\left[\frac{h\sqrt{\alpha t}}{k}\right] \tag{6}$$

where

$$\alpha = \frac{k}{\rho C_p} \tag{7}$$

In classical heat convection problems, the reference temperature, T_r, is readily available, i.e. equal to the temperature of the mainstream or bulk flow. Liquid crystal imaging can provide a relationship between T_w and t over the entire capturing domain, the local heat transfer coefficient, h, can be solved from the above equation.

While the one-dimensional approach mentioned above is generally valid for channel wall, it is largely invalid for the turbulator elements that are small in size and made of metal. To obtain the heat transfer coefficient of a turbulator, lump capacitance method has been used under the assumption that the element has uniform temperature (small Biot number) at all times. The governing equation for lumped heat capacity model can be described as

$$hA(T - T_r) = -mC_p \frac{dT}{dt} \tag{8}$$

and the initial condition is

$$T\big|_{t=0} = T_i \tag{9}$$

From above equation, analytic solution can be obtained as

$$\frac{T - T_i}{T_r - T_i} = 1 - \exp\left[-\frac{hAt}{mC_p} \right] \tag{10}$$

The acquired heat transfer coefficient can be transformed into dimensionless term which is known as Nusselt number and its definition is

$$Nu = \frac{hD_h}{k} \tag{11}$$

The resulted Nusselt number could be normalized by the fully developed value of the turbulent flow in smooth duct without turn which widely known as the Dittus-Boelter equation [52];

$$Nu_0 = 0.023\,\mathrm{Re}^{0.8}\,\mathrm{Pr}^{0.4} \tag{12}$$

On the pressure loss, the dimensionless friction factor of the channel can be calculated from

$$f_{ave} = \frac{\Delta p}{(\frac{L}{D_h})\left(\frac{\rho U^2}{2}\right)} \tag{13}$$

where Δp is the pressure drop across the channel, L is the length of the channel and U is the velocity of the flow and D_h is hydraulic diameter. The friction factor above can be normalized by the approximation friction factor of the smooth channel without turn [53], i.e.

$$\begin{aligned} f_0 &= 0.316\,\mathrm{Re}^{-0.25} \qquad \mathrm{Re} \le 2\times10^4 \\ f_0 &= 0.184\,\mathrm{Re}^{-0.20} \qquad \mathrm{Re} \ge 2\times10^4 \end{aligned} \tag{14}$$

To compare the cooling performance of different channels, one must have reference definition. According to the analysis by Gee and Webb [54, 55] presented the definition of overall cooling performance factor can be expressed as

$$f_{PF} = \frac{f_N}{f_F^{1/3}} = \frac{Nu_{ave}/Nu_0}{(f_{ave}/f_0)^{1/3}} \tag{15}$$

3.0 EXPERIMENT SETUP AND APPARATUS

While significant level of studies have been focused on either surface enhancement, such as turbulators/vortex generators, or turn effects, virtually no study in the open literature has been directed to the combined effects of sharp turn and surface-feature induced heat transfer enhancement. In this study, a series of experiments were performed to investigate the heat transfer and pressure characteristics in a high aspect ratio, (4.5:1 width-to-height), two-pass channel, with delta-wing-shaped, cube-shaped and diamond-shaped element arrays placed in both channel passes before and after a 180-degree sharp turn.

3.1 OVERALL TEST SETUP

Figure 10 is the schematic of the experiment set up. A laboratory compressed air tank provides the main flow. The air in the tank is kept constant by building main air supply line at around 620 kPa (90 psi). To begin the experiment, air is released from the compressed air tank. The flow rate, measured by standard ASME orifice, is adjustable by ball valve before the orifice. After passing through the orifice, the flow goes through an inline 2000 W heater controlled by a variable voltage controller. The temperature of flow for the present study is set at 80°C. While the flow warm is warming up, it is diverted away from the test section. When the flow reaches the desired steady temperature, the ball valve is turned to direct the flow to the test section.

Meanwhile, the CCD digital camcorder is recording the color changing video image of the surface and the data acquisition equipment is recording the temperature of the mainstream flow. After the digital video file and the temperature data history have been combined and analyzed with *Liquid Crystal Imaging Analyzer (LCIA)* software, the local heat transfer coefficient is obtained. Figure 11 shows the experiment setup in the laboratory with test section already attached.

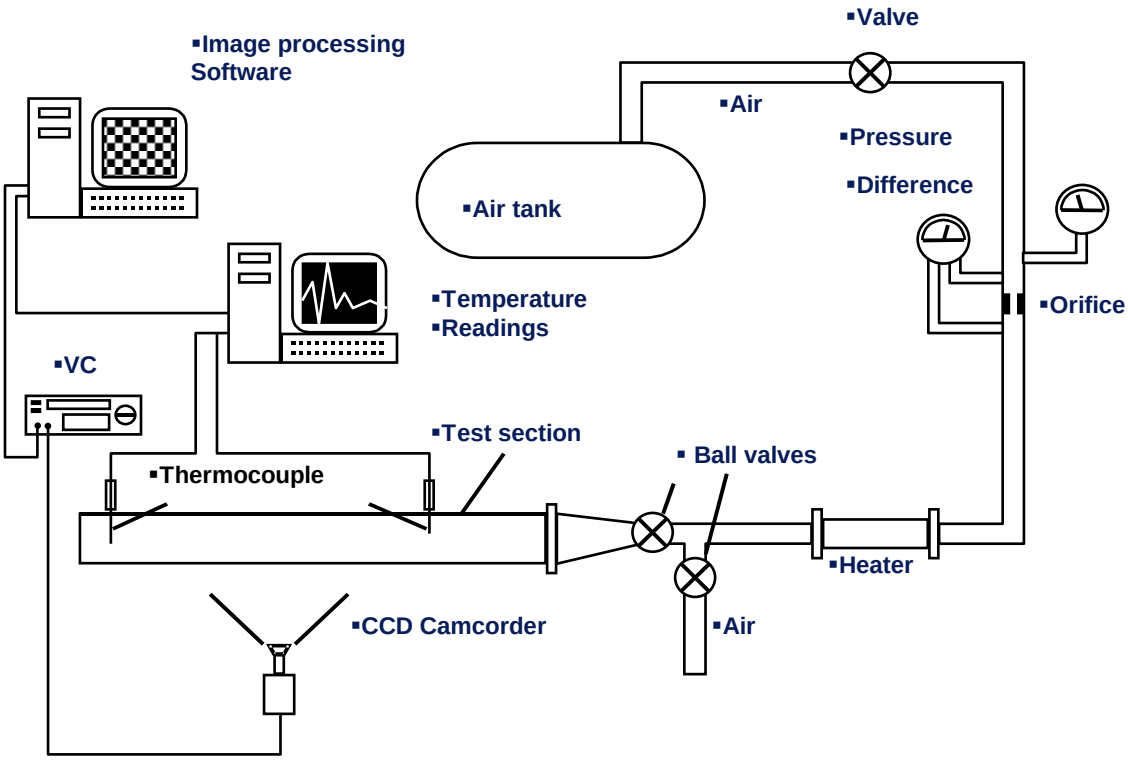

Figure 10 Experiment setup diagram

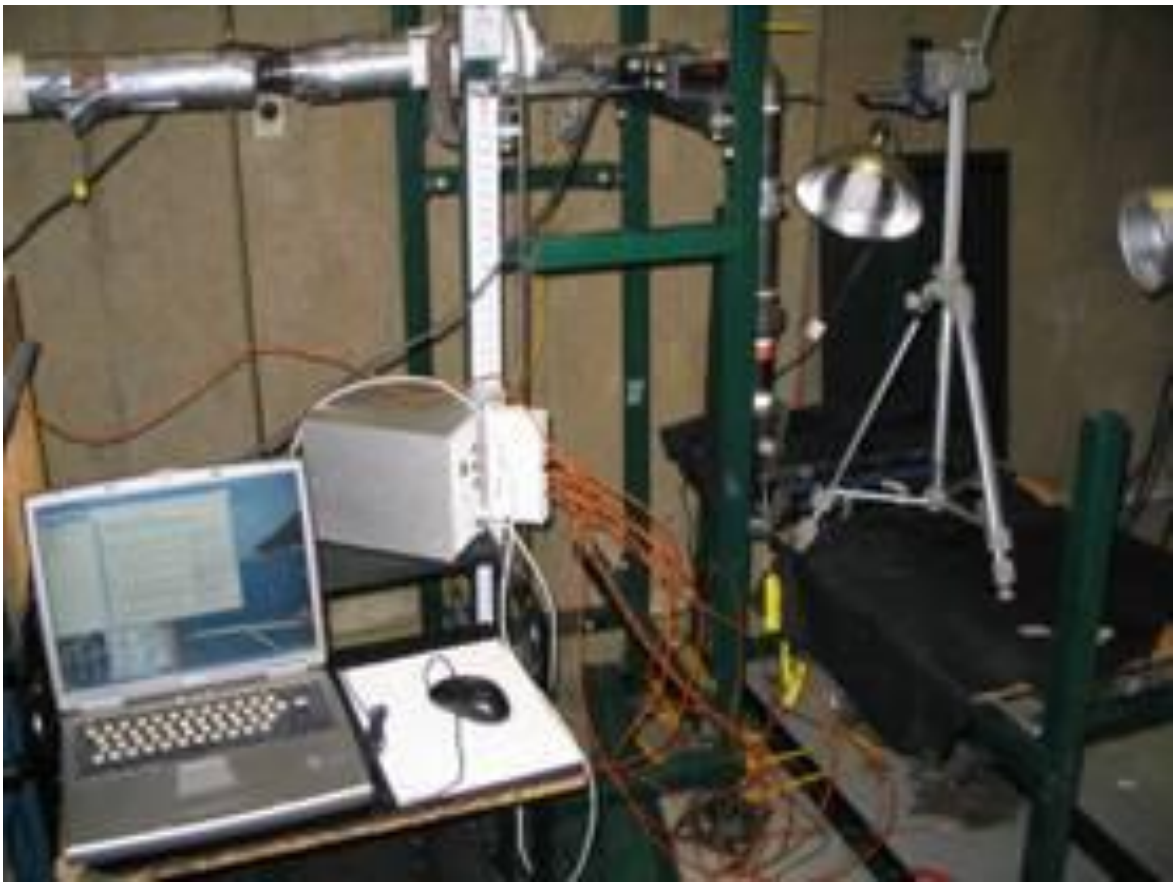

Figure 11 Experiment setup

3.2 TEST SURFACE PREPARATION

The surface of the test section has to be cleaned after the machining process and left to dry completely. Next, it is coated with a thin uniform layer of black paint to help increasing color contrast of reflecting light from liquid crystal. Then, a thin uniform layer of liquid crystal is sprayed on top. The most effective applying method is to use hobby paint sprayer to apply both the black paint and the liquid crystal on the surface. When the liquid crystal dries, the top

part of the test section, which is a flat plexiglass plate is secured on to the bottom part with machine screws. The test section is then connected to the experiment setup and left for a few hours to ensure that the test section's temperature stabilizes with the surrounding environment before starting the test.

3.3 EXPERIMENT PROCEDURE

Temperature readings from the thermocouples at the inlet and along the test section are recorded by a data acquisition system from National Instruments. Before starting the test, the digital camcorder is set to view appropriate image domain. The lighting has to be adjusted to light up the test section and not create the shadow that is hindering the post processing analyzation.

First, the ball valve is set at the position to divert the flow away from test section. The air is release from the air tank to the desire flow rate. Then the heater is turned on to heat the flow to the set temperature at 80 °C. When the flow's temperature reaches the required temperature, the ball valve is turn to suddenly divert the flow to the test section. Simultaneously, the camcorder records the video image and the data acquisition system records the thermocouple readings. The test usually lasts approximately 2-4 minutes. A test ends when the liquid crystal through out the surface turns into blue color. When the test ends, the flow is diverted away from the test section and the heater is turned off. The flow is not shut down until the system is cool down to the safe level. All the data are saved for post processing by the in-house LCIA software. Each test takes about 1 hour to run. Before starting the next test, the test section is left for at least 4 hours to cool down to the room temperature.

4.0 HEAT TRANSFER ENHANCEMENT EXPERIMENT

4.1 2-PASS SMOOTH CHANNEL

Figure 12a shows the bottom part of the 2-pass smooth channel test section made of 12.7 mm (0.5") thick plexiglass. The channel height (H), width (D) and Length are 12.7 mm (0.5"), 57.2 mm (2.25") and 381 mm (15.0") respectively. The wall and the center partition are made of 12.7 mm (0.5") square strips of plexiglass. They are glued to the flat plexiglass plate to form the bottom part of the test section as shown. The channel is formed by securing top plexiglass plate to the bottom section using machine screws. When connecting the channel to the test system, the flow is directed into the channel as shown in Figure 12b.

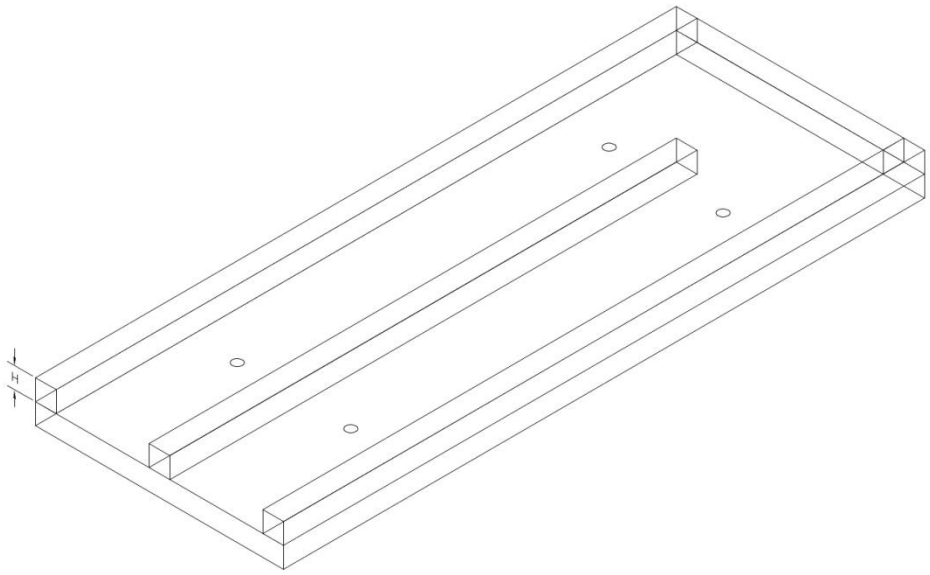

(a)

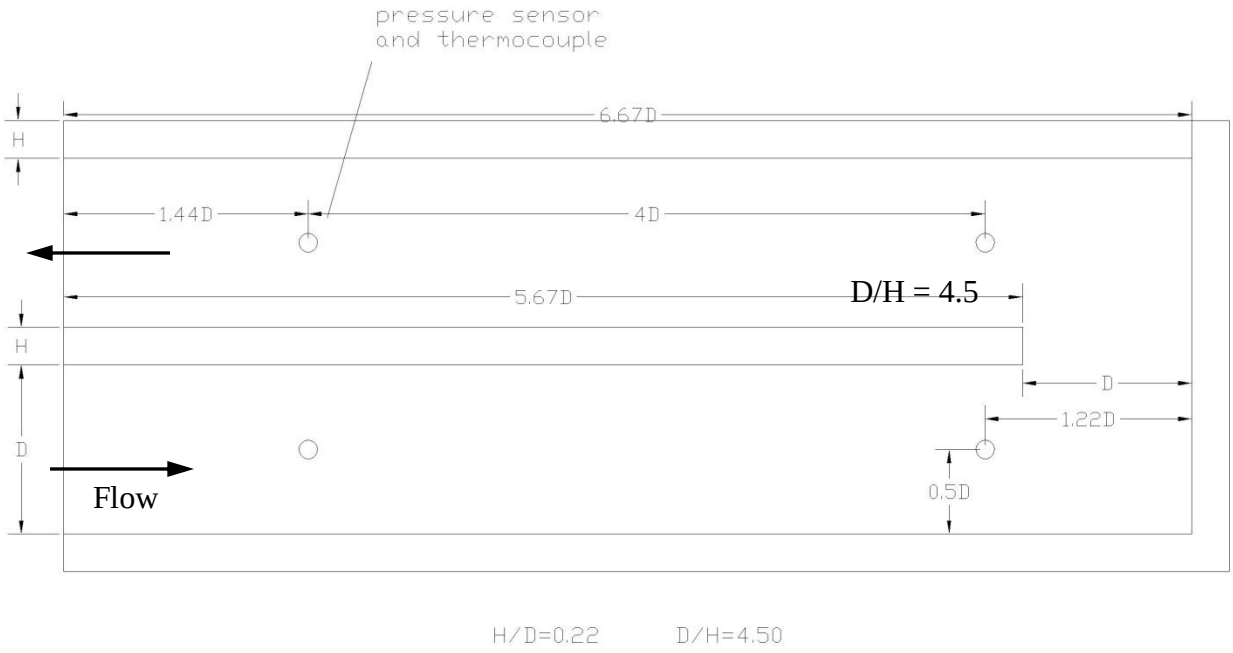

(b)

Figure 12 2-pass smooth channel test section

4.1.1 Result and discussion

The heat transfer result of the smooth channel with 180-degree turn is as expected. As shown in Table 1, h_0 is the coefficient value of the fully developed turbulent flow in smooth channel without turn. The average heat transfer in the second pass of the channel is much higher as a result of the sharp turn effect. The sharp turn induced strong secondary flow and turbulence in the second pass; thus the heat transfer in the second pass is approximately 60% higher than that of the first pass over the range of 13000-32000 Reynolds number. Figure 15 shows the local heat transfer coefficient in the 2-pass channel with the Reynolds number of 13000, 20000, 28000 and 32000 respectively. The results show similar heat transfer distribution trend as the study by Wang and Chyu [8]. The other significant feature observed in Figure 13 is that the heat

transfer coefficient is rather low at the turn corners and at the tip of the partition wall. This phenomenon occurs mainly due to the nature of flow and geometry (sharp corner) of the test section that create a recirculation zone at those particular regions.

Figure 14 reviews that the peak column average Nu/Nu_0 in the second pass increases significantly with increasing Reynolds number while the overall average Nu/Nu_0 does not increase as much. This result suggests that the Reynolds number has strong influent on heat transfer at the area where the flow impacts the channel wall downstream of the turn.

Table 1: Average heat transfer coefficient in the 2-pass smooth channel

Re_{Dh}	Heat transfer coefficient (W/m^2-K)			
	h_0	h_{1st}	h_{2nd}	h total ave
13000	54.2	66.4	99.8	83.2
20000	76.5	93.4	137.0	115.2
28000	100.1	109.1	180.2	144.7
32000	111.4	126.9	215.2	171.0

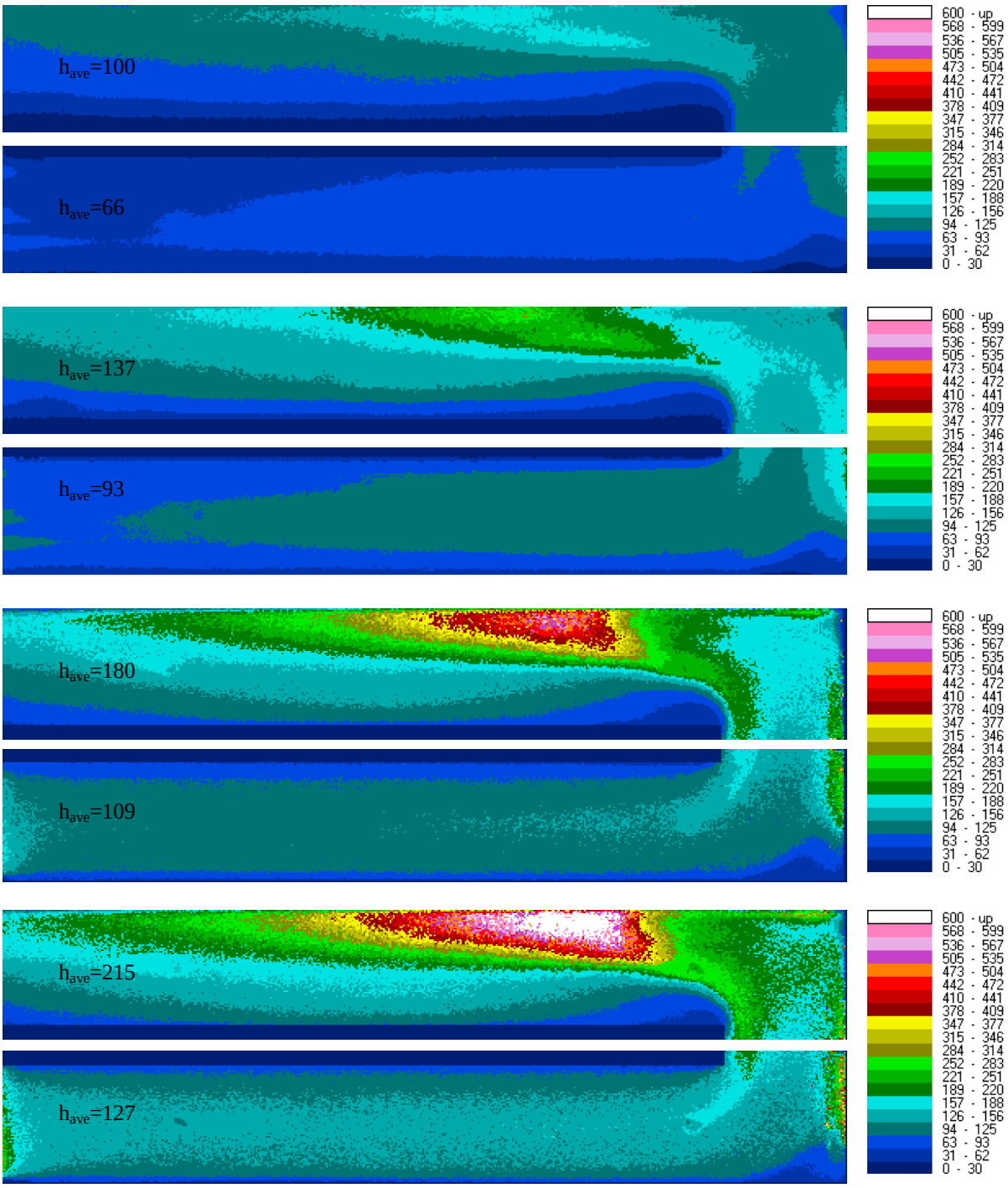

Figure 13 Local heat transfer coefficient of 2-pass channel with Reynolds number of 13000, 20000, 28000 and 32000 respectively

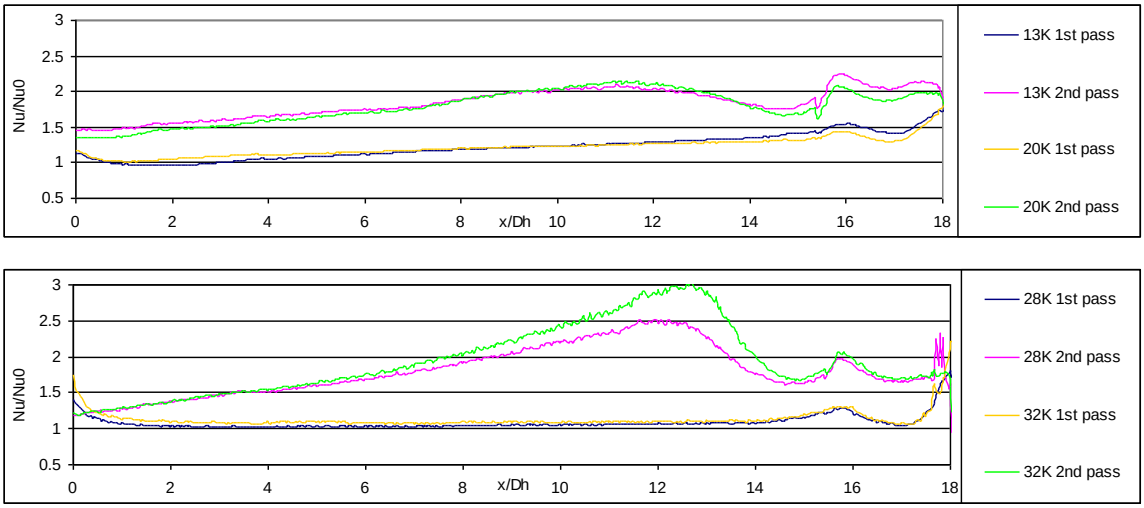

Figure 14 Column average Nu/Nu_0 of 2-pass channel with Reynolds number of 13000, 20000, 28000 and 32000 respectively

4.2 3-PASS SMOOTH CHANNEL

The experimental study of the 3-pass smooth channel is conducted to compare the result with the 2-pass smooth channel. The tested channel has the same geometry as in the 2-pass channel with the addition of one 180-degree sharp turn as shown in Figure 15.

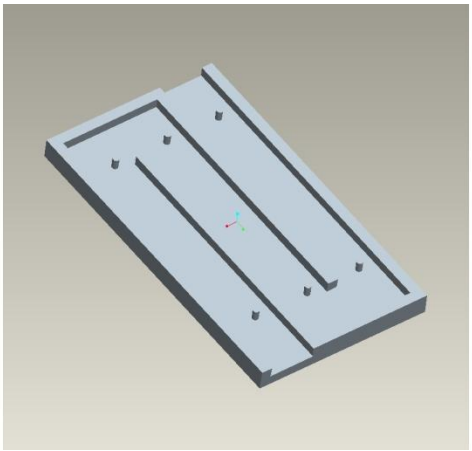

Figure 15 3-pass channel

4.2.1 Result and discussion

The heat transfer coefficient of 3-pass smooth channel is shown in Figure 16-Figure 17. The overall average heat transfer coefficient of the 3-pass smooth channel is approximately 23% higher than that of the 2-pass smooth channel. The first passes of both channels have comparable flow characteristic and heat transfer. For the second pass of the 3-pass channel, it has the highest heat transfer among the three passes and its heat transfer is approximately 1.3 folds of that of the 2-pass channel. The flow in the third pass is affected by the sharp turn similar to the flow in the second pass. Heat transfer in the third pass is lower than that of the second pass but still considerably higher than that of the first pass. The sharp turn geometry creates recirculation zones at the corners and partition wall tips in the 3-pass channel similar to that of the 2-pass channel. These results suggest that the flow characteristic of the last passes, i.e. second pass in 2-pass channel and third pass in 3-pass channel, of the channels with 180-degree sharp turn are similar.

Table 2: Average heat transfer coefficient in the 3-pass smooth channel

Re_{Dh}	Heat transfer coefficient (W/m^2-K)			
	h_{1st}	h_{2nd}	h_{3rd}	h total ave
13000	67.6	129.7	118.0	105.1
20000	90.9	173.3	151.3	138.5
28000	116.0	216.1	193.6	175.2

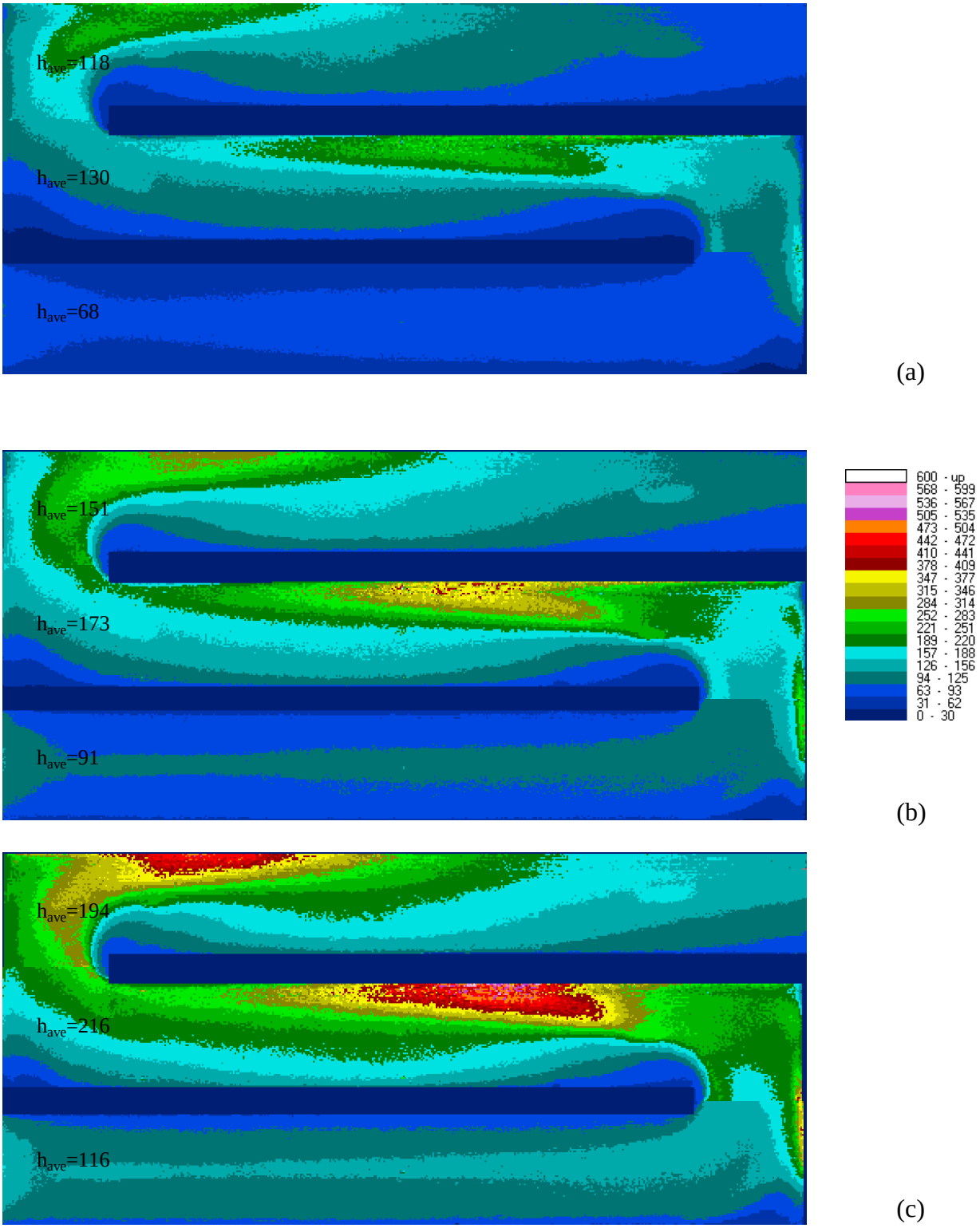

Figure 16 Local heat transfer coefficient of 3-pass channels at 3 different Reynolds number;

(a) 13000, (b) 20000, (c) 28000

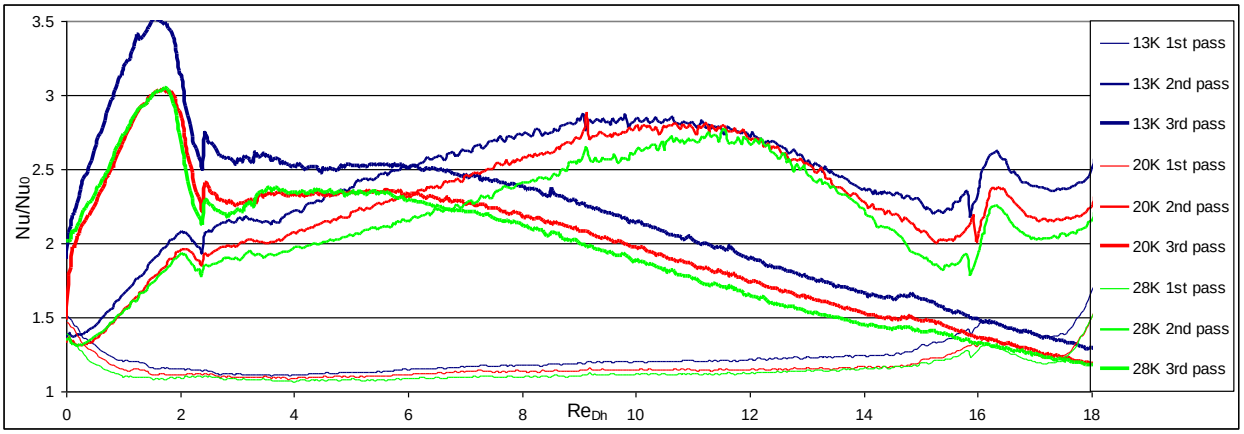

Figure 17 Column average Nu/Nu_0 of 3-pass channel at Re_{Dh}=13000, 20000 and 28,000

4.3 2-PASS CHANNEL WITH SPARSE DELTA WING ARRAYS

An array of delta-wing-shaped vortex generators is added into both passes of the channel following the experiment with the smooth channel. The delta wing elements are made of aluminum which have high thermal conductivity to ensure very small Biot number so that each element can be consider as a lump unit with uniform temperature. The dimension of the delta wing is 12.7x12.7x6.4 mm (0.5"x0.5"x0.25") in length, width and height. The pitch, P, of the delta wings array is 101.6mm (4.0"). Figure 18 show the sparse array configuration of the turbulators within the channel. The delta wing vortex generators in this study are different from the delta-shaped elements studied by the Han et al. [33]. One of the advantages of the present delta wing elements is that not only they create vortices but they also direct part of the flow to enhance heat transfer at the top endwall.

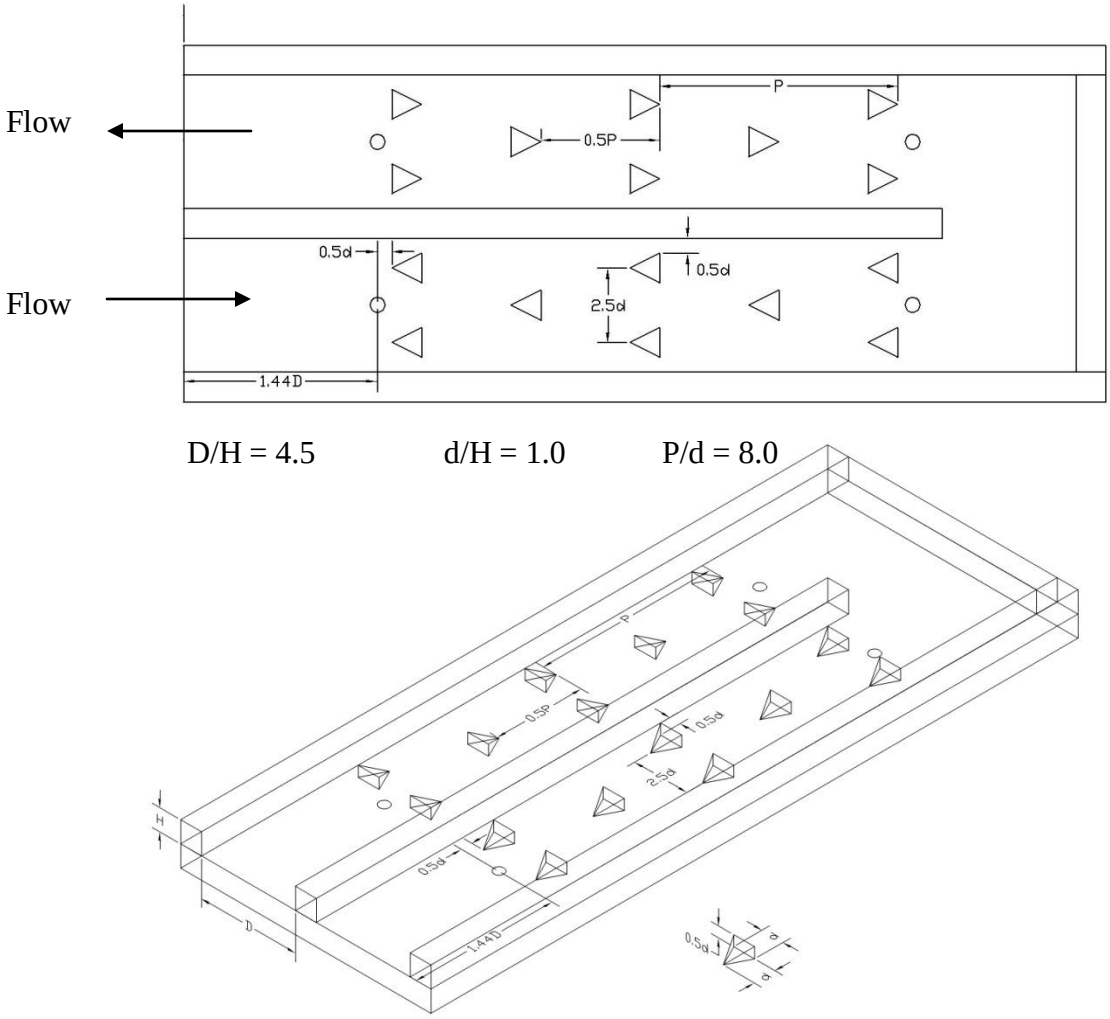

Figure 18 2-pass channel with sparse delta wing arrays configuration

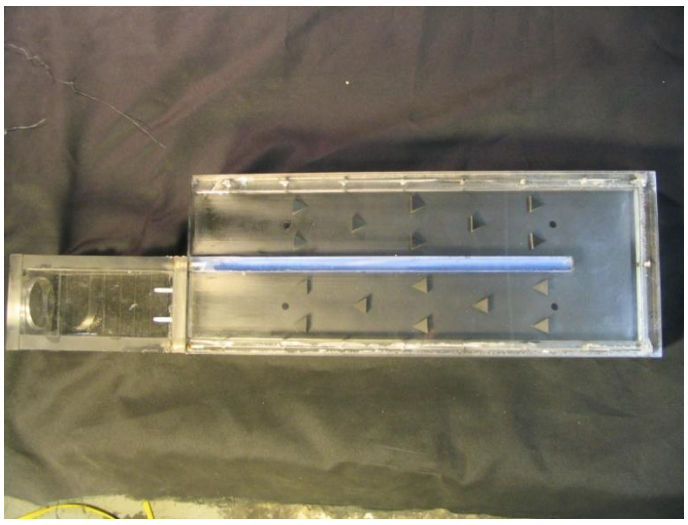

Figure 19 Test section with sparse delta wing arrays

4.3.1 Result and discussion

The flow characteristic and heat transfer change significantly with the delta wing vortex generators placed on the channel surface. The overall heat transfer enhancement is approximately 1.2 fold, relative to the smooth channel counterpart. Figure 20-Figure 23 show the local heat transfer and column average Nu/Nu_0 of the sparse array delta wings at Reynolds number of 13k, 20k, 28k and 32 k respectively.

Figure 22-Figure 25 reveal that the flow is obviously more turbulent in the first pass, resulting in up to 1.6 fold heat transfer enhancement, compared to the smooth channel. While the gain in the second pass is only up to 1.1 fold, the local heat transfer distributes more evenly over the surface and the recirculation zone at the inner of the turn is smaller. The different of the average heat transfer between first pass and second pass also reduces to about 12%, where as the heat transfer of the second pass is still higher.

While the delta wings enhance heat transfer at the bottom endwall, they also direct part of the flow to enhance heat transfer at the top endwall. Even though, the bottom endwall heat transfer coefficient is approximately 11% higher than that of the top endwall, they are considered to be comparable.

According to Table 3, the turbulators account for approximately 9% of heat transfer in both the first and the second passes. The turbulators obviously change the flow and heat transfer characteristic significantly. They distribute the flow more evenly over the entire channel and create more turbulent; thus the heat transfer is higher and distributes more evenly on the endwall surfaces, comparing to the smooth channel.

Table 3: Average heat transfer coefficient of 2-pass channel with sparse delta-wing arrays

Re_d	Heat transfer coefficient (W/m^2-K)					
	h_0	h_{1st}	h_{2nd}	h total ave	1st pass pins(%)	2nd pass pins(%)
13000	54.2	97.4	113.9	105.7	11.8	11.6
20000	76.5	135.2	154.4	144.8	9.4	10.0
28000	100.1	176.2	193.0	184.5	7.3	8.0
32000	111.4	192.4	207.6	200.0	7.0	7.8

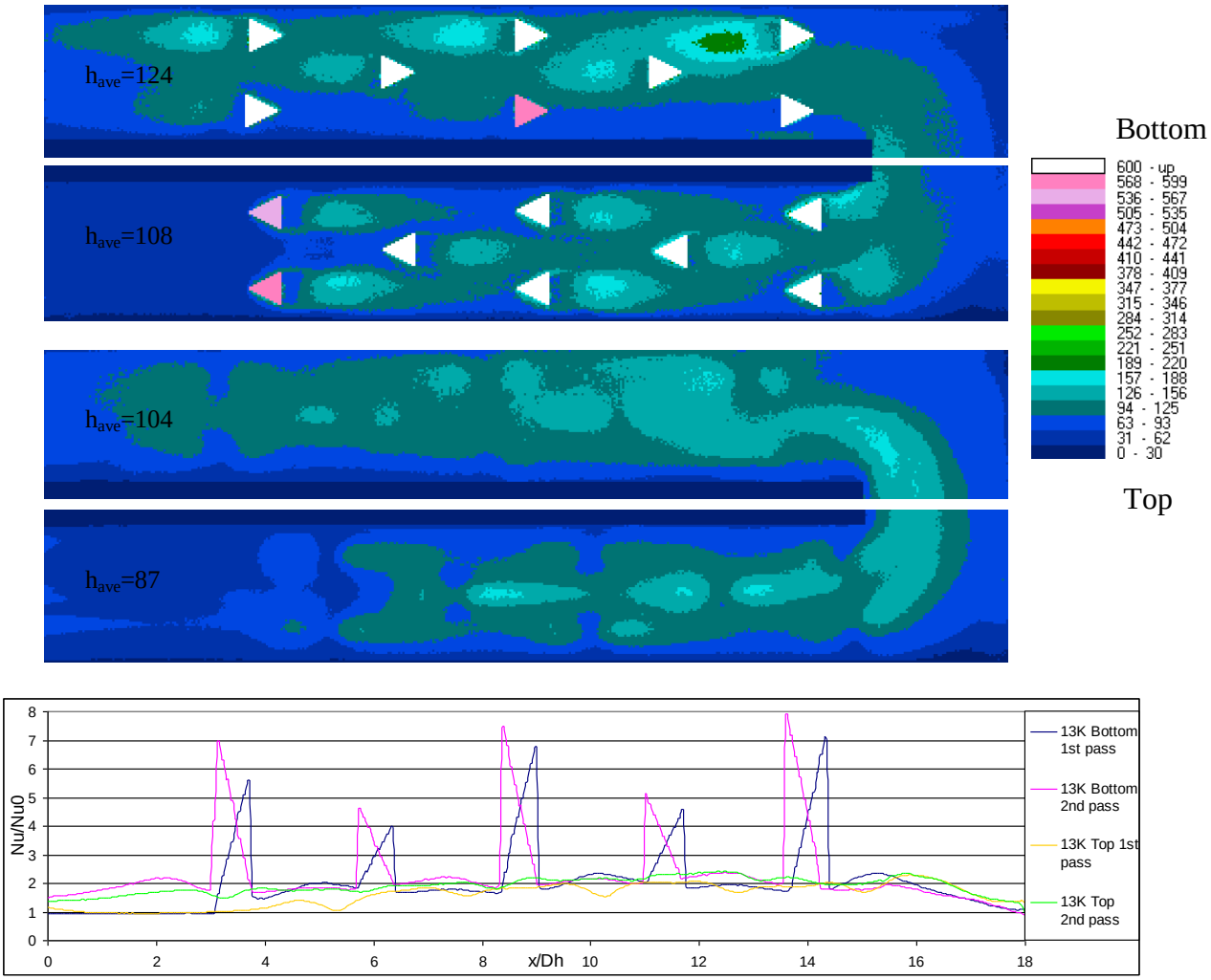

Figure 20 Local heat transfer coefficient and column average Nu/Nu_0 of 2-pass channel with sparse array delta wings configuration at Re_{Dh}=13000

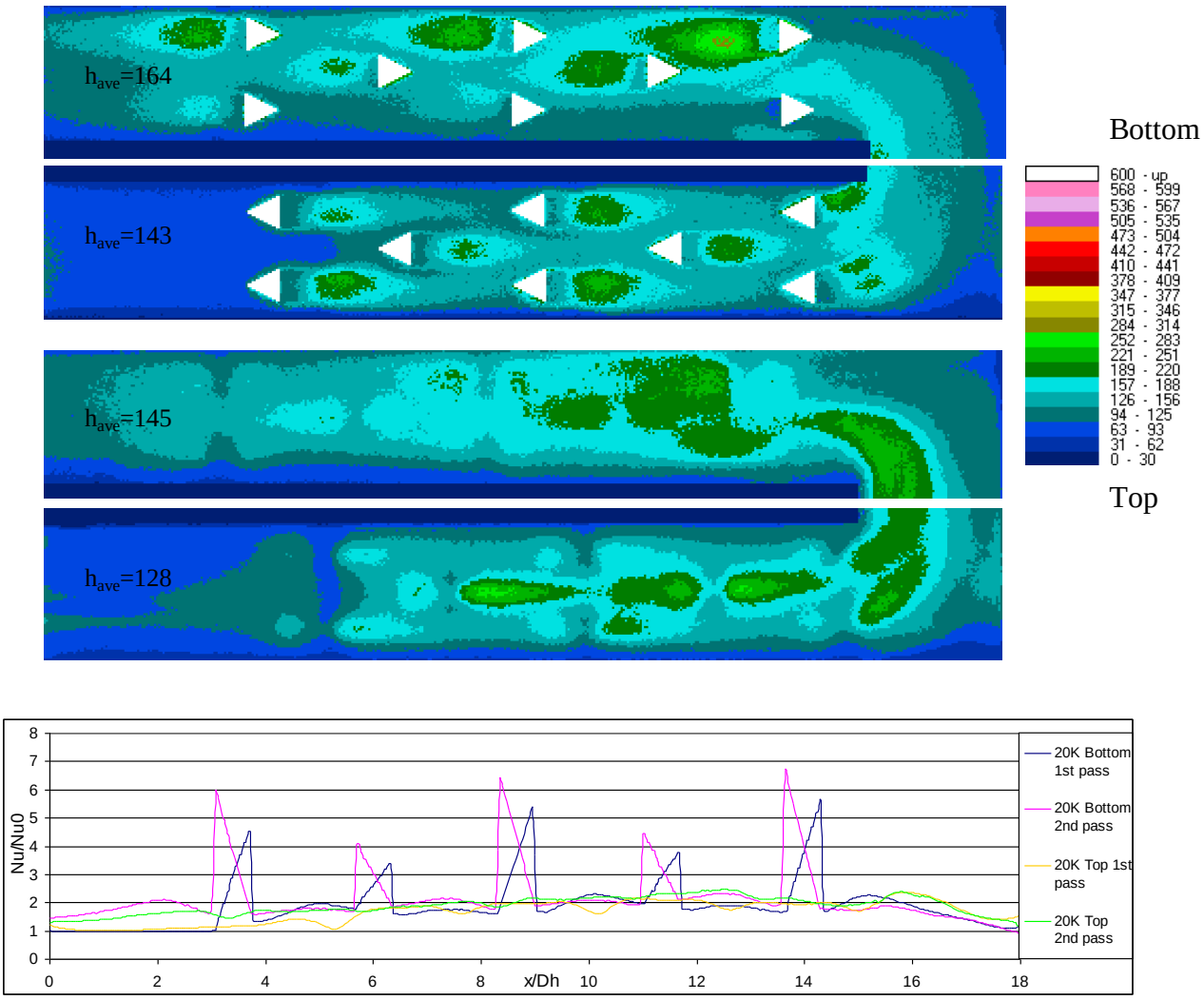

Figure 21 Local heat transfer coefficient and column average Nu/Nu_0 of 2-pass channel with sparse array delta wings configuration at Re_{Dh}=20000

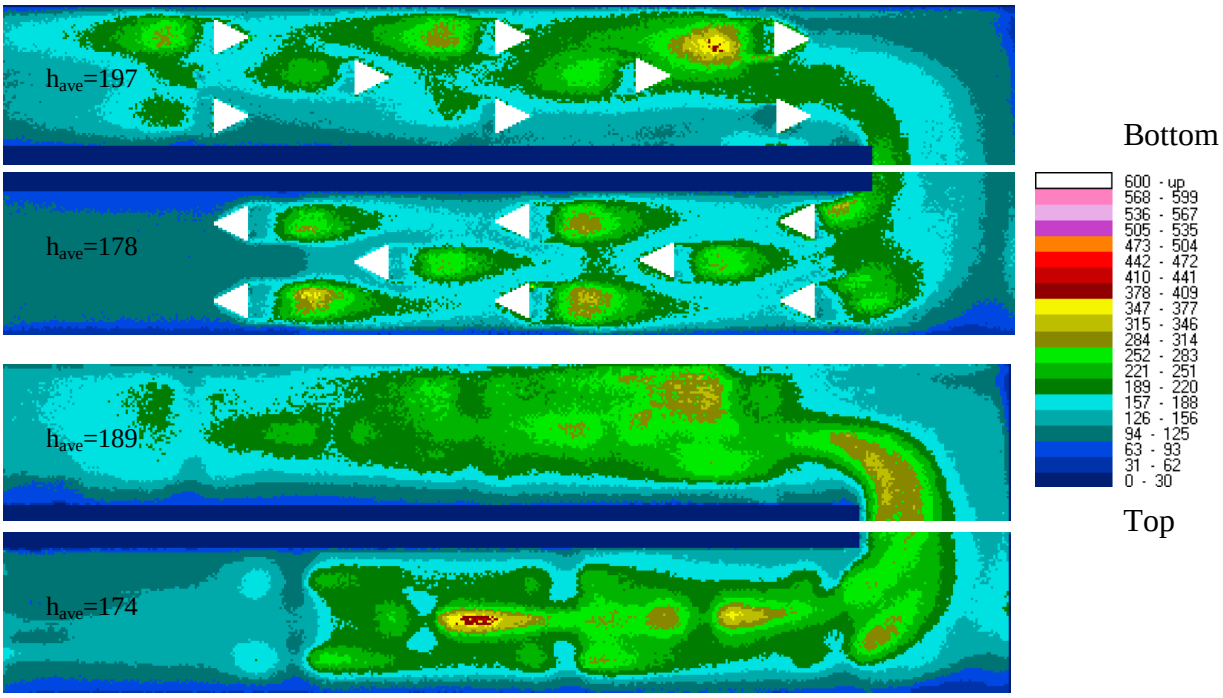

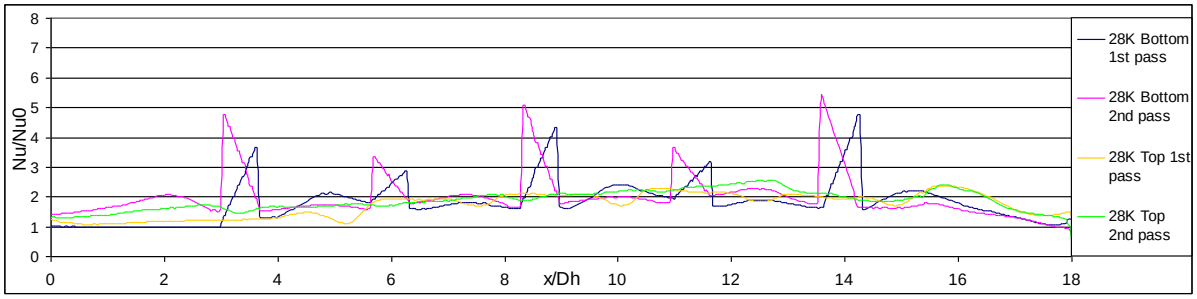

Figure 22 Local heat transfer coefficient and column average Nu/Nu_0 of 2-pass channel with sparse array delta wings configuration at Re_{Dh}=28000

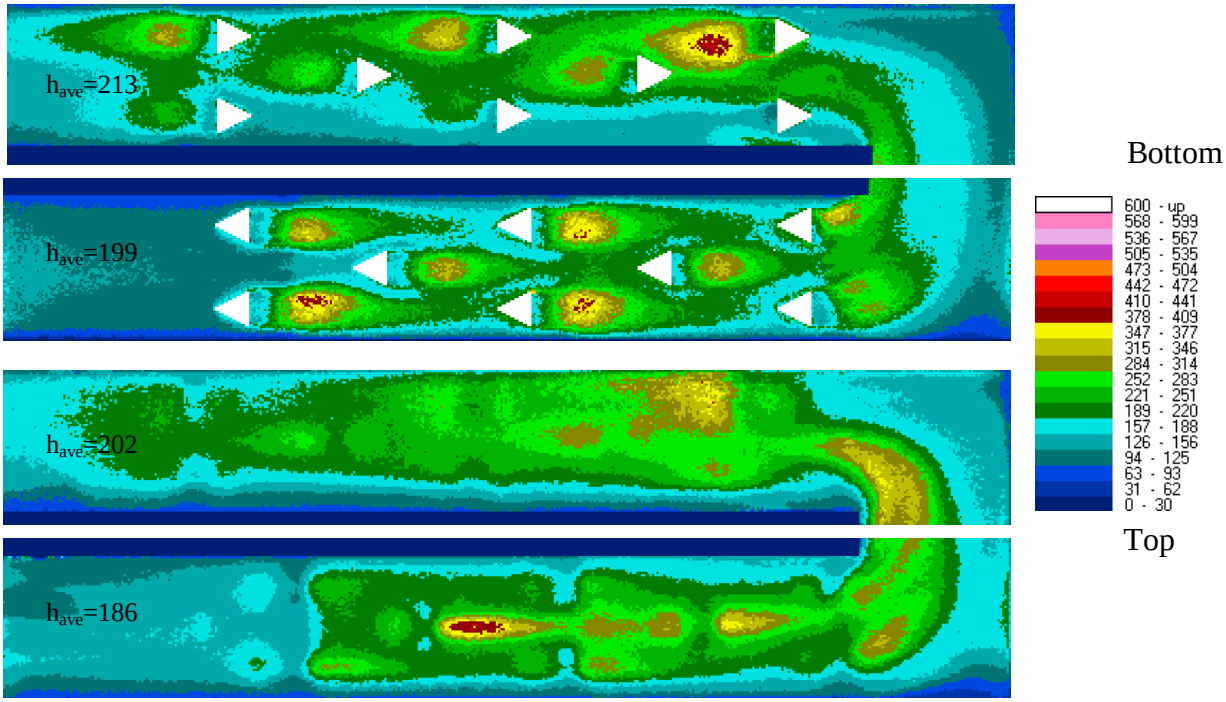

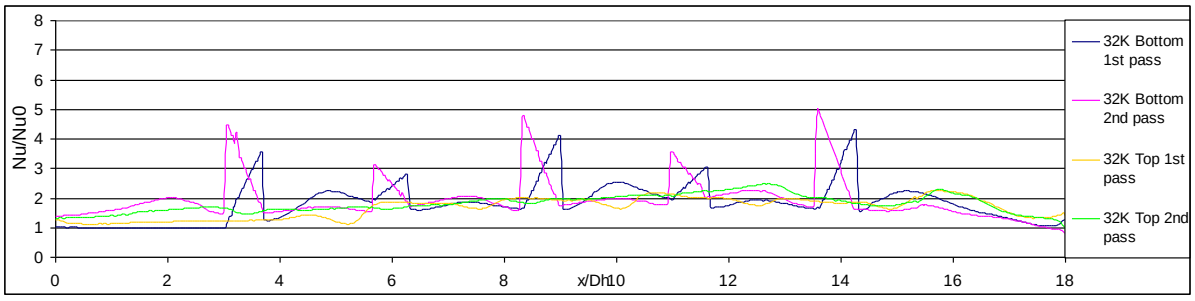

Figure 23 Local heat transfer coefficient and column average Nu/Nu_0 of 2-pass channel with sparse array delta wings configuration at Re_{Dh}=32000

4.4 2-PASS CHANNEL WITH DENSE DELTA WING ARRAYS

Stronger turbulence flow can be induced by adding more vortex generators to the channel surface. The dense array configuration, shown below in Figure 24-Figure 25, utilizes the same pins as in the sparse array configuration but with denser placement. The first row of pin is 25.4mm (1.0") from the center of the thermocouple hole. The pitch, P, is 50.8mm (2.0").

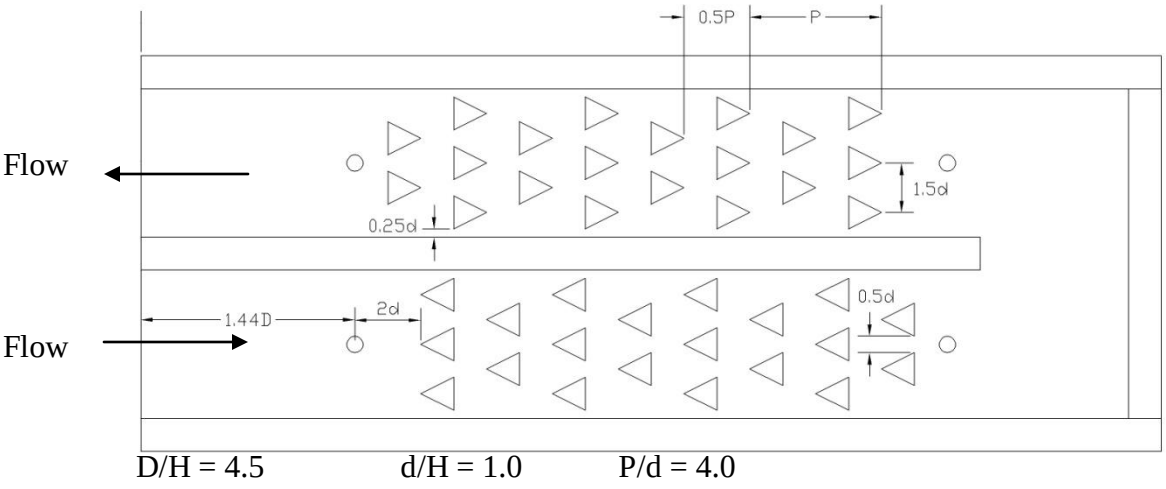

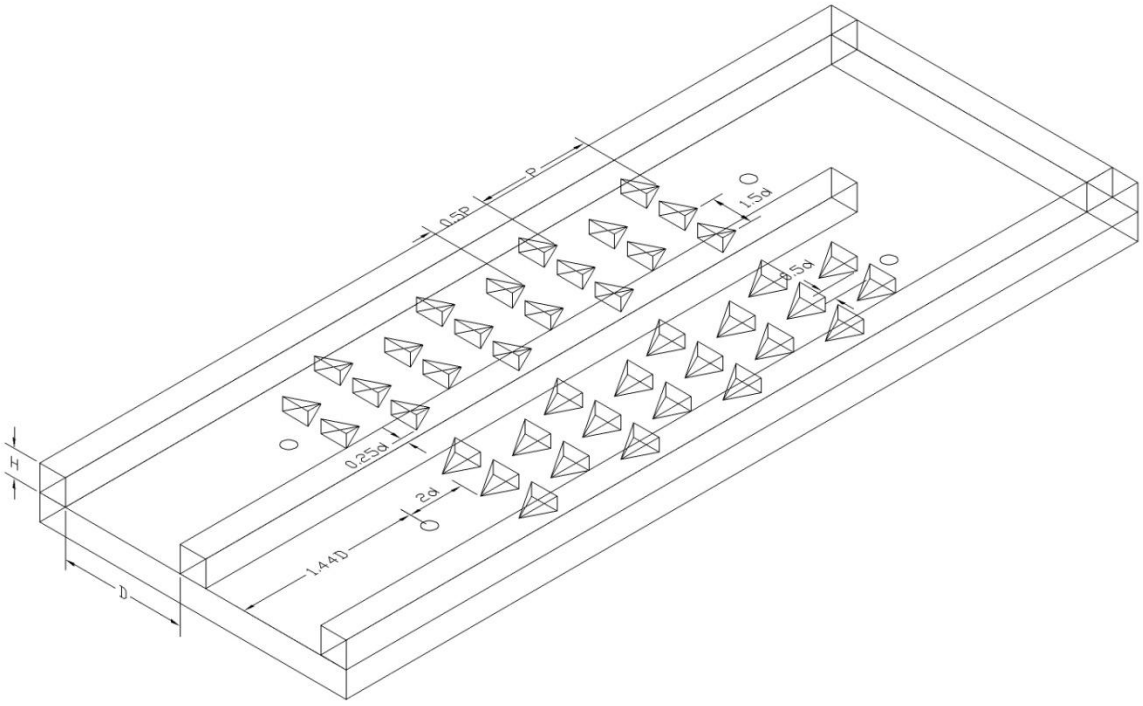

Figure 24 2-pass channel with dense delta wing arrays configuration

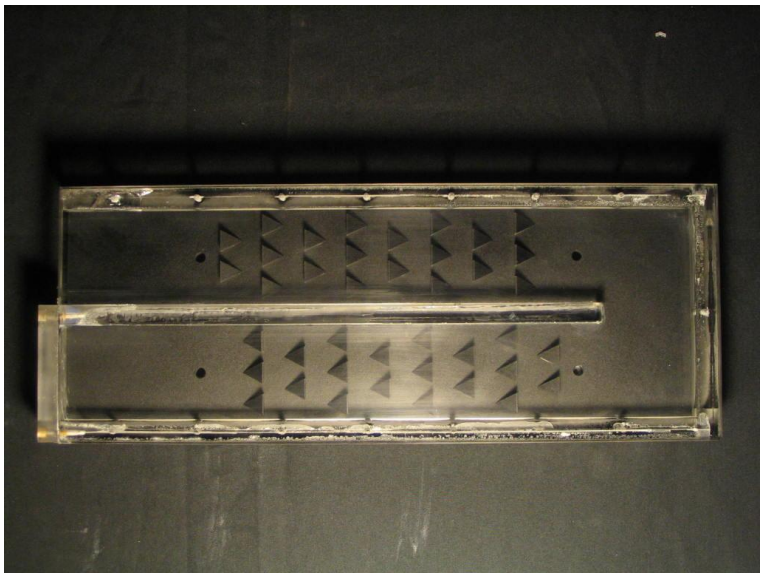

Figure 25 Test section with dense delta wing arrays

4.4.1 Result and discussion

The dense delta wing arrays change the flow characteristic and heat transfer of the channel even more significantly than the sparse arrays, as shown in Figure 26-Figure 29. At lower Reynolds number, 13000 and 20000, the second pass has higher heat transfer than the first pass. On the contrary, at Reynolds number of 28000 and 32000, the heat transfer in the first pass become much higher than that of the second pass. The overall heat transfer coefficient of the dense array configuration is approximately 1.5 fold of that of the smooth channel.

Comparing the result from the dense delta wing arrays to the smooth channel, heat transfer enhancement is up to 3.1 and 1.6 fold in the first and second pass respectively. Similar to the sparse configuration, the gain in the first pass is more prominent than that of the second pass. However, contrary to the smooth channel and the sparse configuration, the average heat transfer in the first pass of the dense configuration surpasses that in the second pass by 11%.

These results suggest that when the number of vortex generators increase, heat transfer enhancement in the first pass increase more prominently than that in the second pass.

According to Table 4, the vortex generators in dense configuration account for approximately 17% and 21% of heat transfer in the first and second pass respectively. The dense arrays configuration changes the flow and heat transfer characteristic significantly more than the sparse arrays configuration. While the heat transfer at the bottom and top endwall of the sparse configuration are comparable, the heat transfer of the dense configuration at the bottom endwall dominates the top endwall. There is more wetted area and more vortices/turbulent generated at the bottom endwall, resulting in significant higher heat transfer than that of the top endwall.

Table 4: Average heat transfer coefficient of 2-pass with dense delta-wing arrays

Re_{Dh}	Heat transfer coefficient (W/m^2-K)					
	h_0	h_{1st}	h_{2nd}	h total ave	1st pass pins(%)	2nd pass pins(%)
13000	54.2	135.1	160.3	147.7	24.3	26.1
20000	76.5	204.1	208.2	206.2	18.7	23.4
28000	100.1	302.1	266.9	284.5	13.0	17.8
32000	111.4	396.3	297.2	346.8	10.6	16.3

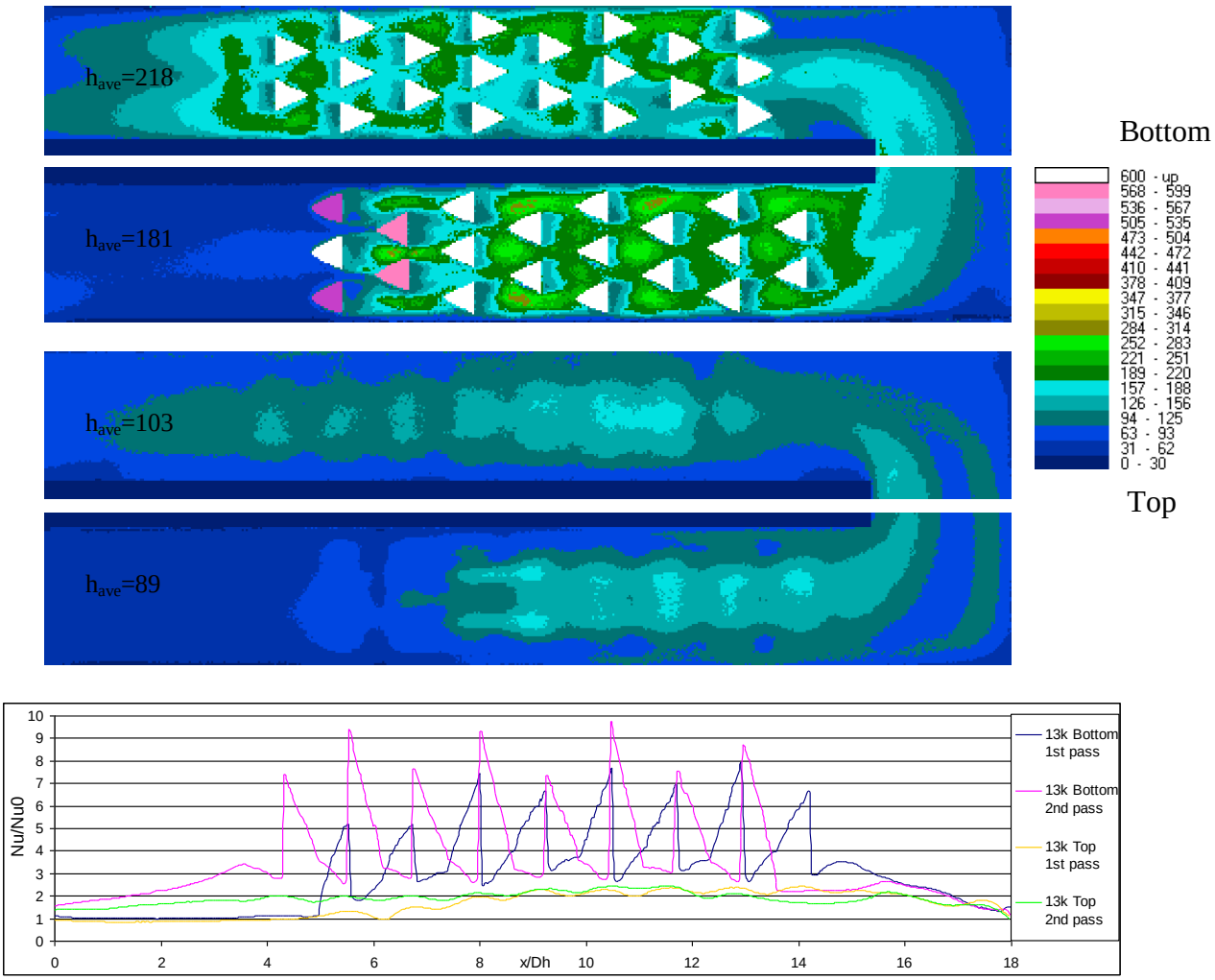

Figure 26 Local heat transfer coefficient and column average Nu/Nu_0 of 2-pass channel with dense array delta wings configuration at Re_{Dh}=13000

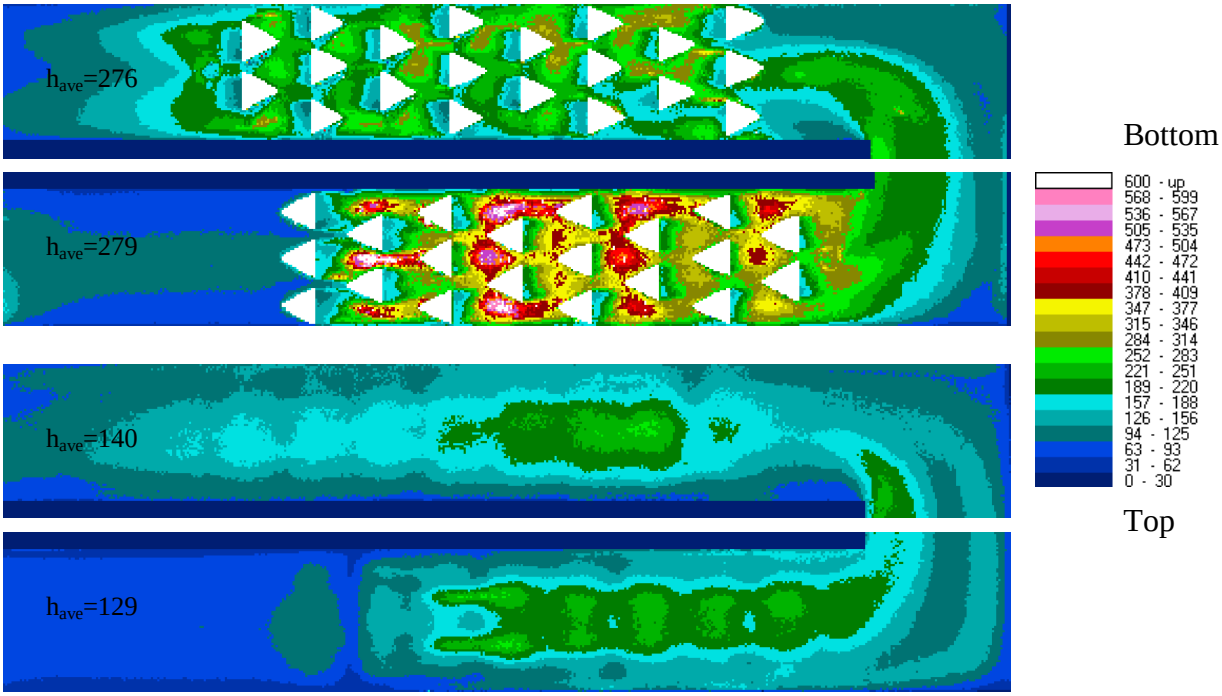

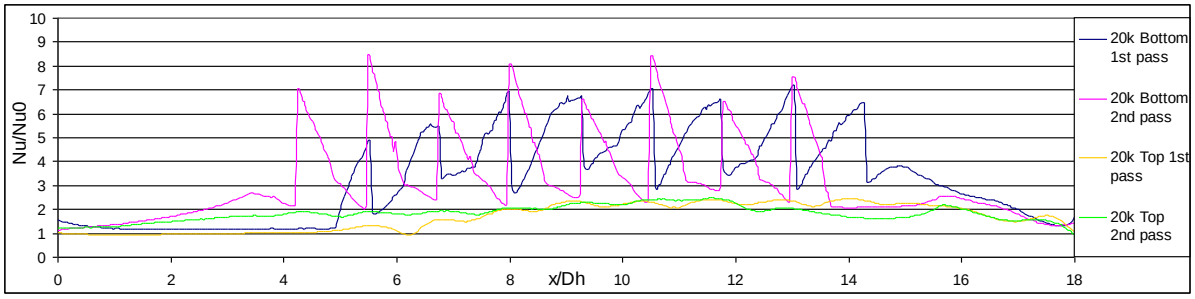

Figure 27 Local heat transfer coefficient and column average Nu/Nu_0 of 2-pass channel with dense array delta wings configuration at Re_{Dh}=20000

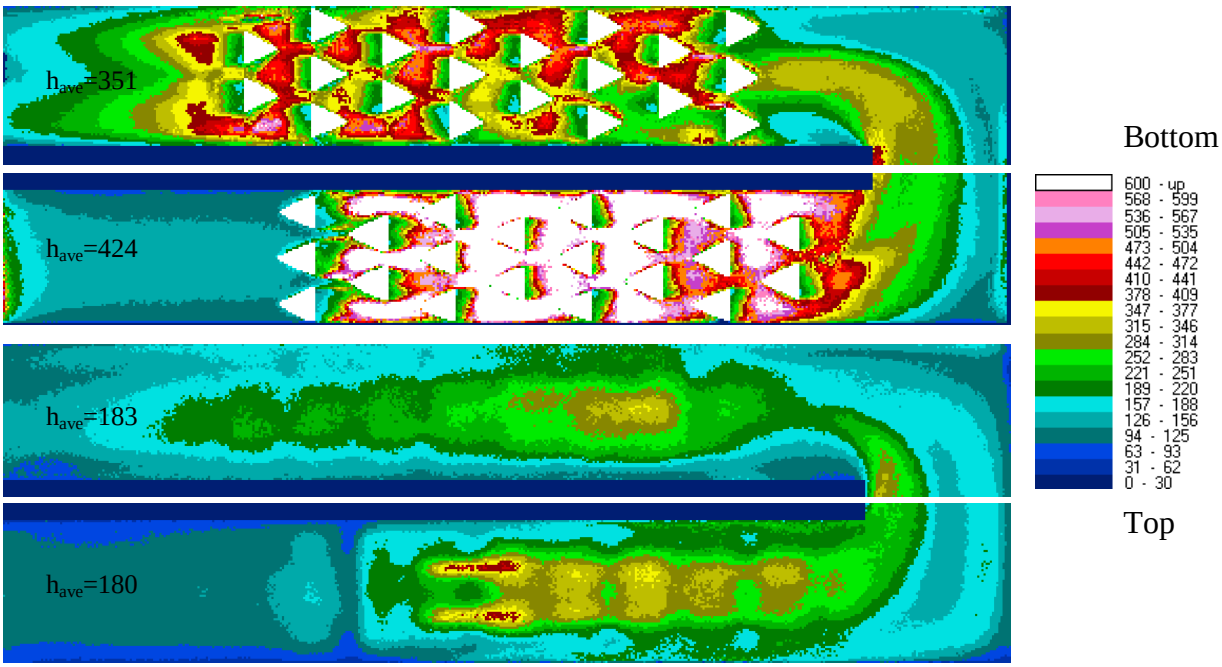

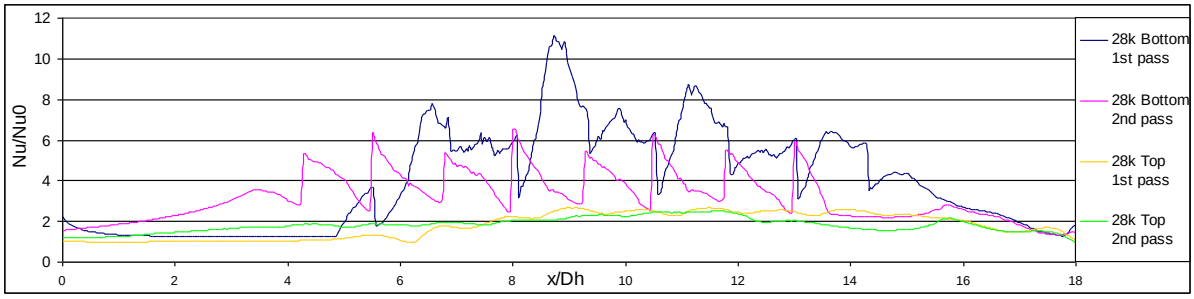

Figure 28 Local heat transfer coefficient and column average Nu/Nu_0 of 2-pass channel with dense array delta wings configuration at Re_{Dh}=28000

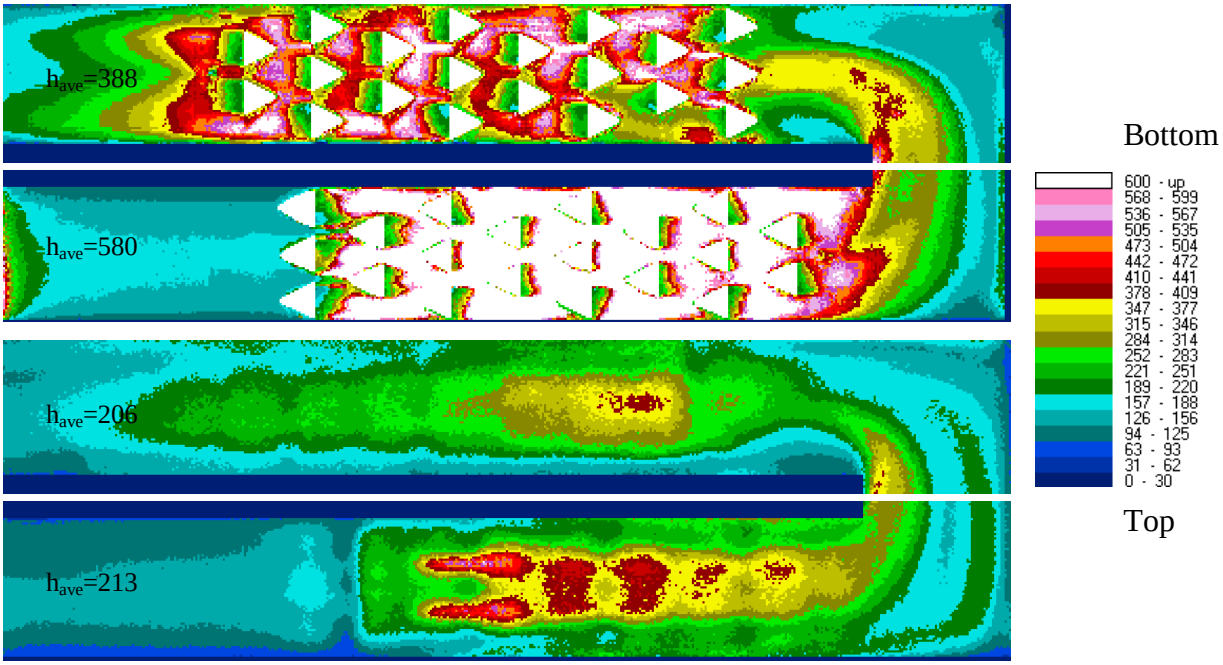

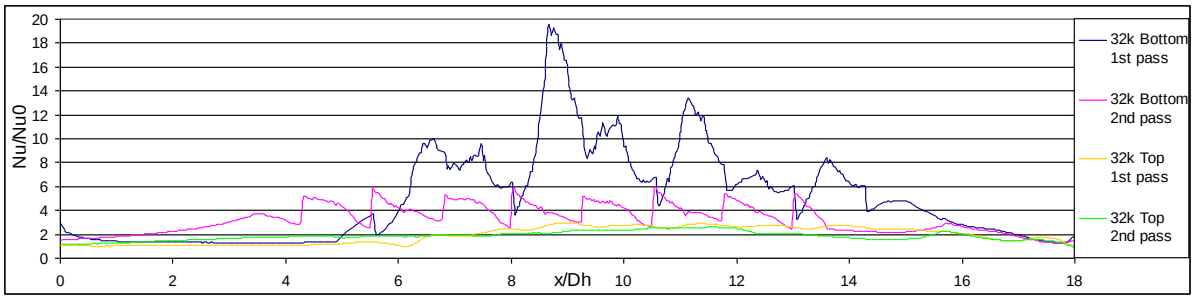

Figure 29 Local heat transfer coefficient and column average Nu/Nu_0 of 2-pass channel with dense array delta wings configuration at Re_{Dh}=32000

4.5 90-DEGREE BEND INLET

To further explore potential design alternatives for enhancement cooling, the effect of the 90-degree bend inlet on the heat transfer in the 2-pass channel at Re=20,000 is studied and then compare with the result of the straight inlet. Figure 30 shows the 90-degree bend inlet drawing and the assembly to the channel. The inner and the outer radii of the bend are 19.1mm (0.75") and 31.8mm (1.25") respectively.

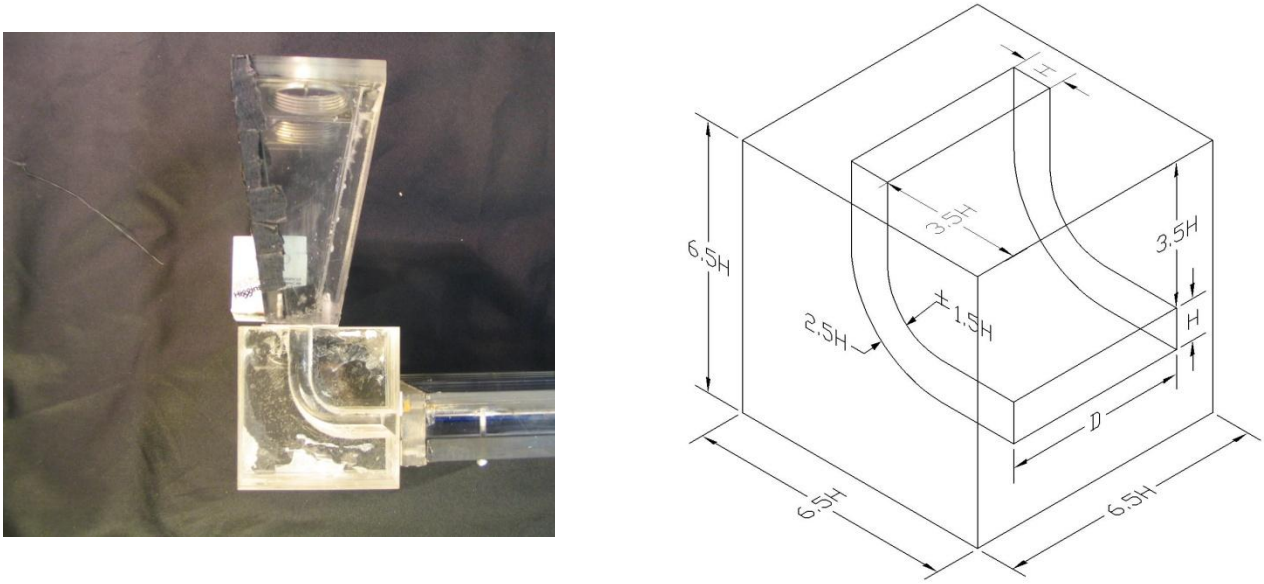

Figure 30 90-degree bend inlet

4.5.1 Result and discussion

Heat transfer distribution of the smooth channel with 90-degree bend inlet is shown in Fig. 31. With bend inlet, the total average heat transfer coefficient of the smooth channel is

enhanced approximately 1.1 fold relative to the smooth channel with straight inlet at the same Reynolds number. In the first pass, the enhancement is higher than the second pass (15% versus 11%) because at the entrance the flow is affected by the bend which induces strong turbulent but subsides while passing through the channel.

For the sparse delta wing arrays configuration with the 90-degree bend inlet, shown in Figure 32, the overall heat transfer enhancement is up to 1.6 fold relative to the straight inlet counterpart. The bend inlet enhances heat transfer in the first and second pass up to 1.9 and 1.3 fold respectively. The increase is in similar manner as with smooth channel but much more significant in the first pass. Thus the heat transfer in the first pass becomes greater than the second pass by 28%.

The 90-degree bend inlet can enhance the overall heat transfer of the dense delta wings configuration, shown in Figure 33, up to 1.2 fold. The first pass heat transfer enhancement is up to 1.4 fold while there is virtually no gain in the second pass. The bend inlet is less effective in the dense configuration than in the sparse configuration. In dense configuration, it only further enhances the heat transfer in the first pass, of which becomes 37% greater than that in the 2nd pass.

The effect of 90-degree bend inlet is prominent in the first pass while the gain in the second pass is much less. It is more effective when coupled with the channel with vortex generators than when coupled with the smooth channel.

Table 5: Average heat transfer coefficient of 2-pass channel with straight and 90-degree bend inlet at Re=20,000

	Smooth w/straight	Smooth w/bend	Sparse w/straight	Sparse w/bend	Dense w/straight	Dense w/bend
h_{1st} (W/m^2-K)	93.4	107.9	135.2	257.4	204.1	285.2
h_{2nd} (W/m^2-K)	137.0	152.7	154.4	196.5	208.2	208.6
h total ave	115.2	130.3	136.3	227.0	206.2	246.9

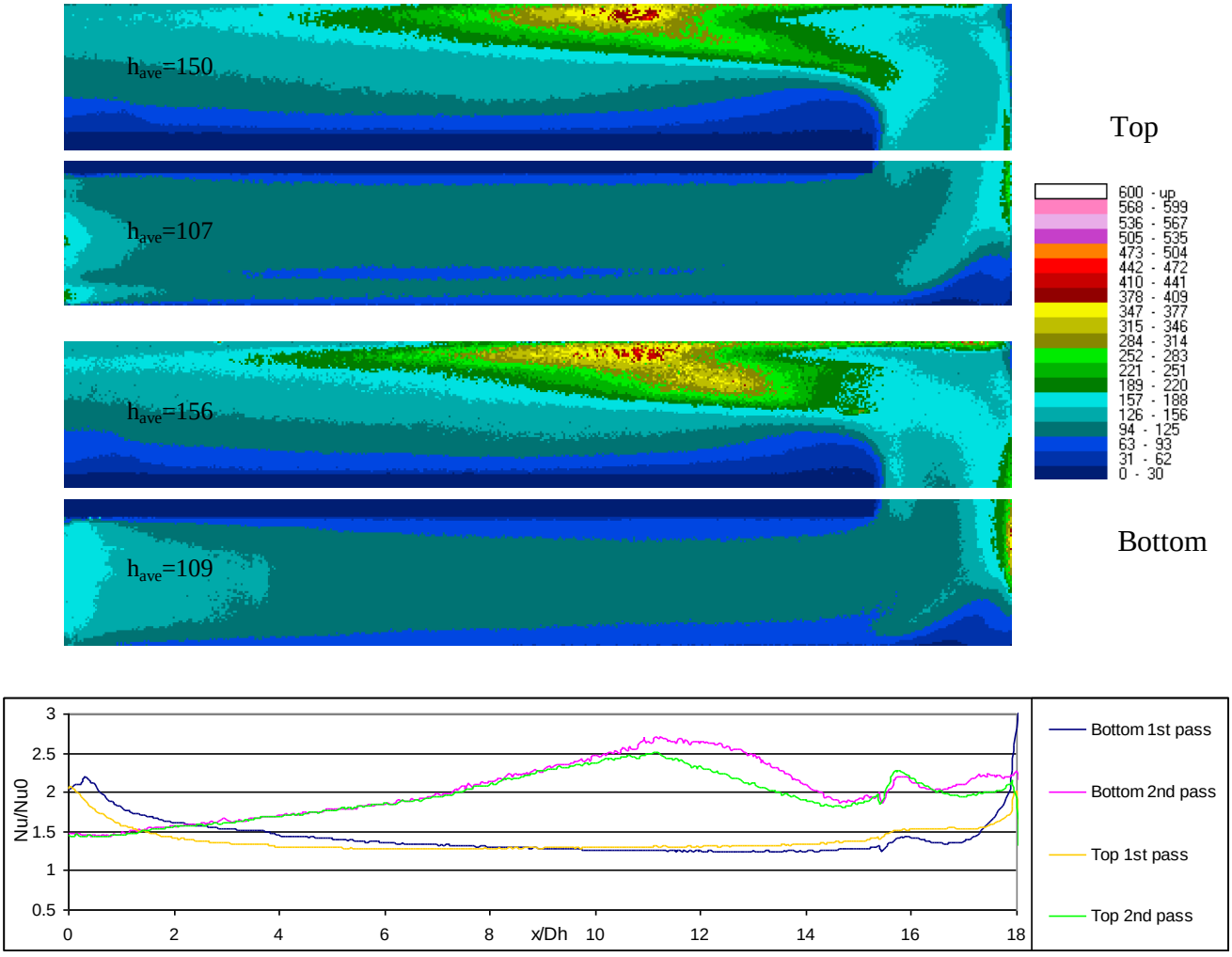

Figure 31 Local heat transfer coefficient and column average Nu/Nu_0 of 2-pass channel with 90-degree bend inlet at Re_{Dh}=20000

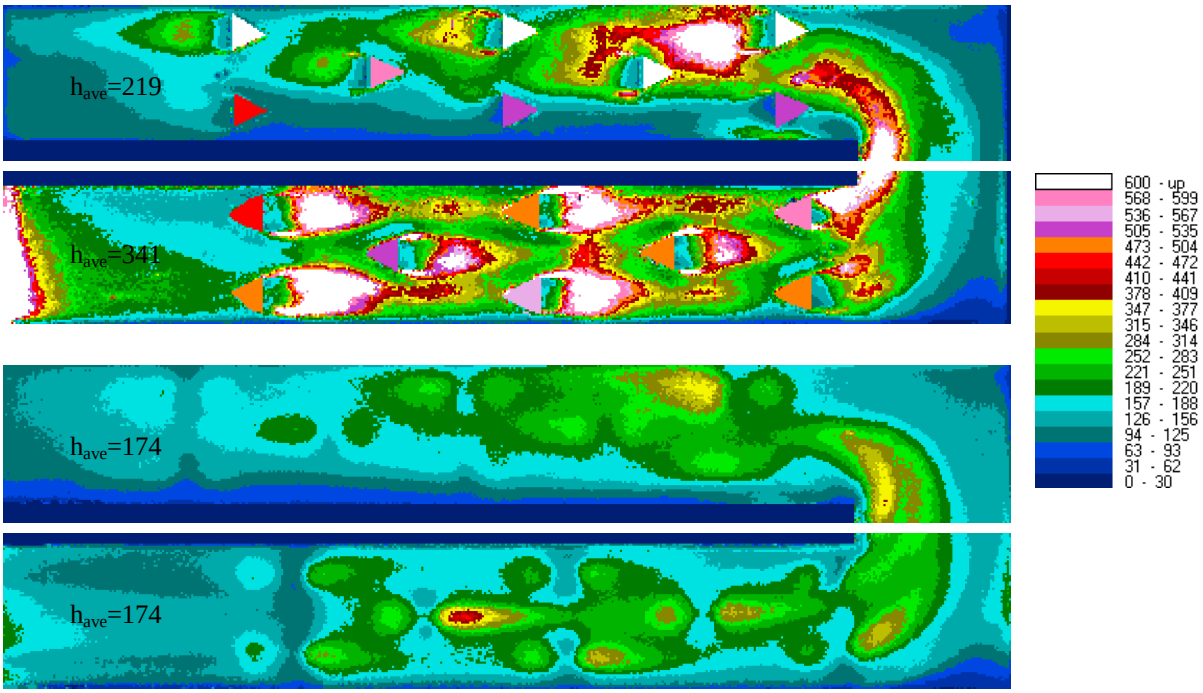

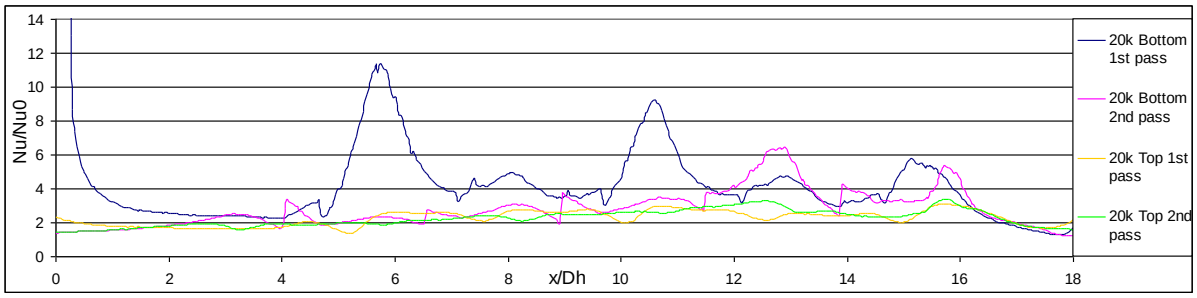

Figure 32 Local heat transfer coefficient and column average Nu/Nu_0 of 90-degree bend inlet 2-pass channel with sparse array delta wings configuration at Re_{Dh}=20000

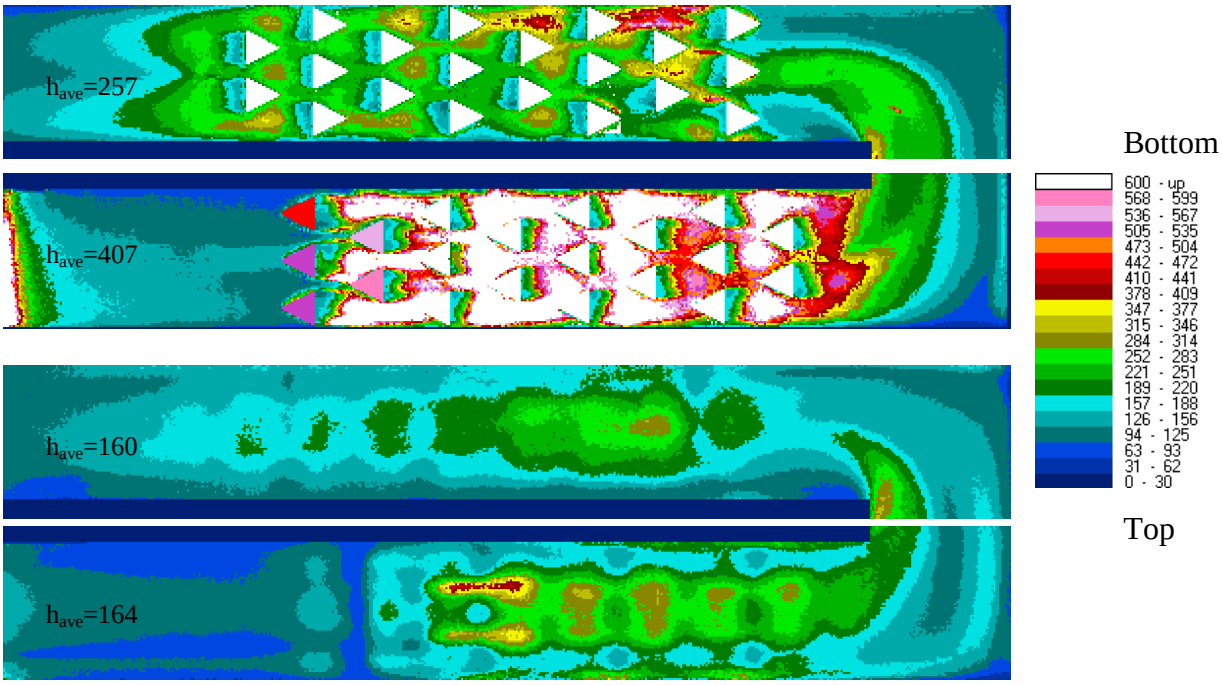

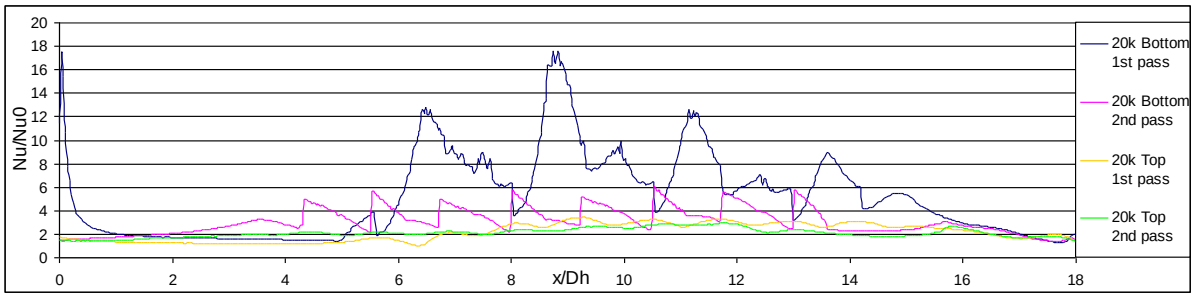

Figure 33 Local heat transfer coefficient and column average Nu/Nu_0 of 90-degree bend inlet 2-pass channel with dense array delta wings configuration at Re_{Dh}=20000

4.6 2-PASS CHANNEL WITH PIN-FIN ARRAYS

A set of experiments were performed to investigate the heat transfer and pressure characteristics in the two-pass channel with pin-fin arrays placed in both channel passes before and after a 180-degree sharp turn. The results from this set of experiments are used as the baseline reference for the following experiments of the cubic and diamond block arrays.

Similar to the previous experiments, transient liquid crystal technique was applied to acquire detailed local heat transfer data both on the channel surface and pin-fin elements, for Reynolds number between 13000 and 28000. Figure 34 shows 2-pass channel, which has the same dimension as previous experiment test channel, with pin-fin arrays. The pin-fin elements are 9.5 mm (0.375") diameter, d, and their height, h, is 12.7 mm (1/2"), same as channel height. The pitch, P, of the cube-shaped block arrays is 47.6 mm (1.875").

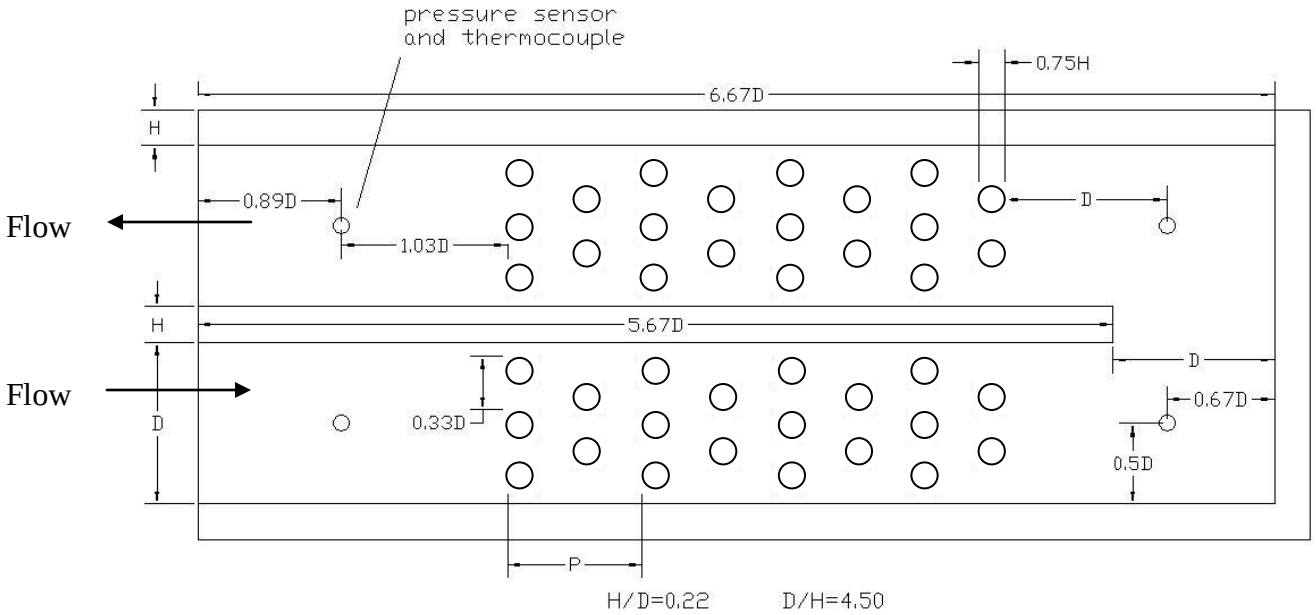

Figure 34 2-pass channel with pin-fin arrays

4.6.1 Result and discussion

With pin-fin arrays place within both passes of the channel, the flow characteristic and heat transfer are significantly different from the smooth channel. The overall heat transfer enhancement is approximately 2.2 fold, relative to fully developed value of the turbulent flow in smooth duct without turn. Figure 35 shows the local heat transfer of the channel with pin-fin arrays at the Reynolds number of 13k, 20k and 28k respectively.

Figure 35 reveals that the flow is obviously more turbulent than the flow in the smooth channel counterpart, resulting in up to 1.9 and 1.2 fold heat transfer enhancement in the first and second passes respectively. While the overall heat transfer significantly increases and distributes more evenly over the surface, the heat transfer in the turning region is lower than that of the smooth channel. The heat transfer coefficient in first pass is generally higher than that of the second pass.

The pins are found to have higher heat transfer coefficient than the endwall which is consistent with the study by Chyu et al [37]. The heat transfer contour in the first pass is also similar to the results of the straight channel reported by Chyu et al [44] whereas the contour in the second pass are different since there is 180-degree sharp turn effect combined.

According to Table 6: Average heat transfer coefficient of 2-pass channel with pin-fin arrays, the pin-fins account for approximately 26% of heat transfer in both the first and the second passes. They obviously change the flow and heat transfer characteristic significantly. They distribute the flow more evenly over the entire channel and create more turbulent; thus the heat transfer is higher and distributes more evenly on the endwall surfaces, comparing to the smooth channel.

Table 6: Average heat transfer coefficient of 2-pass channel with pin-fin arrays

Re_{Dh}	Heat transfer coefficient (W/m^2-K)					
	h_0	h_{1st}	h_{2nd}	h total ave	1st pass pins(%)	2nd pass pins(%)
13000	54.2	121.2	121.6	121.4	27.7	26.5
20000	76.5	161.2	153.7	157.5	26.8	26.7
28000	100.1	245.1	204.9	225.0	24.3	26.2

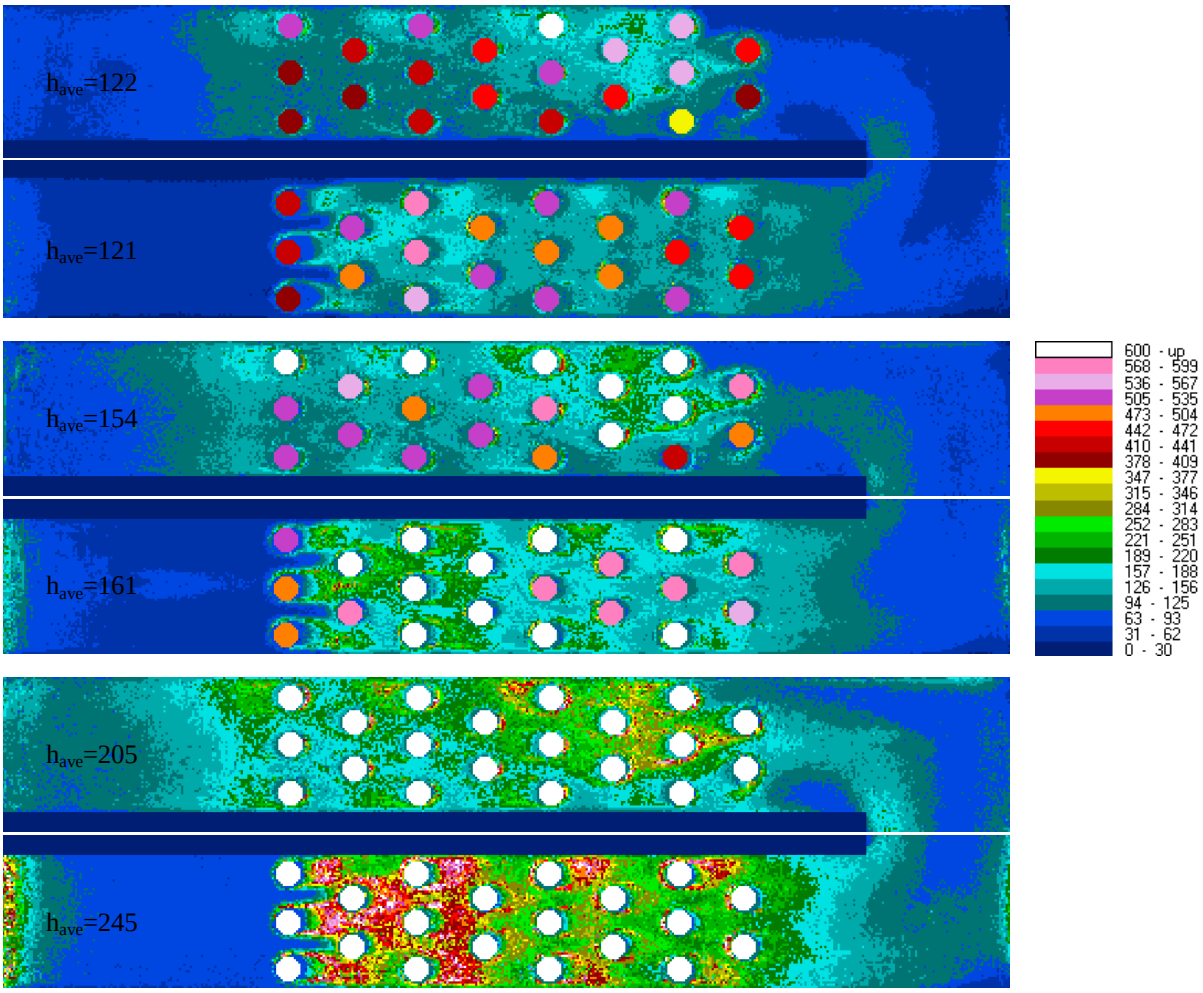

Figure 35 Local heat transfer coefficient of 2-pass channel with pin-fin arrays at Re_{Dh}=13000, 20000 and 28000

4.7 2-PASS CHANNEL WITH CUBE-SHAPED BLOCK ARRAYS

Series of experiments were performed to investigate the heat transfer and pressure characteristics in the two-pass channel with cube-shaped block arrays placed in both channel passes before and after a 180-degree sharp turn. Similar to the previous experiments, transient liquid crystal technique was applied to acquire detailed local heat transfer data both on the channel surface and block elements, for Reynolds number between 13000 and 28000. Moreover, the effects of block height, ranging from ¼, ½, ¾ and full span of the channel height were also evaluated. Figure 36 shows 2-pass channel, which has the same dimension as previous experiments, with cube-shaped block arrays. The cube-shaped elements are 9.5 mm (0.375") square and their height is 3.2, 6.4, 9.5 or 12.7 mm (1/8", 1/4", 3/8" or 1/2") corresponding to the experimental series. The pitch, P, of the cube-shaped block arrays is 47.6 mm (1.875").

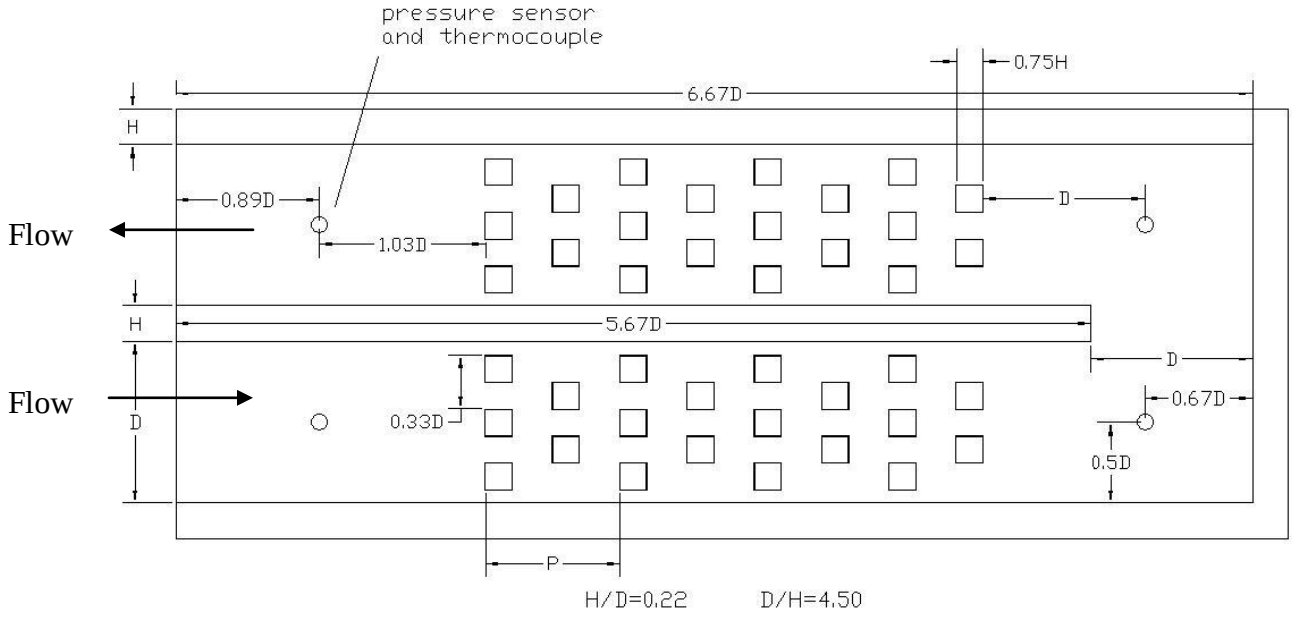

Figure 36 2-pass channel with cube-shaped block arrays

4.7.1 Result and discussion

The Local heat transfer distribution and column average Nu/Nu_0 of 2-pass channel with cube-shaped block arrays is shown in Figure 37-Figure 40. The overall results show significant improvement over the channel without turbulators especially in the first pass before the turn. With lowest height block arrays, the ¼ height of the channel, the sharp turn effect in the second pass is prominent while the pins fail to affect flow and heat transfer.

The comparison of the colored contour values in Figure 37-Figure 40 clearly suggests that the block arrays of ½ height to full span change the flow and heat transfer characteristic significantly. The top endwalls of the ½, ¾ and full height block arrays show significant improvement in heat transfer rate over that of the ¼ height block arrays. In general, while the pin-fin arrays significantly improve the heat transfer on the bottoms endwall, they exhibit higher heat transfer than the endwall, except the case with ¼ height block arrays.

Further examination suggests that, the top endwall of the case with ¾ height block arrays exhibits the highest heat transfer rate among all the top endwalls while the bottom endwall of the full span block arrays case exhibits the highest heat transfer rate among the bottom endwalls of all case. Generally, the cubic block arrays create more turbulent flow and spread the flow in the channel, which resulting in more evenly heat transfer distribution in the channel. When the gaps between top endwall and pins is in appropriate distance, the turbulent flow is enhanced; thus promoting better heat transfer enhancement on the endwall as shown in the case with ¾ height pin arrays.

Table 7 shows average heat transfer coefficient in two-pass channel with cube-shaped block arrays with four different height variation. The data from the tables suggest that, the ¼ height block elements can increase heat transfer only in the first pass at high Reynolds number

(33% increase at 28k), otherwise there is virtually no gain over the smooth channel. The ½ height elements yield up to 2.6 and 1.4 fold in the first pass and second pass respectively. While the increase to 3.0 and 1.6 fold can achieve from ¾ height cube turbulators, the highest enhancement come from full height cube elements at 3.5 and 1.9 fold in the first and second pass respectively.

The results suggest that the staggered cube-shaped arrays are highly effective in the first pass of the channel which raise the heat transfer rate up to 13% surpassing that of the second pass. Except for the ¼ height elements, the cube-shaped block elements account for approximately half of the total heat transfer in the channel.

The full height cubic block arrays have similar heat transfer trend to the pin-fin arrays but the enhancement is higher, up to 3.5 fold versus 1.9 fold in the first pass and up to 1.9 fold versus 1.2 fold in the second pass, compared to the smooth channel. These results consistent with the study by Chyu et al [44] that cubic block arrays enhance higher heat transfer than the pin-fin arrays.

Table 7: Average heat transfer coefficient of 2-pass channel with cube-shaped block arrays

	Re_d	h_0 (W/m^2-K)	h_{1st} (W/m^2-K)	h_{2nd} (W/m^2-K)	h total ave (W/m^2-K)	1^{st} pass pins(%)	2^{nd} pass pins(%)
1/4 height	13000	54.2	69.7	94.9	82.3	13.8	13.8
	20000	76.5	94.7	130.9	112.8	13.1	11.2
	28000	100.1	145.6	182.4	164.0	15.2	10.4
1/2 height	13000	54.2	132.7	138.6	135.6	50.1	40.2
	20000	76.5	191.7	188.0	189.8	51.0	40.4
	28000	100.1	285.1	260.2	272.7	54.6	41.7
3/4 height	13000	54.2	185.5	170.3	177.9	55.6	50.1
	20000	76.5	245.8	223.8	234.8	54.8	48.5
	28000	100.1	330.9	297.6	314.2	52.1	47.3
Full height	13000	54.2	194.3	182.8	188.6	55.5	55.5
	20000	76.5	260.8	252.4	256.6	56.9	56.9
	28000	100.1	381.5	336.9	359.2	57.2	57.2

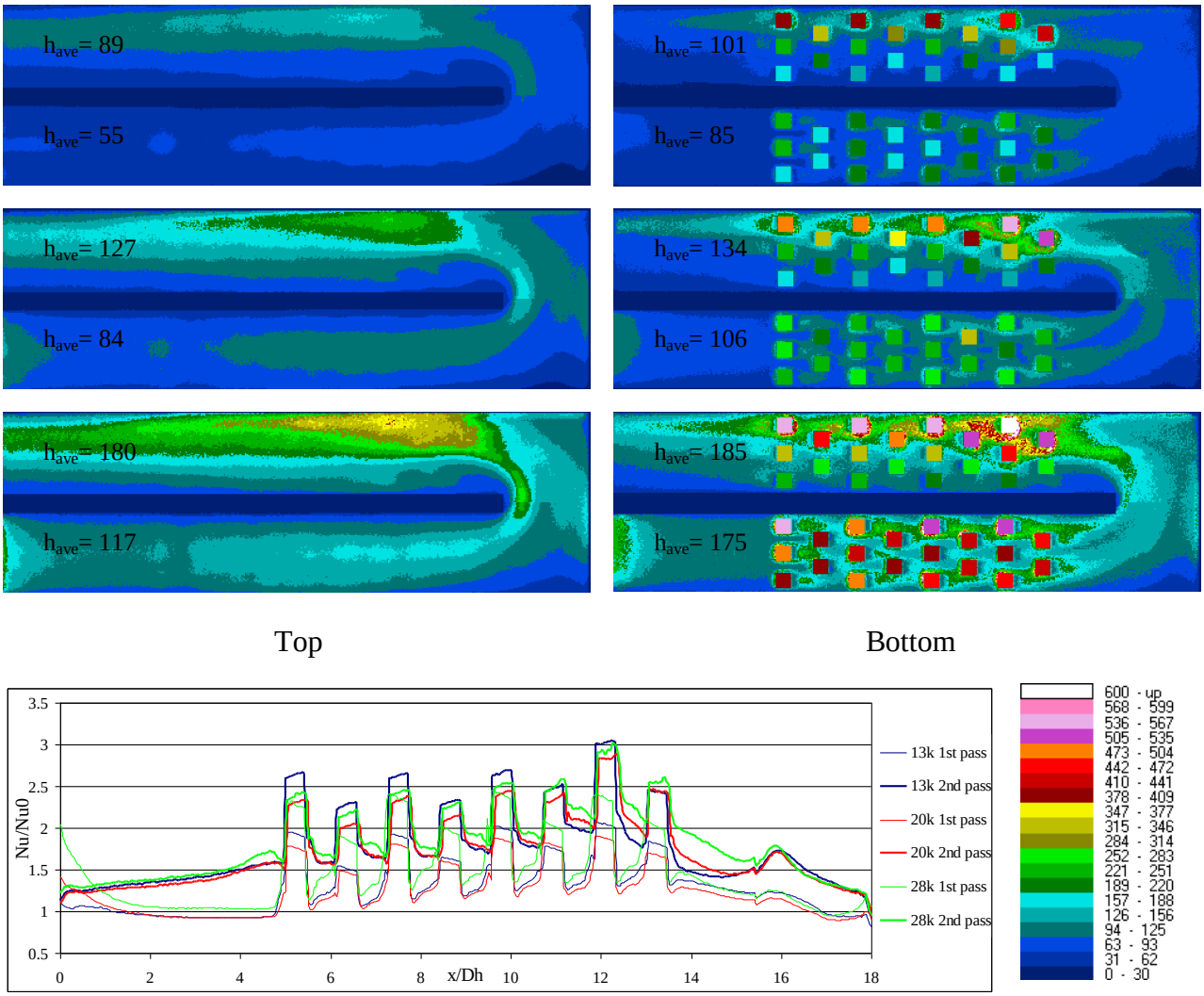

Figure 37 Local heat transfer coefficient of 2-pass channel with ¼ channel height cube-shaped block arrays at Re_{Dh}=13000, 20000, 28000 and column average Nu/Nu_0

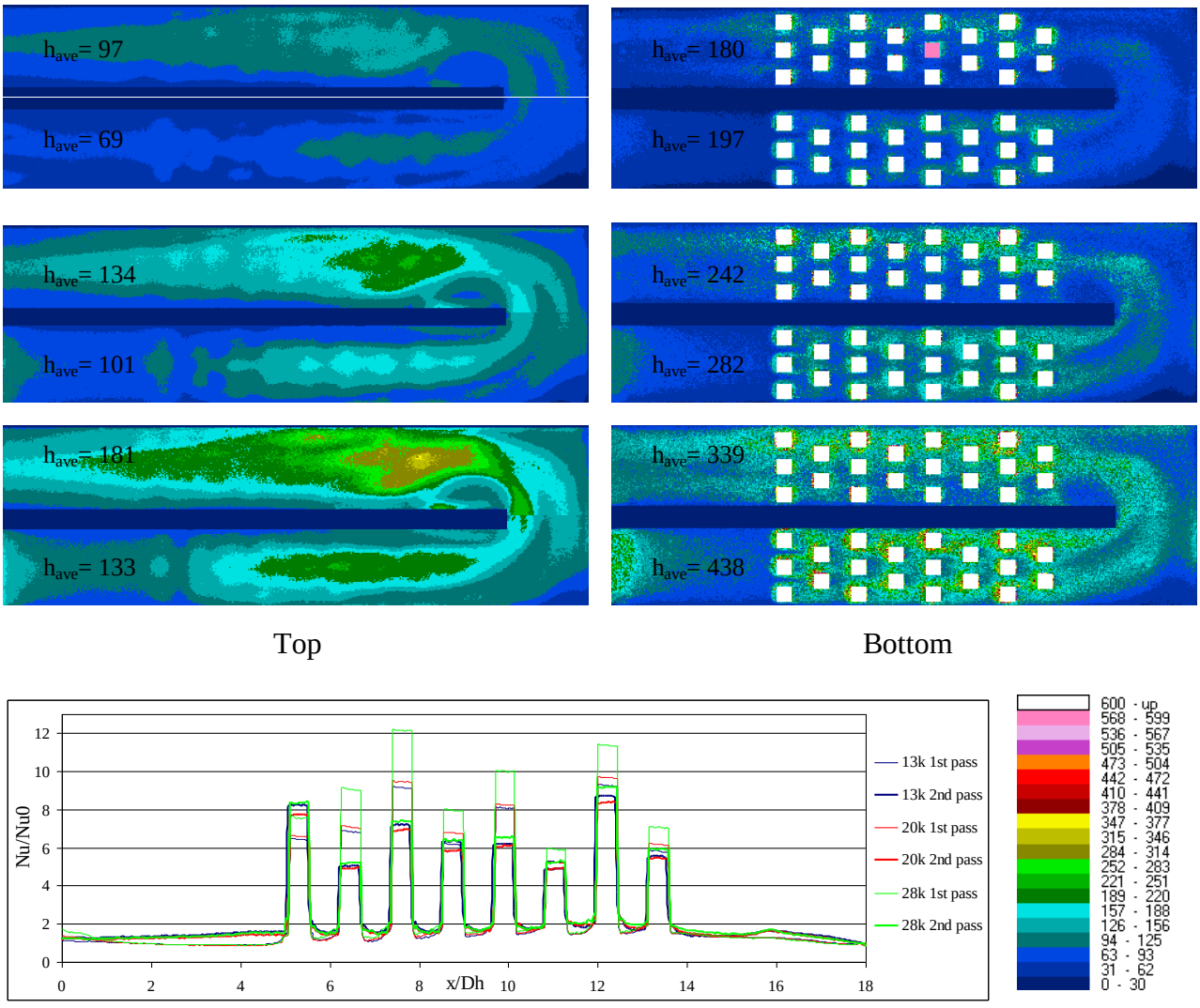

Figure 38 Local heat transfer coefficient of 2-pass channel with ½ channel height cube-shaped block arrays at Re_{Dh}=13000, 20000, 28000 and column average Nu/Nu_0

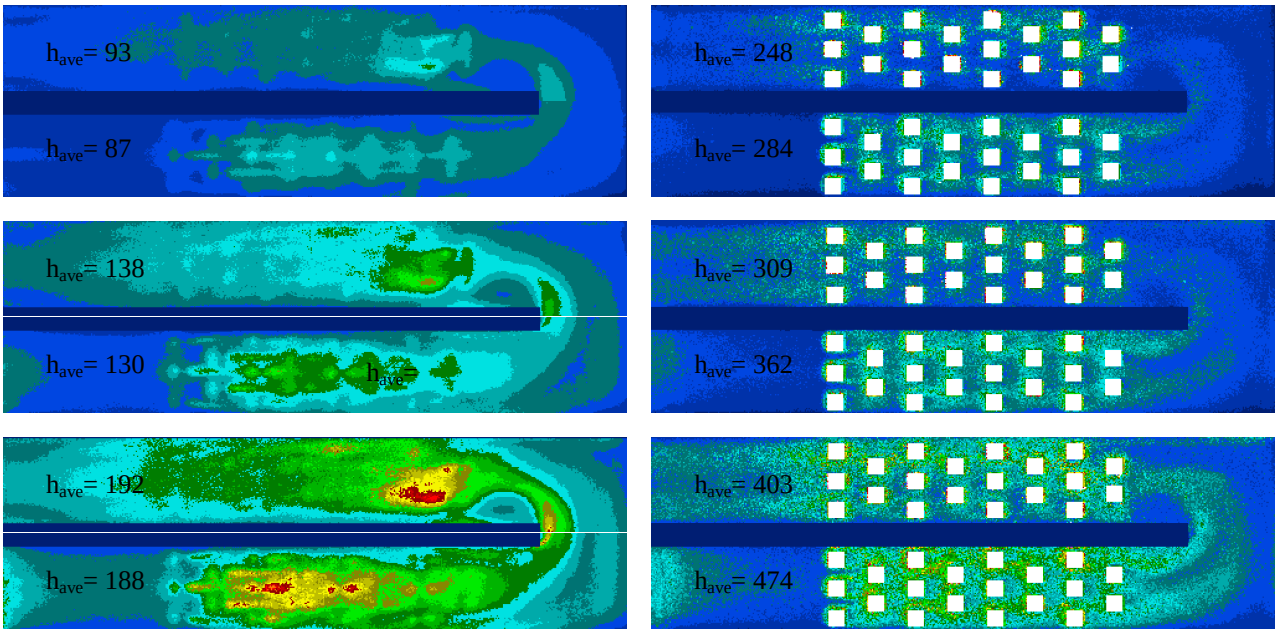

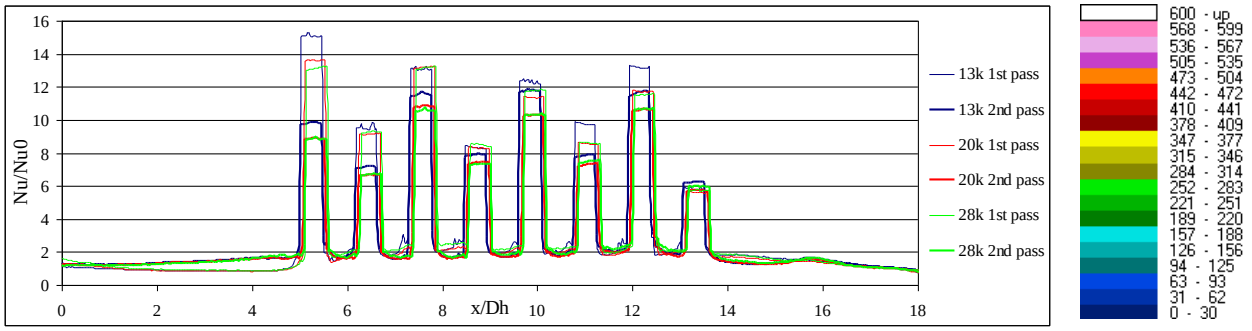

Figure 39 Local heat transfer coefficient of 2-pass channel with ¾ channel height cube-shaped block arrays at Re_{Dh}=13000, 20000, 28000 and column average Nu/Nu_0

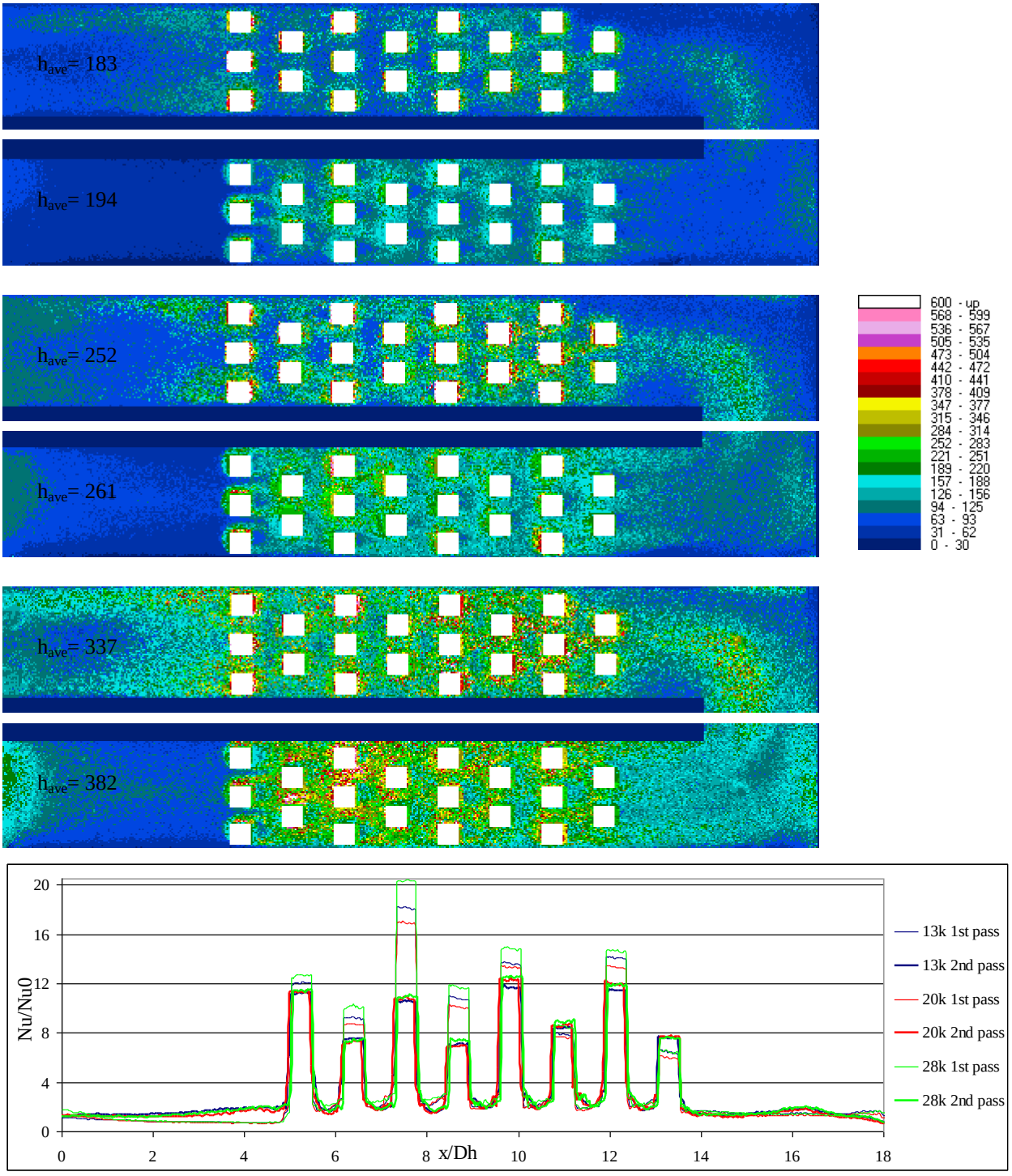

Figure 40 Local heat transfer coefficient of 2-pass channel with full channel height cube-shaped block arrays at Re_{Dh}=13000, 20000, 28000 and column average Nu/Nu_0

4.8 2-PASS CHANNEL WITH DIAMOND-SHAPED BLOCK ARRAYS

The cube-shaped block arrays are rotated 45 degree to become diamond-shaped configuration. Similar to the cube-shaped block arrays experimental series, the heat transfer and pressure characteristics were investigated. The effects of block height, ranging from ¼, ½, ¾ and full span of the channel height were also evaluated. Figure 41 shows 2-pass channel with diamond-shaped block arrays. The diamond-shaped elements are 9.5 mm (0.375") square and their height is 3.2, 6.4, 9.5 or 12.7 mm (1/8", 1/4", 3/8" or 1/2") corresponding to the experimental series. The pitch, P, of the diamond-shaped block arrays is 47.6 mm (1.875").

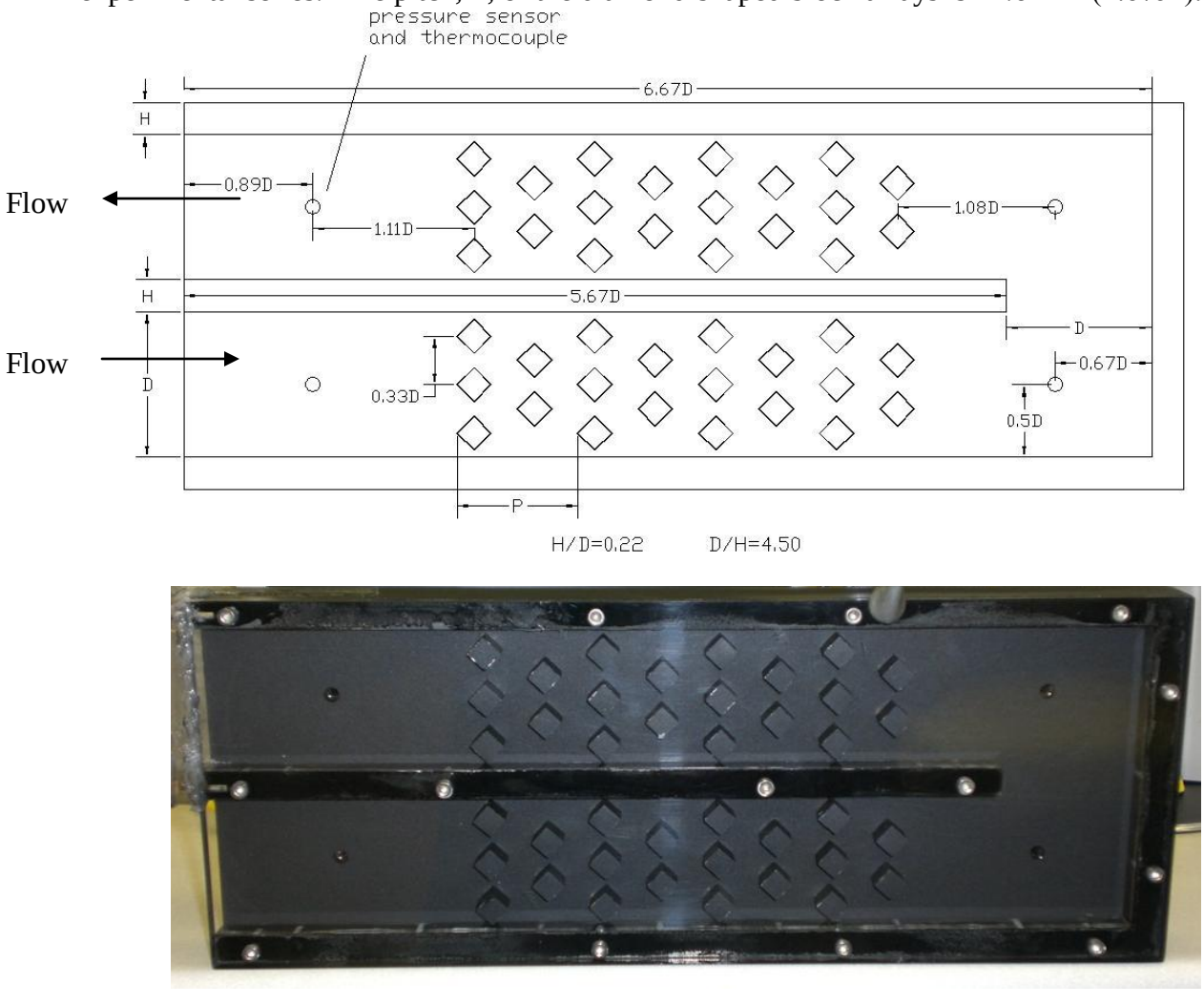

Figure 41 2-pass channel with diamond-shaped block arrays

4.8.1 Result and discussion

The Local heat transfer distribution and column average Nu/Nu_o of 2-pass channel with diamond-shaped block arrays is shown in Figure 42-Figure 45. The effects of the diamond-shaped block arrays are similar to that of the cube-shaped block arrays but the heat transfer is more prominent.

With ¼ height block arrays, the sharp turn effect in the second pass is still prominent but the diamond pins affect flow and enhance heat transfer more than cubic pin counterpart. The diamond block arrays of ½ and ¾ height of the channel change the flow and heat transfer characteristic even more drastically than the cubic arrays; however, with full span diamond arrays, the heat transfer rate is lower than that of ¾ height block arrays. The full height diamond elements suffer from the highest restriction which causes part of the flow to be directed to the side space between the channel wall and block arrays; thus reducing the effectiveness of the pin-fin arrays.

Table 8 shows average heat transfer coefficient in two-pass channel with diamond-shaped block arrays with four different height variation. Comparing the result with the smooth channel from Table 1, they suggest that the ¼ height block elements can increase heat transfer in the first pass up to 1.5 fold at high Reynolds number but the heat transfer in the second pass suffers a little. The ½ height elements yield up to 2.8 and 1.5 fold in the first pass and second pass respectively. The highest gain is achieved from ¾ height diamond turbulators at 3.4 and 1.7 fold in the first and second pass respectively.

The experimental results show that, generally, the staggered diamond-shaped arrays achieve higher heat transfer rate than the cube-shaped array except at full height. The diamond elements also account for about half of the heat transfer in the channel, except at ¼ height.

These results are consistent with the other report [44] that generally diamond arrays yield higher heat transfer enhancement than cubic arrays.

Table 8: Average heat transfer coefficient of 2-pass channel with diamond-shaped block arrays

	Re_{Dh}	h_0 (W/m^2-K)	h_{1st} (W/m^2-K)	h_{2nd} (W/m^2-K)	h total ave (W/m^2-K)	1^{st} pass pins(%)	2^{nd} pass pins(%)
1/4 height	13000	54.2	74.6	85.2	79.9	16.1	12.3
	20000	76.5	112.8	128.1	120.4	17.0	14.5
	28000	100.1	167.9	176.9	172.4	14.8	13.8
1/2 height	13000	54.2	151.4	147.1	149.2	48.8	43.4
	20000	76.5	235.3	208.0	221.6	50.5	42.2
	28000	100.1	306.8	275.2	291	46.6	39.6
3/4 height	13000	54.2	196.7	192.3	194.5	50.6	46.2
	20000	76.5	279.8	247.5	263.7	48.9	46.3
	28000	100.1	373.2	303.9	338.5	47.2	44.1
Full height	13000	54.2	186.7	177.8	182.3	53.7	47.0
	20000	76.5	258.0	223.6	240.8	55.0	49.7
	28000	100.1	336.1	275.3	305.7	53.3	48.8

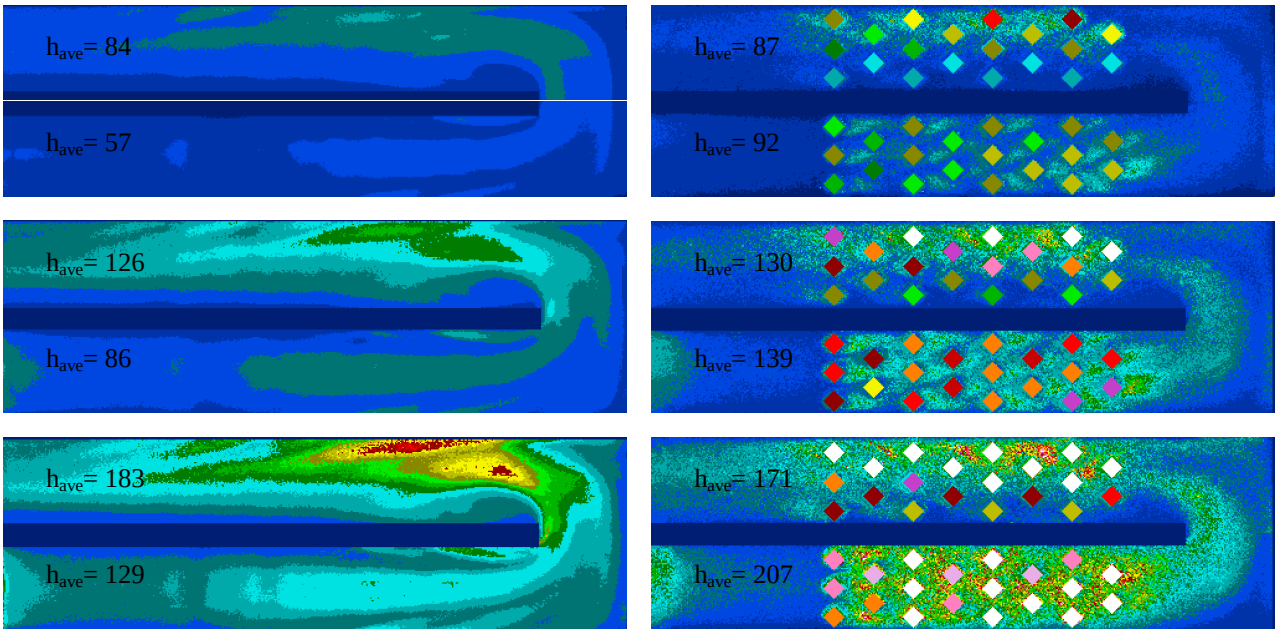

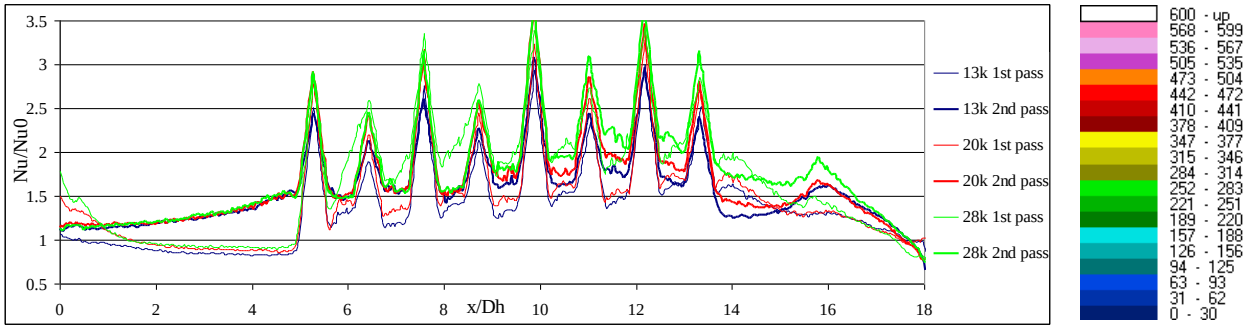

Figure 42 Local heat transfer coefficient of 2-pass channel with ¼ channel height diamond-shaped block arrays at Re_{Dh}=13000, 20000, 28000 and column average Nu/Nu_0

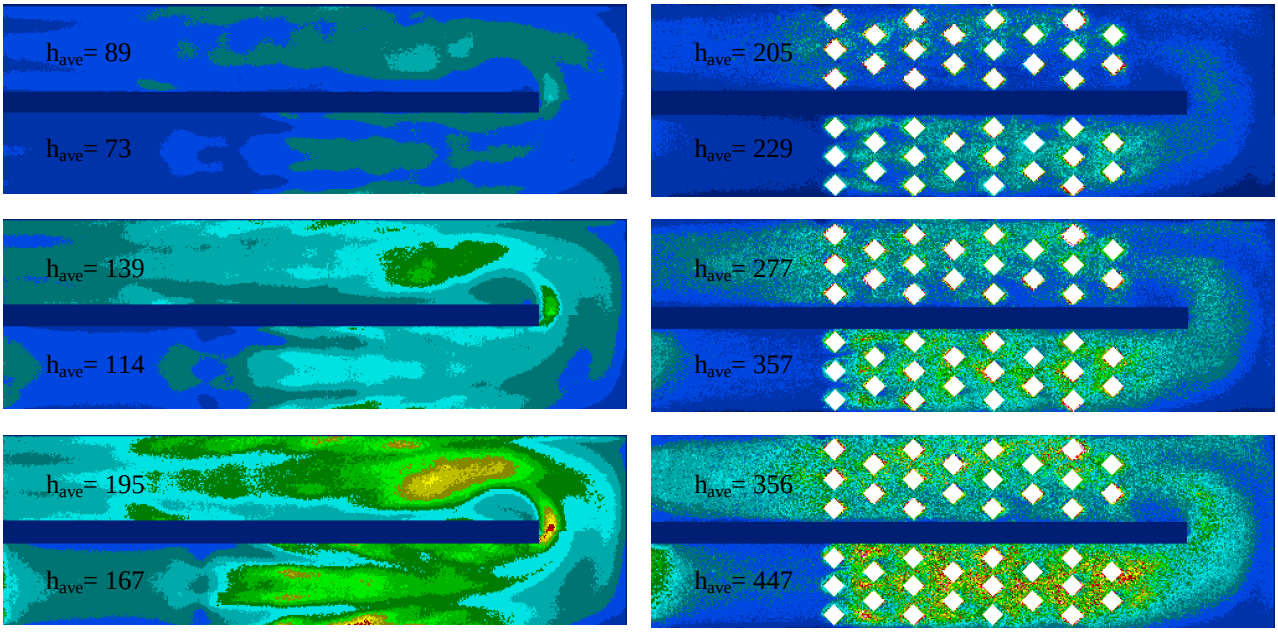

Figure 43 Local heat transfer coefficient of 2-pass channel with ½ channel height diamond-shaped block arrays at Re_{Dh}=13000, 20000, 28000 and column average Nu/Nu_0

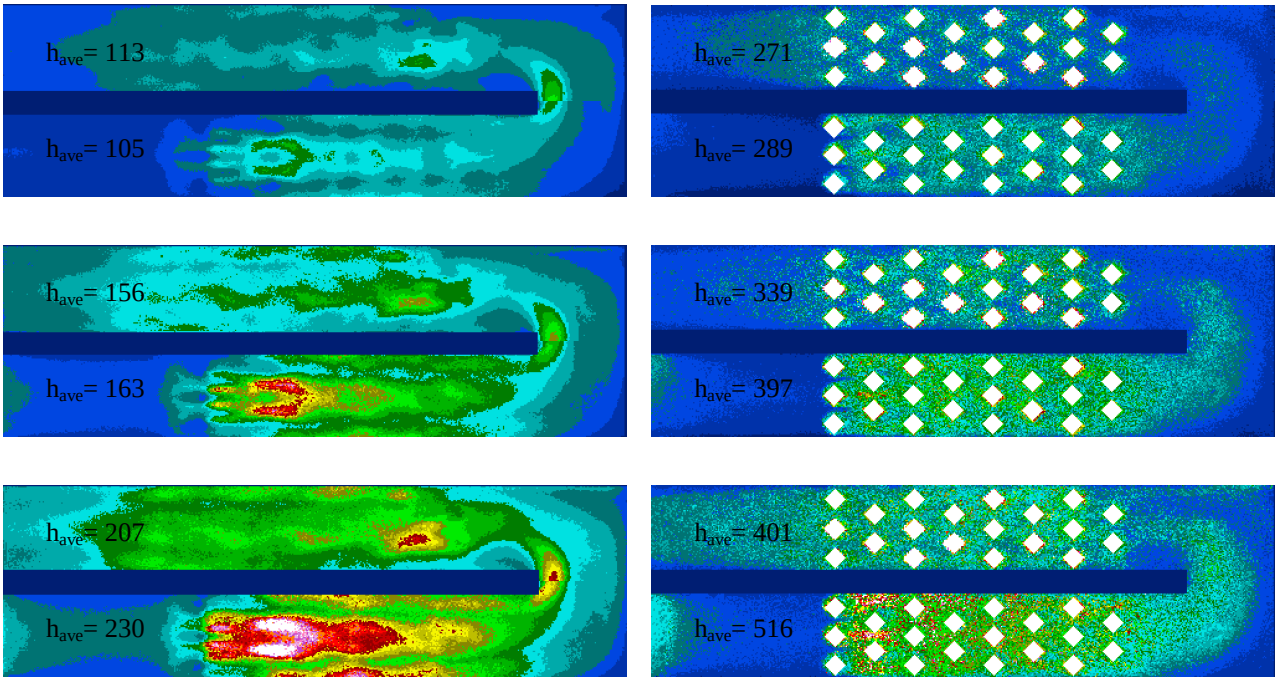

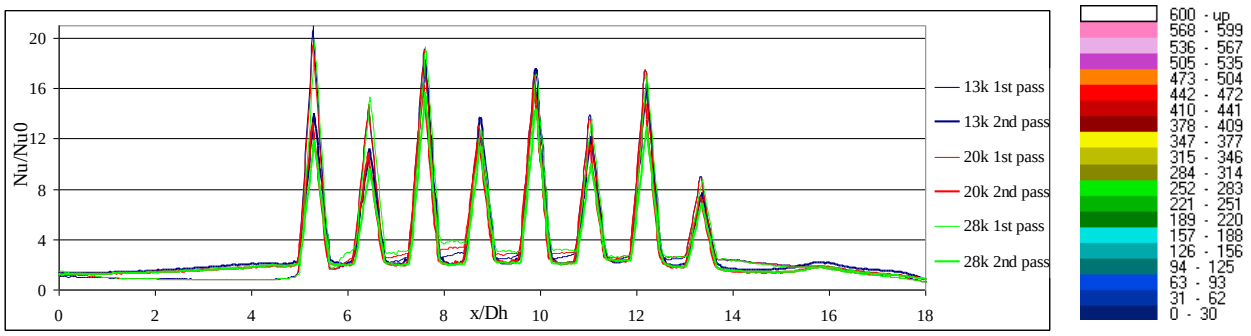

Figure 44 Local heat transfer coefficient of 2-pass channel with ¾ channel height diamond-shaped block arrays at Re_{Dh}=13000, 20000, 28000 and column average Nu/Nu_0

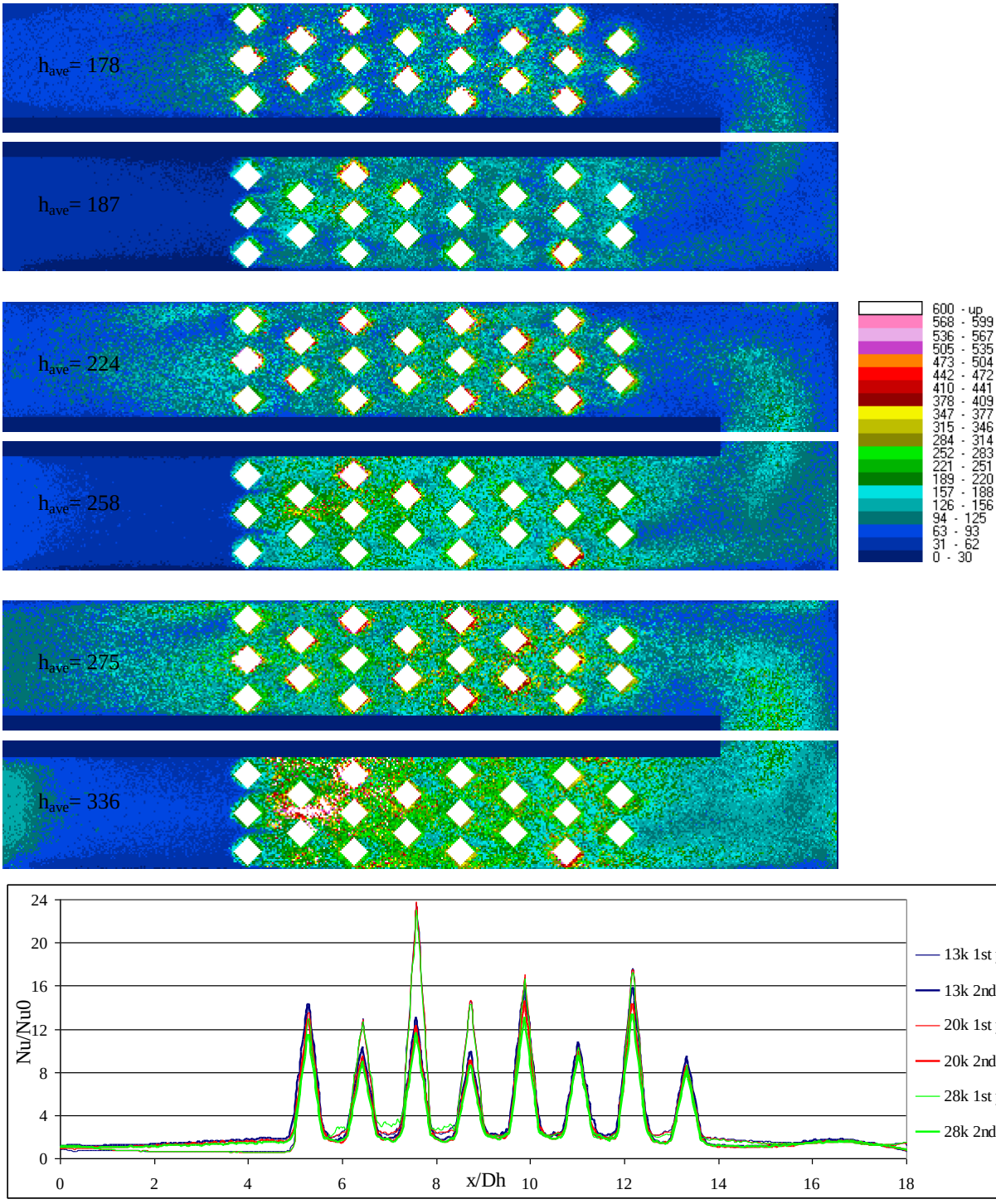

Figure 45 Local heat transfer coefficient of 2-pass channel with full channel height diamond-shaped block arrays at Re_{Dh}=13000, 20000, 28000 and column average Nu/Nu_0 conclusion

5.0 RESULTS COMPARISON

The results of each configuration are compared in Figure 46-Figure 48. The overall average heat transfer relation with the Reynolds number is shown in Figure 46. The experimental results show that, generally, the staggered diamond-shaped arrays achieve higher heat transfer rate than the cube-shaped array except at full height. The dense delta wings heat transfer enhancement falls between those of the ½ height cubic and diamond block arrays while the sparse delta wings heat transfer enhancement is just higher than those of the ¼ height block arrays. Most of the configuration in this study have substantial higher heat transfer enhancement compared to the full span round pins in straight channel studied by Chyu [40]. The results suggest that the sharp turn affects heat transfer enhancement significantly.

Heat transfer enhancement is always achieved with the expense of pressure loss. Figure 47 shows pressure loss characteristic of the different configurations. Generally, the pressure lost of the diamond arrays is higher and can be up to 2.5 times of the cube block arrays pressure loss. Depend on the height of the block elements, the pressure loss penalty can be several folds over the smooth channel. The pressure loss of the sparse and dense delta wing arrays is comparable to that of the ½ height cubic and diamond arrays respectively. The 180-degree sharp turn also contributes to several folds pressure loss compared to the straight channel.

Figure 48 represent the Overall cooling performance factors versus Reynolds number of different channel configurations. At ¼ height, both the cube and diamond configurations have

approximately the same cooling performance as the smooth channel and sparse delta wing configuration. In all cases with the same pins height, cubic array configurations have higher cooling performance factor than the diamond array configurations. The cooling performance factor of the full span diamond pin array is the lowest since it suffers from the biggest penalty in pressure loss. Most of the two-pass channel configurations in this study have higher performance factor than the full span round pins in straight channel studied by Chyu [40].

The heat transfer enhancement of the diamond block arrays is higher than that of the corresponding cube block arrays but the pressure lost of the diamond arrays is much higher in general. Thus in term of cooling performance factor, the cube block arrays surpass the diamond block arrays by a considerable degree. Dense delta wing arrays perform significantly better than the sparse arrays but they are outperformed by some of the block arrays. The best configuration in term of heat transfer enhancement is the diamond block at ¾ height of the channel while the best in term of cooling performance is the cube block at ½ height of the channel.

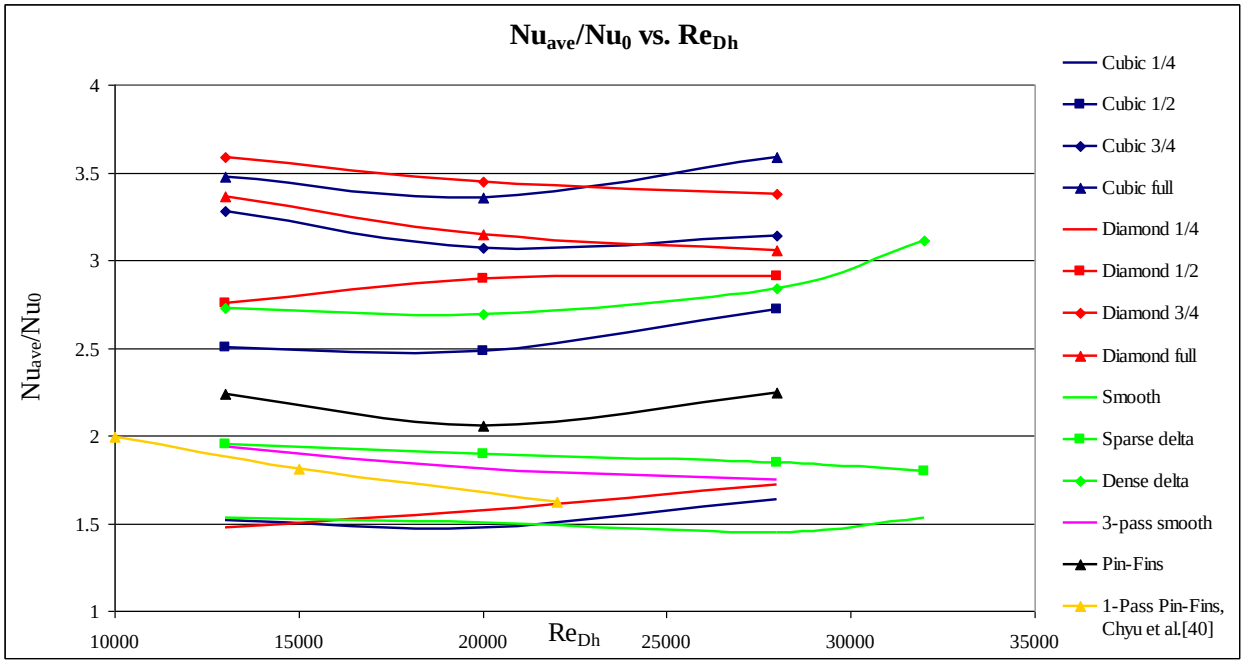

Figure 46 Comparison of Nu_{ave}/Nu_0 vs. Re_{Dh} with different channel configurations

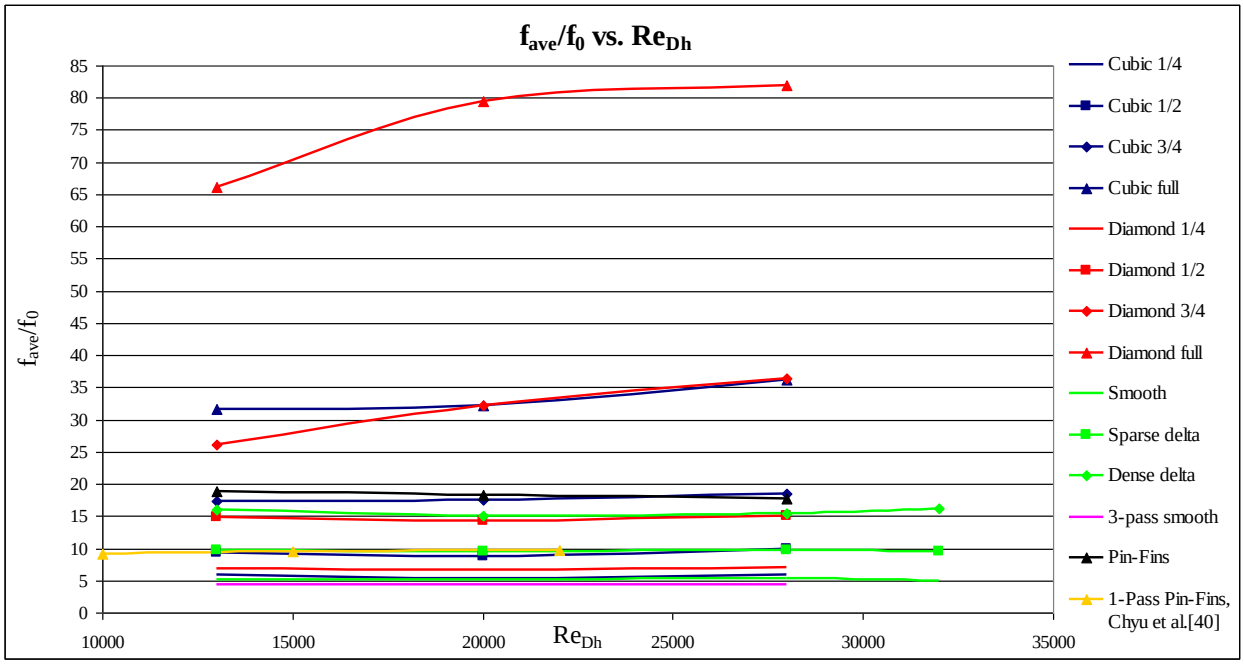

Figure 47 Comparison of f_{ave}/f_0 vs. Re_{Dh} with different channel configurations

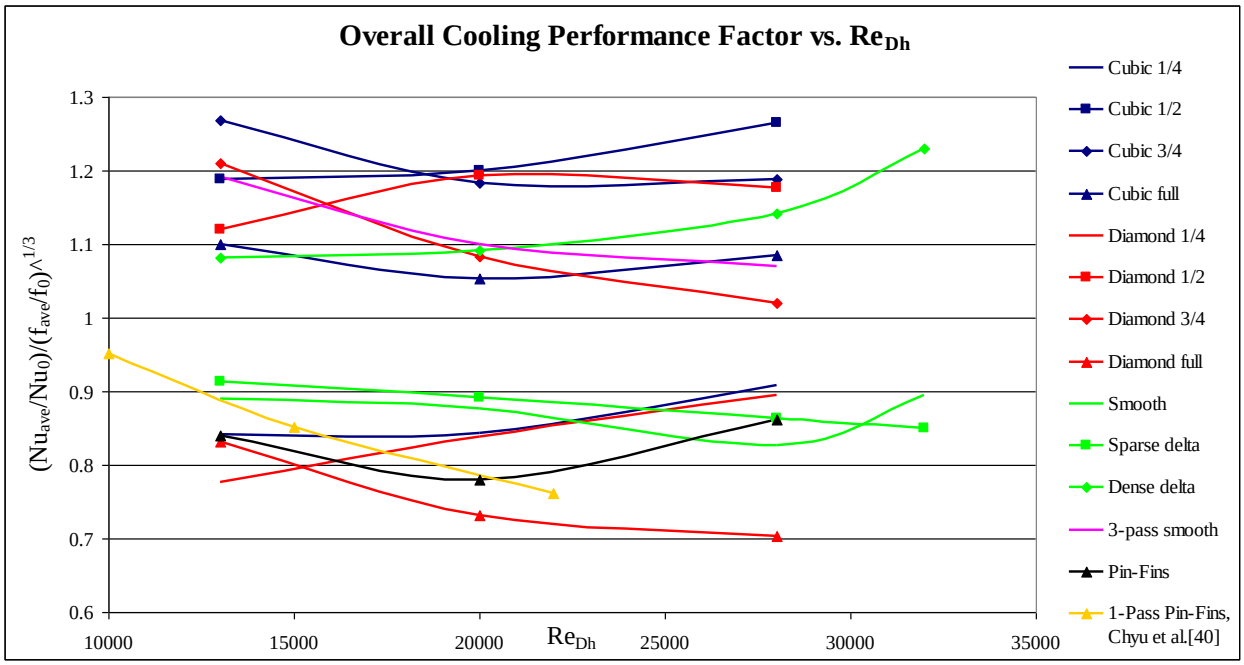

Figure 48 Overall cooling performance factor vs. Re_{Dh} with different channel configurations

6.0 CONCLUSIONS

Due to the sharp turn effect, the second pass in 2-pass smooth channel have approximately 60% higher heat transfer rate than the first pass. As a result of having two 180-degree sharp turn, the 3-pass smooth channel posts higher overall average heat transfer coefficient than the 2-pass smooth channel by approximately 23% while the first passes of both channels have similar flow and heat transfer characteristics.

With the delta wing vortex generators placed in the channel, the flow characteristic and heat transfer have change significantly. The flow in the first pass of the channel with sparse delta-wing arrays is obviously more turbulent which resulting in heat transfer enhancement up to 1.6 folds of the smooth channel while the enhancement in the second pass is only up to about 1.1 folds. While the gain in the second pass is nominal, the heat transfer distributes more evenly over the surface and the different between first and second pass reduces to 12% (2^{nd} pass heat transfer is still higher).

When the density of the delta wing increases, the change is even more significant. The dense delta wing arrays can enhance heat transfer rate up to 3.1 folds and 1.6 folds in the first pass and second pass respectively. Same as the sparse configuration, the gain in the first pass is greater than the gain in the second pass. The average heat transfer in the first pass of the dense configuration is surpassing that of the second pass by 11%.

The effect of 90-degree bend inlet is prominent in the first pass. It can magnify the heat transfer rate up to 1.9 folds relative to the straight inlet counterpart. The gain in the second pass is much less. It is most effective when coupled with sparse delta-wing configuration.

Present results suggest that a staggered cube-array can enhance heat transfer rate up to 3.5 folds in the first pass and approximately 1.9 folds in the second pass, relative to the fully-developed smooth channel counterpart. For the corresponding diamond-shaped block array, the enhancement is 3.4 and 1.9 respectively. Both ¼ height cube and diamond block arrays do not post significant gain over smooth channel. In general, the heat transfer enhancement of the diamond block arrays is higher than that of the corresponding cube block arrays but the pressure lost of the diamond arrays is much higher. Thus in term of cooling performance factor, the cube block arrays surpass the diamond block arrays by a considerable degree. Furthermore, when the flow is too restrictive, i.e. full height diamond blocks, the heat transfer rate reduces because the flow tends to flow toward the space between the block arrays and the channel wall instead; thus reducing the effectiveness of the block arrays.

Among the full height arrays, the study reveals that the cubic and diamond arrays can enhance heat transfer higher than the pin-fin arrays. Except the full height diamond arrays that suffer from excessive restriction, this study is consistent with the report from other researchers [44]. It is interesting to note that even though the post-turn turbulence transport in the second pass is generally higher than the first turn, the effects of surface-element induced heat transfer enhancement are, in fact, less prominent, in the post-turn region in the second pass.

The vortex generators can change the flow field and enhance heat transfer significantly if they sufficiently protrude out of the endwalls. Each type of element array has advantages and disadvantage of its own. Dense delta wing arrays reduce the recirculation zones and enhance

heat transfer in the turning region better than the block arrays but the block arrays have higher overall heat transfer enhancement. While dense delta wings configuration posts good result, it is outperformed by some of the cubic and diamond arrays configurations. The best configuration in term of heat transfer enhancement is the diamond block at ¾ height of the channel while the best in term of cooling performance is the cube block at ½ height of the channel.

7.0 FUTURE WORK

Based on this dissertation study, the recommended future studies are;

- Investigate 90-degree inlet jet impingement.

  90-degree bend inlet is a typical geometry for the cooling channel in turbine blades. The bend inlet promote turbulent and heat transfer. With 90-degree jet inlet instead of bend inlet, heat transfer in the cooling channel could be further enhanced.

- Explore different array configurations.

  The flow field in the 2-pass channel with vortex generators is affected by the position of the vortex generators significantly. Different array configurations need to be studied to further enhanced heat transfer and reduce pressure loss.

- Improve heat transfer in the turning region by adding elements in the turning area.

  The vortex generators can change the flow field and promote turbulent in the tip turn area. Different element configurations need to be explored.

- Investigate rotating effects on 2-pass channel with vortex generators.

  To better understand the real world operating condition, the rotating effects need to be investigated.

BIBLIOGRAPHY

[1] World Energy Outlook, 2006, International Energy Agency.

[2] Todd, D. M., 2000, "Gas Turbine Improvements Enhance IGCC Viability," Gasification Technologies Conference, San Francisco, CA, October 8-11, 2000.

[3] Martini, P., and Schulz, A., 2004, "Experimental and Numerical Investigation of Trailing Edge Film Cooling by Circular Coolant Wall Jets Ejected from a Slot with Internal Rib Arrays," Journal of Turbomachinery, 126, pp.229-236.

[4] Schilke, P. W., "Advanced Gas Turbine Materials and Coatings," GE Energy, Schenectady, NY.

[5] Bathie, W. W., 1984, "Fundamentals of Gas Turbines," John Wiley & Sons, New York.

[6] Chyu, M. K., 2010, "Recent Advances in Turbine Heat Transfer with a View of Transition to Coal Gas Based Systems," International Heat Transfer Conference IHTC-14, Washington, D.C., USA

[7] Dean, W. R., 1928, "Fluid Motion in a Curved Channel," Proceedings of the Royal Society of London, Series A: Mathematical and Physical Sciences, Vol. 121, pp. 402-420.

[8] Wang, T., and Chyu, M. K., 1994, "Heat Convection in a 180-Deg Turning Duct with Different Turn Configurations," Journal of Thermophysics and Heat Transfer, Vol. 8, No. 3., pp. 595-601.

[9] Metzger, D. E., Pelvich, C. W., and Fan, C. S., 1984, "Pressure Loss Through Sharp 180 Degree Turns in Smooth Rectangular Channels," Journal of Engineering for Gas Turbines and Power, Vol. 106, No. 3, pp. 677-681.

[10] Metzger, D. E., and Sahm, M. K., 1986, "Heat Transfer Around Sharp 180-Deg Turn in Smooth Rectangular Channels," Journal of Heat Transfer, Vol. 108, No. 3, pp. 500-506.

[11] Chyu, M. K., 1989, "Regional Heat Transfer and Pressure Drop in Two-Pass and Three-Pass flow Passages with 180-Degree Sharp Turns," ASME Paper 89-GT-191

[12] Chyu, M. K., 1991, "Regional Heat Transfer Two-Pass and Three-Pass Passages with 180-Degree Sharp Turns," Journal of Heat Transfer, Vol. 113, No. 1, pp. 63-70.

[13] Cheng, K. C., Shi, L., Kurokawa, M., and Chyu, M. K., 1992, "Visualization of Flow Patterns in a 180-Degree Sharp Turn of a Square Duct," Fourth International Symposium on Transport Phenomena and Dynamics Rotating Machinery, Honolulu, HI

[14] Liou, T., Tzeng, Y., and Chen, C., 1998, "Fluid Flow in a 180 Deg Sharp Turning Duct with Different Divider Thicknesses," ASME Paper 98-GT.

[15] Syuhada, A., Hirota, M., Fujita, H., Araki, S., Yanagida, M., and Tanaka, T., 2001, "Heat (Mass) Transfer in Serpentine Flow Passage with Rectangular Cross-Section," Energy Conversion and Management, Vol. 42, pp. 1867-1885.

[16] Chyu, M. K., and Natarajan, V., 1995, "Surface Heat Transfer From a Three-Pass Blade Cooling Passage Simulator," Transactions of the ASME, Vol. 117, pp. 650-656.

[17] Cravero, C., Giusto, C., and Massardo, A. F., 1999, "Fluid Flow and Surface Heat Transfer Analysis in a Three-Pass Trapezoidal Blade Cooling Channel," An International Journal of Aircraft Engineering and Aerospace Technology, Vol. 71, No. 2, pp. 142-153.

[18] Choi, J. M., and Anand, N. K., 1995, "Turbulent Heat Transfer in a Serpentine Channel with a Series of Right-Angle Turns," International Journal of Heat and Mass Transfer, Vol. 38, No. 7, pp. 1225-1236.

[19] Fan, C. S., and Metzger, D. E., 1987, "Effects of Channel Aspect ratio on Heat Transfer in Rectangular Passage Sharp 180-Deg turns," ASME Paper 87-GT-113.

[20] Joye, D. D., 1994, "Optimum Aspect Ratio for Heat Transfer Enhancement in Curved Rectangular Channels," Heat Transfer Engineering, Vol. 15, No. 2, pp. 32-38.

[21] Cai, L., Ota, H., Hiroto, M., Nakayama, H., and Fujita, H., 2004, "Influence of Channel Aspect Ratio on Heat Transfer Characteristics in Sharp-Turn Connected Two-Pass Channels with Inclined Divider Wall," Experimental Thermal and Fluid Science, Vol. 28, No. 6, pp. 513-523.

[22] Han, J. C., Glicksman, L. R., and Rohsenow, W. M., 1978, " An Investigation of Heat Transfer and Friction for Rib-Roughened Surfaces," International Journal of Heat and Mass Transfer, Vol. 21, pp. 1143-1156.

[23] Han, J. C., 1984, "Heat Transfer and Friction in Channels with Two Opposite Rib-Roughened Walls," ASME Journal of Heat Transfer, Vol. 106, pp. 774-781.

[24] Han, J. C., Park, J. S., and Lei, C. K., 1985, "Heat Transfer Enhancement in Channels with Turbulence Promoters," Journal of Engineering for Gas Turbines and Power, Vol. 107, pp. 628-635.

[25] Han, J. C., Chandra, P. R., and Lau, S. C., 1988, "Local Heat/Mass Transfer Distributions Around Sharp 180 Deg Turns in Two-Pass Smooth and Rib-Roughened Channel," ASME Journal of Heat Transfer, Vol. 110, pp. 91-98.

[26] Metzger, D. E., and Vedula, R. P., 1987, "Heat Transfer in Triangular Channels with Angles Roughness Ribs on Two walls," Experimental Heat Transfer, Vol. 1, pp. 31-44.

[27] Metzger, D. E., Fan, C. S. and Plevich, C. W., 1988, "Effects of Transverse Rib Roughness on Heat Transfer and Pressure Losses in Rectangular Ducts with Sharp 180 Degree Turns," AIAA-88-0166, AIAA 26th Aerospace and Sciences Meeting, Jan. 11-14, 1988, Reno, Nevada

[28] Han, J. C., 1988, "Heat Transfer and Friction Characteristics in Rectangular Channels Rib Turbulators," ASME Journal of Heat Transfer, Vol. 110, pp. 321-328.

[29] Han, J. C., and Zhang, P., 1989, "Pressure loss Distribution in Three-Pass Rectangular Channels with Rib Turbulators," ASME Journal of Turbomachinery, Vol. 111, pp. 515-521.

[30] Park, J. S., Han, J. C., Huang, Y., Ou, S., and Boyle, R. J., 1992, "Heat Transfer Performance Comparisons of Five Different Rectangular Channels with Parallel Angles Ribs," International Journal of Heat and Mass Transfer, Vol. 35, No. 11, pp. 2891-2903.

[31] Ekkad, S. V., Han, J. C., 1997, "Detailed Heat Transfer Distributions in Two-Pass Square Channels with Rib Turbulators," International Journal of Heat and Mass Transfer, Vol. 40, No. 11, pp. 2525-2537.

[32] Chandra, P. R., Alexander, C. R., and Han, J. C., 2003, "Heat Transfer and Friction Behaviors in Rectangular Channels with varying number Ribbed-Walls", International Journal of Heat and Mass Transfer, Vol. 46, pp. 481-495.

[33] Han, J. C., Huang, J. J., and Lee, C. P., 1993, "Augmented Heat Transfer in Square Channels with Wedge-Shaped and Delta-Shaped Turbulence Promoters," Enhanced Heat Transfer, Vol. 1, No. 1, pp. 37-52.

[34] Armstrong, J., and Winstanley, D., 1988, "A Review of Staggered Array Pin Fin Heat Transfer for Turbine Cooling Applications," ASME Journal of Turbomachinery, Vol. 110, pp. 94-103.

[35] Ames, F. E., and Dvorak, L. A., 2006, "Turbulent Transport in Pin Fin Arrays: Experimental Data and Predictions," Journal of Turbomachinery, Vol. 128, No.1, pp. 71-81.

[36] Chyu, M. K., and Goldstein, R. J., 1991, "Influence of an Array of Wall-Mounted Cylinders on the Mass Transfer from a Flat Surface," International Journal of Heat and Mass Transfer, Vol. 34, No. 9, pp. 2175-2186.

[37] Chyu, M. K., Hsing, Y. C., Shih, T. I. P., and Natarajan, V., 1999, "Heat Transfer Contributions of Pins and Endwall in Pin-Fin Arrays: Effects of Thermal Boundary Condition Modeling," ASME Journal of Turbomachinery, Vol. 121, Vol. 2, pp. 257-263.

[38] Metzger, D. E., Fan, Z. X., and Shepard, W. B., 1982, "Pressure Loss and Heat Transfer Through Multiple Rows of Short Pin Fins," Heat Transfer, Proceedings of the International Heat Transfer Conference, pp. 137-142.

[39] Metzger, D. E., Fan, C. S., and Haley, S. W., 1984, "Effects of Pin Shape and Array Orientation on Heat Transfer and Pressure. Loss in Pin Fin Arrays," Journal of Engineering for Gas Turbine and Power, Vol. 106 (1), pp. 252-257.

[40] Chyu, M. K., 1990, "Heat Transfer and Pressure Drop for Short Pin-Fin Arrays with Pin-Endwall Fillet," ASME Journal of Heat Transfer, Vol. 12, pp. 926-932.

[41] Goldstein, R. J., Jabbari, M. Y., and Chen, S. B., 1994, "Convective Mass Transfer and Pressure Loss Characteristics of Staggered Short Pin-Fin Arrays," International Journal of Heat and Mass Transfer, Vol. 37, Suppl. 1, pp. 149-160.

[42] Chyu, M. K., Oluyede, E. O., and Moon, H. K., 2007, "Heat Transfer on Convective Surfaces with Pin-Fins Mounted in Inclined Angles," Proceedings of the ASME Turbo Expo 4, Part B, pp. 991-999.

[43] Chyu, M. K., Hsing, Y. C., and Natarajan, V., 1998, "Convective Heat Transfer of Cubic Fins Arrays in a Narrow Channel," ASME Journal of Turbomachinery, Vol. 120, pp. 362-367.

[44] Chyu, M. K., Yen, C. H., Siw, S., 2007, " Heat Transfer Characterization of Staggered Pin Fin Arrays using Transient Liquid Crystal Method," Proceedings of GT2007, ASME Turbo Expo 2006: Power for Land, Sea and Air, May 14-17, 2007, Montreal, Canada

[45] Baughn, J. W., 1995, "Liquid Crystal Methods for Studying Turbulent Heat Transfer", International Journal of Heat and Fluid Flow, Vol. 16, No. 5, pp. 364-375.

[46] Ekkad, S. V., and Han, J. C., 1995, "Local Heat Transfer Measurements near a Sharp 180^0 Turn of a Two-Pass Smooth Square Channel with a Transient Liquid Crystal Image Technique," Journal of Flow Visualization and Image Processing, Vol. 2, pp. 285-297

[47] Ekkad, S. V., Zapata, D., and Han, J. C., 1997, "Heat Transfer Coefficient over a Flat Surface with Air and CO2 Injection through Compound Angle Holes Using a transient Liquid Crystal Image Method", Journal of Turbomachinery, Vol. 119, pp.580-586

[48] Chyu, M. K., Ding, H., Downs, J. P., and Soechting, J. P., 1998, "Determination of Local Heat Transfer Coefficient Based on Bulk Mean Temperature Using a Transient Liquid Crystals Technique", Experimental Thermal an Fluid Science, Vol. 18, pp. 142-149.

[49] Yu, Y., and Chyu, M. K., 1998, "Influence of Gap Leakage Downstream of the Injection Holes on Film Cooling Performance", ASME Journal of Turbomachinery, Vol. 120., pp.779-807.

[50] Yu, Y., Yen, C.-H., Shih, T.I.-P., Chyu, M. K., and Gogineni, S., 2002 "Film Cooling Effectiveness and Heat Transfer Coefficient Distributions Around Diffusion Shaped Holes," Transaction of ASME, 124, Oct.. pp. 820-827.

[51] Chen, S. P., Li, P.W., Chyu, M. K., Cunha, F. J., and Messeh, W. A., "Heat Transfer in an Airfoil Trailing Edge Configuration with Shaped Pedestals Mounted Internal Cooling Channel and Pressure Side Cutback", Proceedings of GT2006, ASME Turbo Expo 2006: Power for Land, Sea and Air, May 8-11, 2006, Barcelona, Spain.

[52] Dittus, F. W., and Boelter, L. M. K., 1930, University of California, Berkley, Publications on Engineering, Vol. 2, pp. 443.

[53] Chapman, A. J., 1984, Heat Transfer, 4th Edition, Macmillan, New York, pp. 261.

[54] Gee, D. L., and Webb, R. L., 1980, "Forced convection Heat Transfer in Helically Rib-Roughened Tubes," International Journal of Heat and Mass Transfer, Vol. 23, pp. 1127-1136.

[55] Webb, R. L., "Performance Evaluation Criteria for Use of Enhanced Heat Transfer Surfaces in Heat Exchanger Design, 1981, "International Journal of Heat and Mass Transfer", Vol. 24, pp. 715-726.